MODELING, IDENTIFICATION, SIMULATION AND CONTROL OF HYDRAULIC ACTUATED FATIGUE TESTING MACHINES

Diego Pereira Dias

Dissertação de Mestrado apresentada ao Programa de Pós-graduação em Engenharia Elétrica, COPPE, da Universidade Federal do Rio de Janeiro, como parte dos requisitos necessários à obtenção do título de Mestre em Engenharia Elétrica.

Orientadores: Ramon Romankevicius Costa
Alessandro Jacoud Peixoto

Rio de Janeiro
Junho de 2014

MODELING, IDENTIFICATION, SIMULATION AND CONTROL OF HYDRAULIC ACTUATED FATIGUE TESTING MACHINES

Diego Pereira Dias

DISSERTAÇÃO SUBMETIDA AO CORPO DOCENTE DO INSTITUTO ALBERTO LUIZ COIMBRA DE PÓS-GRADUAÇÃO E PESQUISA DE ENGENHARIA (COPPE) DA UNIVERSIDADE FEDERAL DO RIO DE JANEIRO COMO PARTE DOS REQUISITOS NECESSÁRIOS PARA A OBTENÇÃO DO GRAU DE MESTRE EM CIÊNCIAS EM ENGENHARIA ELÉTRICA.

Examinada por:

Prof. Ramon Romankevicius Costa, D.Sc.

Prof. Alessandro Jacoud Peixoto, D.Sc.

Prof. Marco Antonio Meggiolaro, Ph.D.

Prof. Aldayr Dantas de Araújo, D.Sc.

RIO DE JANEIRO, RJ – BRASIL
JUNHO DE 2014

Dias, Diego Pereira

Modeling, Identification, Simulation and Control of Hydraulic Actuated Fatigue Testing Machines/Diego Pereira Dias. – Rio de Janeiro: UFRJ/COPPE, 2014.

XX, 124 p. 29, 7cm.

Orientadores: Ramon Romankevicius Costa

Alessandro Jacoud Peixoto

Dissertação (mestrado) – UFRJ/COPPE/Programa de Engenharia Elétrica, 2014.

Referências Bibliográficas: p. 108 – 115.

1. Hydraulic Control. 2. Fatigue Testing Machines. 3. Control of Hydraulic Actuated Fatigue Testing Machines. I. Costa, Ramon Romankevicius *et al.* II. Universidade Federal do Rio de Janeiro, COPPE, Programa de Engenharia Elétrica. III. Título.

To my beloved family.

Acknowledgments

I take the freedom of expressing my sincere gratitude and appreciation in my native language ...

A Deus, primeiramente pela graça da minha vida e por sempre estar comigo guiando-me nas estradas da vida.

Aos meus pais, Altamir e Maria de Lourdes, pelo carinho, apoio e amor incondicional. Minha eterna gratidão, por tudo isso e pelos valores de caráter, honestidade e humanidade que sempre transmitem.

Aos meus irmãos, Bruno e Francis, pelo companheirismo e pela confiança que depositaram em mim. Sinceramente, não existem irmãos melhor do que vocês – grande presente de Deus em minha vida.

Ao Prof. Ramon Romankevicius Costa, meu orientador, expresso meus sinceros agradecimentos pela receptividade, acolhida e incentivo ao desenvolvimento deste trabalho. As suas orientações foram essenciais na formulação e fundamentação do problema da tese, de modo a extrair o meu melhor trabalho.

Ao Prof. Alessandro Jacoud Peixoto, meu co-orientador, deixo um agradecimento especial, pela clareza dos conhecimentos repassados e pela oportunidade/honra de trabalhar ao seu lado. As suas contribuições foram fundamentais e me impulsionaram na superação de meus limites.

Ao Prof. Oscar Rosa Mattos, pela confiança e apoio para a realizando meu trabalho. Ao acolher-me no LNDC/COPPE/UFRJ e disponibilizar infraestrutura do laboratório um mundo de possibilidades fez-se presente. Agradeço pela liberdade dada para o desenvolvimento deste trabalho.

À minha *hermosa* namorada Ligia Marcela Tarazona Alvarado pelo carinho,

compreensão e paciência.

Aos professores do PEE/COPPE/UFRJ e aos colegas de mestrado. Em especial aos amigos: Alessandro Santos de Lima, Igor M. Moreira, Ivanko Yannick Yanque Tomasevich, Luciano Menezes Júnior, Kleberson M. de Lima, Nerito O. Aminde e Trevor Matheus Carlos Vilella do Carmo Dobbin, pelo comprometimento de construirmos o conhecimento coletivamente e por compartilharmos bons momentos juntos. Continuemos trabalhando juntos por um mundo melhor!

Aos colegas de trabalho do LNDC/COPPE/UFRJ, em especial aos amigos Alan Machado de Araújo, Demerson Silva Alves de Sá e Rafael Pincos de Mattos, que contribuíram diretamente na realização da parte experimental deste trabalho, além de proporcionarem um ambiente de trabalho agradável e estenderem suas amizades.

Aos professores: Marco Antonio Meggiolaro e Aldayr Dantas de Araújo, pela participação em minha banca e pela contribuições.

Ao Prof. Antonio Carlos Valdiero da UNIJUÍ, pela disponibilidade em discutir conceitos e pelo presente literário dado.

Aos funcionários do PEE/COPPE/UFRJ, Daniele Cristina Oliveira da Silva, Rosa Maria Fontes, Mauricio de Carvalho Machado pela presteza e gentileza.

A todos que participaram de forma direta e indireta da minha formação acadêmica e profissional. Por fim, agradeço ao LNDC/COPPE/UFRJ e CNPq pelo suporte financeiro e à COPPE/UFRJ pela oportunidade de realizar o mestrado.

"The most beautiful things in the world cannot be seen or touched, they are felt with the heart".

Antoine de Saint-Exupéry,
The Little Prince

Resumo da Dissertação apresentada à COPPE/UFRJ como parte dos requisitos necessários para a obtenção do grau de Mestre em Ciências (M.Sc.)

MODELAGEM, IDENTIFICAÇÃO, SIMULAÇÃO E CONTROLE DE UMA MÁQUINA HIDRÁULICA DE ENSAIO DE FADIGA

Diego Pereira Dias

Junho/2014

Orientadores: Ramon Romankevicius Costa
Alessandro Jacoud Peixoto

Programa: Engenharia Elétrica

Esta dissertação aborda a modelagem, identificação, simulação e controle de uma máquina de ensaio de fadiga atuada hidraulicamente. Foi realizada uma revisão bibliográfica detalhada sobre atuadores hidráulicos para máquinas de ensaios de fadiga e um protótipo foi construído no Laboratório de Ensaios Não Destrutivos, Corrosão e Soldagem (LNDC)/COPPE da Universidade Federal do Rio de Janeiro. Um simulador foi desenvolvido a partir de parâmetros obtidos durante um processo de identificação e teste experimentais foram realizados para validar o comportamento dos ensaios de fadiga. Baseado em uma metodologia apropriada de mínimos quadrados, a identificação da força de atrito foi realizada assumindo-se um modelo de Stribeck. Foi verificado através de simulações numéricas que o corpo de prova comporta-se como uma mola equivalente que varia no tempo. Para atenuar este fenômeno, foi projetado uma compensação por realimentação de força. Porém, um controlador proporcional via ganho fixo mostrou-se satisfatório somente para o caso de rastreamento de posição. Verificou-se que um esquema de controle mais elaborado é necessário para solucionar o problema de rastreamento de força quando há propagação de trinca ao longo do tempo. Simulações e resultados experimentais são apresentados para mostrar a eficácia do processo de identificação da força de atrito e os esquemas de controle.

Abstract of Dissertation presented to COPPE/UFRJ as a partial fulfillment of the requirements for the degree of Master of Science (M.Sc.)

MODELING, IDENTIFICATION, SIMULATION AND CONTROL OF HYDRAULIC ACTUATED FATIGUE TESTING MACHINES

Diego Pereira Dias

June/2014

Advisors: Ramon Romankevicius Costa
Alessandro Jacoud Peixoto

Department: Electrical Engineering

This thesis addresses the modeling, identification and control of hydraulic actuated fatigue testing machines. A literature review on hydraulic actuation for fatigue testing machines is provided and a prototype for fatigue test is implemented in the Non-destructive Testing, Corrosion and Welding Laboratory (LNDC)/COPPE of Federal University of Rio de Janeiro. A simulator is developed with parameters obtained during the identification process and experimental tests are conducted to validate the fatigue testing behavior. An appropriate least square based methodology for force friction identification is proposed by considering the Stribeck force friction model. It is verified via numerical simulations that the specimen equivalent spring constant variation must be compensated via force feedback. A conventional proportional control with fixed gain can solve satisfactorily only the position tracking problem. It is verified that a more elaborate control scheme is needed to solve the force tracking problem while the crack grows with time. The crack growth results in a equivalent spring with a time varying stiffness. Simulations and experimental results are provided to show the effectiveness of the proposed friction force identification and control schemes.

Table of Contents

List of Figures

List of Tables

List of Abbreviations and Symbols

List of Abbreviations and Acronyms

CT	compact tension
FPGA	field-programmable gate array
HPU	hydraulic power unit
HSS	hydraulic servo-system
HTM	hydraulic actuated fatigue testing machine
I/O	input-output
LS	least squares
LS	non-linear least squares
RT	real-time
SISO	single-input single-output
SV	servo valve

List of Symbols

Symbol	Description	Units
Latin Notation		
A_n	piston annular area or effective piston surface	[m^2]
B_{co}	parameter for Coulomb friction force	[N]
B_s	parameter for static friction force	[N]
B_v	parameter for viscous friction force	[N s/m]
C_s	parameter for static friction (also known as Stribeck velocity) force	[m/s]
F	algebraic force applied at the specimen	[N]
F_f	total friction force in the cylinder	[N]
F_g	gravitational force	[N]
F_H	fluid net force on the piston surface produced by the load pressure	[N]
F_s	parameter for static friction force	[N]
k_{vel}	velocity gain	[V m/s]
M_p	total mass of the piston mass	[Kg]
M_t	total mass consists of the piston mass, and the mass of hydraulic fluid in the cylinder chambers and in the pipelines	[Kg]
P_A	pressure at the valve port A, connected to chamber A of the actuator	[N/m^2]
P_B	pressure at the valve port B, connected to chamber B of the actuator	[N/m^2]
P_L	difference of pressures in the cylinder chambers	[Pa]
P_s	pressure at the valve port P, connected to the pump of the hydraulic power unit	[N/m^2]
Q_N	valve nominal flow rate	[m^3/s]
T_s	sampling time of real-time control and data acquisition system	[s]
u_c	voltage applied at the servo-valve system	[V]
x_v	position of the spool	[m]
y	piston displacement(position)	[m]
$\dot{y}$	piston velocity	[m/s]
y_d	desired reference (or trajectory) for actuation position	[m]

Accents

Δ	variation or difference
$(\hat{\ })$	estimation or measurement
$(\tilde{\ })$	error or difference
$(\ )^*$	approximation or normalized
$(\dot{\ })$	first derivative
$(\ddot{\ })$	second derivative
$(\dddot{\ })$	third derivative
$(\ )_\Gamma$	filtered value
$(\ )^\intercal$	transpose

Indices

co	Coulomb
d	1.desired
	2.discharge
ext	external
f	1.friction
	2.flapper
	3.final
fb	feedback
ff	feedforward
g	gravitational
H	hydraulic
m	measured
max	maximum
min	minimum
N	nominal
n	1.nozzle
	2.annular
p	piston
ref	reference
r	rod
S	supply
T	tank
t	total
v	1.valve
	2.viscous

Operators and Standard Functions

$\lvert\cdot\rvert$	absolute value (of matrix or vector)
$\overline{(\cdot)}$	mean value
$\in$	element of
$\#$	cardinal number
sin	sine function or wave
sign	signal function
sig	smoothed signal function
$\equiv$	defined as
$\sqcap$	square wave
$\approx$	roughly the same

Chapter 1

Introduction

This thesis is part of the development of a hydraulic actuated fatigue testing machine (HTM) for material testing in corrosive environment of the Non-destructive Testing, Corrosion and Welding Laboratory (LNDC)*. HTM has an important role for mechanical fracture and fatigue testing analyses.These machines may improve LNDC's testing infrastructure. This study made an initial evaluation of all the requirement, structure, limitations and advantages of HTM. Moreover, modeling, identification and position control design were developed for HTM.

The first step to develop a high-performance position and force control for HTM is to elaborate a good model of the actuation system. Next, an appropriate identification of the model parameters should be carried out. Then, different control laws can be designed and implemented in order to fulfill the fatigue testing requirements.

Fatigue testing involves the preparation of carefully polished† test specimens. These notched specimens are submitted to a cyclic controlled force range (ΔF) or stress-intensity factor range (ΔK). As fatigue testing evolves, different values of stress levels are applied and the test specimen stiffness may vary. Hence, the HTM

*"Non-destructive Testing, Corrosion and Welding Laboratory (LNDC) was conceived of an initial proposal made in 2001 to Petrobras, where a laboratory devoted to the areas of oil and gas would be created. The main innovative characteristic of the proposal was to gather research areas of the Graduate Program in Metallurgical and Materials Engineering (PEMM), albeit acting independently. The areas of welding, non-destructive testing, corrosion and fracture mechanics would be bundled together in a single place; a new building where researchers could work conjointly. LNDC has conventional test and research laboratories, an auditorium for 75 people among other common use areas" (LNDC/COPPE/UFRJ, 2012).

†The test specimen surface can not have flaws, because they are stress concentrators.

controller should maintain the cyclic loading very close to a desired profile and monitor the rapid critical crack growth. The stored data are condensed, analyzed and reported. An engineer can then use these information to estimate when the tested material will fail as a result of repeated stresses.

The main motivation for the development of HTM with sophisticated controllers are given in the next section. The novelty is the new conditions which the fatigue testing will be conducted at the LNDC: corrosive and pressurized environments. At the present time, no commercial machine is available to perform such test.

1.1 Motivation

More and more material testing is needed for engineering applications and projects. Industries such as Nuclear, Aerospace, and Petroleum, among many others, have been systematically testing materials in order to obtain:

(1) better quality,

(2) increased safety,

(3) assurance of economic merits, and

(4) development of innovative products and materials (PEREIRA-DIAS *et al.*, 2013).

Recently, new petroleum reservoir were discovered in the Pre-Salt layer, where the oil and gas lie below approximately 2000 [m] water deep and more than 6000 [m] depth. At this depth and environment conditions, better understanding on material properties is required. The dimensioning of flexible pipelines demands material testing and fatigue life estimation. These extreme conditions, high pressure and high salinity, produce a greater mechanical load on the production pipelines.

Fatigue and fracture test laboratories are steadily evolving to meet the demands of standards and providing significant improvements for all industries. In previously years, fatigue testing machines were controlled by analog function generators, mechanical relay counters, digital voltmeters and X-Y recorders. A considerable savings in time and money can be made when standard fatigue and fracture tests are conducted

under a well designed conditions combining control and automated systems. A great effort has been made to develop control techniques and computational tools to ensure good system performance (CULLEN *et al.*, 1985).

In the 1960's, many manufacturing companies of hydraulic servo-system (HSS) and electronic devices were being consolidated. Companies such as Instron Engineering Corporation, MTS Systems Corporation and Shimadzu, which are the leading companies in the sector, started the development of automated material testing machines. Generally speaking, the main technologies employed to generate the cyclic stress on the material samples are basically the following (WEIBULL, 1961):

(1) Mechanical deflection,

(2) Hydraulic actuation,

(3) Pneumatic actuation,

(4) Centrifugation and

(5) Electromagnetic actuation.

However, as mentioned before, in this work we focus on the hydraulic actuated machines.

The development of automated testing machines was followed by a great effort to standardize the procedures. The ASTM International is a globally recognized reference for fatigue and fracture testing standards (ASTM E648-11, 2011),(ASTM E647-08e1, 2011), (ASTM E647, 2008).

The ASTM states that:

> "ASTM's fatigue and fracture standards provide the appropriate procedures for carrying out fatigue, fracture, and other related tests on specified materials. These tests are conducted to examine and evaluate the behavior, susceptibility, and extent of resistance of certain materials to sharp-notch tension, tear, axial fatigue, strain-controlled fatigue, surface crack tension, creep crack, and residual strain."
>
> *ASTM International, 2013.*

Figure 1.1 shows the main components of a HTM. This system can generate a

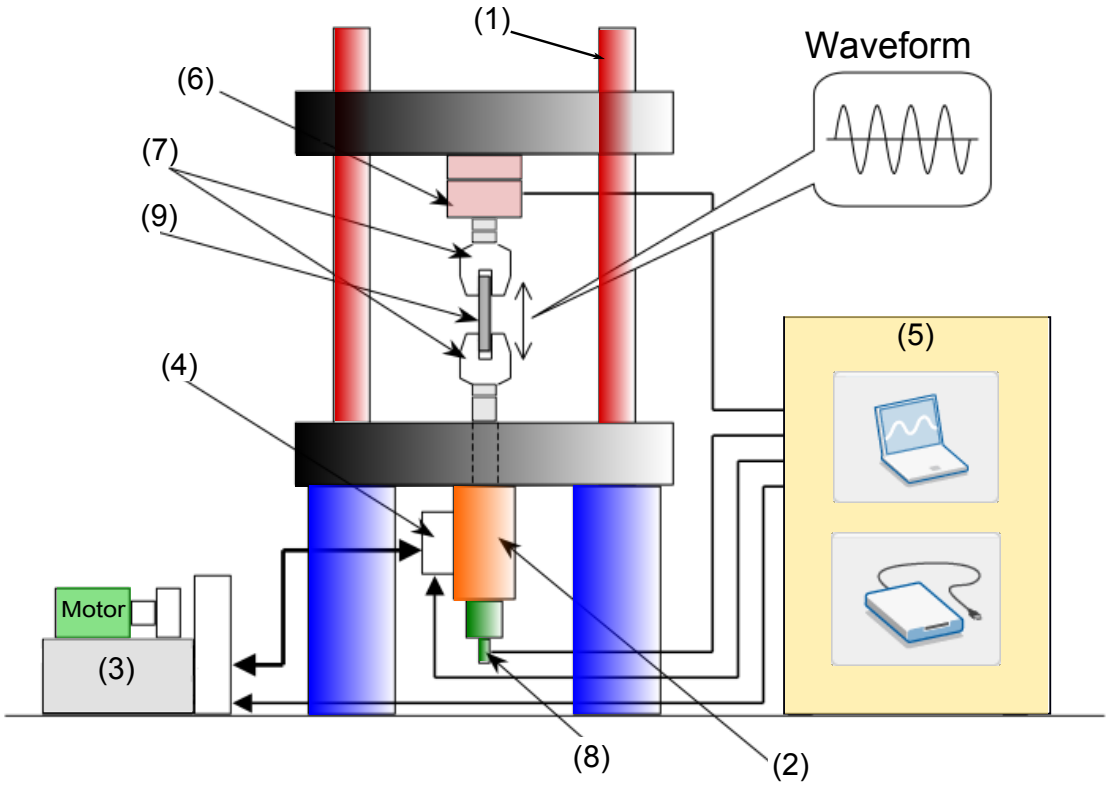

Figure 1.1: Hydraulic actuated fatigue testing machine main components : (1) main frame, (2) hydraulic actuator, (3) hydraulic power unit, (4) servo valve, (5) controller/computer/human-machine interface, (6) load cell, (7) grips, (8) position transducer, (9) specimen to be tested and (10) crack propagation rates measurement system .
Source: adapted from (PEREIRA-DIAS *et al.*, 2013).

vast range of testing conditions. Structures may be subjected to all kinds of dynamic and fluctuating stresses, such as axial (tension-compression), flexural (bending) and torsional (twisting). After a lengthy period of repeated stress, a failure may occur. In general, when applying a fatigue test, the goal is to determine how many load cycles a specimen can sustain or the failure load level for a given number of cycles, the so called *fatigue life* (CALLISTER, 2001), (INTERNATIONAL, 2002). The results of fatigue test may vary from one material to another, so the control system must quickly adapt in order to meet standard requirements.

The most common method of fatigue testing is *constant load*. Different procedures have been developed to solve two objectives (CALLISTER, 2001):

(1) Life distribution at a constant stress level and

(2) Strength distribution at a constant life.

The commercially available HTMs are not capable to perform fatigue testing simulating different environmental conditions. Additionally, the internal control algorithms are not accessible to the user for modification or improvements, thus precluding the implementation of new strategies. In view of these considerations, the possibility of designing and implementing the HTM controller is imperative for a high-performance fatigue testing such as these intended by the LNDC. The controller should be versatile, safe, and adaptable in order to be able to perform fatigue testings in an environment that is at the same time corrosive and pressurized.

1.2 Objectives

The objective of this thesis is to investigate the hydraulic actuated fatigue testing machines and their control algorithms.

Some important aspects of this work are:

- To assess the requirements of HTMs for material fracture,
- To model a hydraulic actuated fatigue testing machine,
- To develop a methodology for hydraulic parameters identification and model validation, and
- To design a position and force control for the HTM.

1.3 HTM and fatigue-corrosion testing

This section is divided into two topics: a brief review of fatigue testing and hydraulic actuation control. Initially, a review on fatigue testing is presented. This review aims to summarize most basic concepts related to fatigue testing. Then, the literature about hydraulic actuation control is reviewed. Since it is not possible to give an extensive list of references for each topic, only the more relevant contributions and concepts are presented.

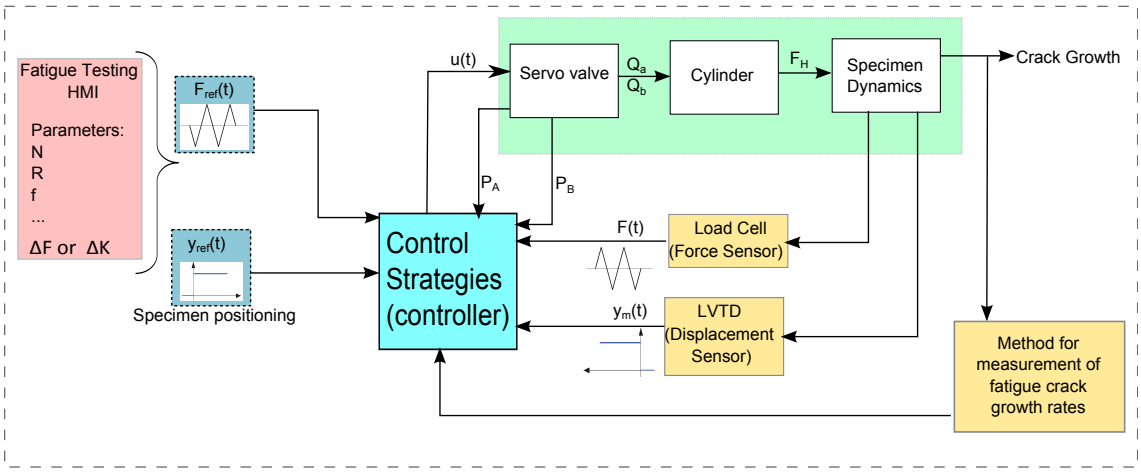

Figure 1.2: Control architecture used for the HTM. The controller for fatigue testing requires information from the method for measurement of fatigue crack growth and force transducer to generate control signal. The module for positioning control is used normally to position the specimen to be tested on the grips of the HTM.
Source: adapted from (PEREIRA-DIAS *et al.*, 2013).

The control architecture used in a **HTM** is depicted in Figure 1.2. Two closed-loop controls are required: (1) position and (2) force. The position controller allows the insertion of the specimen in the correct position. The force controller should keep the load applied to the specimen during the fatigue test strictly inside the bounds defined by the standards.

The controller shown in Figure 1.2 should be able to handle the following variables:

- Crack length a obtained from the fatigue crack growth,
- Position y of the actuator measured by a displacement transducer,
- Force range ΔF applied in a cycle,
- Stress-intensity factor range ΔK, and
- Desired force F_d.

1.3.1 Fatigue testing

Fatigue is a condition whereby the material cracks or fails as result of repeated (cyclic) stress (See Figure 1.3 on page 7). This is an undesirable event that may cause financial losses and, above all, could expose human lives in danger. The causes can be due to inadequate component design, or no prior knowledge of crack growth

rate propagation of a material (CALLISTER, 2001).

Materials can be tested to determine fatigue crack growth rates through experimental investigation. Several different test procedures can be implemented on fatigue testing machines. Thus, fatigue testing gives better understanding of in-service life of material (*fatigue life*). This type of mechanical testing can be performed by different kinds of machines. Different types of load/stress profiles can be applied to perform a fatigue test starting with simple sinusoidal load cycles to complex service life load. Figure 1.3 depicts the same compact tension (CT) specimen before (Fig. 1.3a) and after (Fig. 1.3b) the fatigue testing. Notably, Figure 1.3b shows the effect of a corrosive environment.

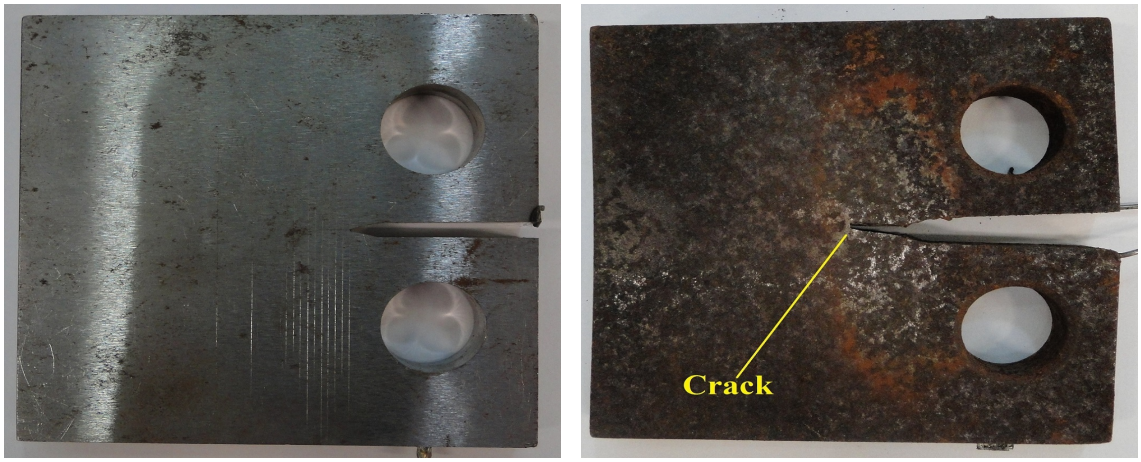

(a) **(b)**

Figure 1.3: Specimen type compact tension behavior before and after fatigue testing, (a) specimen with pre-crack, (b) specimen with crack (*in situ*). The test at constant load was applied during three weeks.

The use of computers to control the machines allowed the complete automation of the testing process. As a result, the time required to perform standard fatigue tests and fatigue crack propagation methods to obtain material characteristics was well reduced (ASTM E647, 2008), (CULLEN *et al.*, 1985). The data acquired by the computer can be processed in accordance with the standards (ASTM E647, 2008), (ISO-12108, 2002) and (ASTM E648-11, 2011). Thus, the material can be completely characterized and the mechanical properties be properly documented.

General purpose machines can be classified according to dynamical and fluctuating

stresses. The machines used in mechanical fracture can be categorized according to (WEIBULL, 1961) as

(1) Axial loading (tension-compression),

(2) Repeated bending,

(3) Rotating bending, and

(4) Torsional (twisting).

Each type of stress requires a specific machine in order to perform the tests (HOSFORD, 2010), (CALLISTER, 2001). The testing machines for special purposes are general purpose machines modified to perform testings such as (WEIBULL, 1961):

- High frequency,
- High or low temperature,
- Cyclic thermal stresses,
- *Corroding environments*,
- Fretting corrosion,
- Multi-stress level tests,
- Contact stresses,
- Repeated impact, and
- Combined creep and fatigue tests.

The choice of an appropriate machine and the right parameters to perform the testings are crucial. In this work, we focus on the axial HTM. Denoting the maximum and the minimum forces[‡] applied in a cycle by F_{max} and F_{min}, respectively. In general, the parameters used to specify how a test should be carried out are the following (ASTM E647, 2008), (ISO-12108, 2002):

(1) **Force range**, $\Delta F = F_{max} - F_{min}$

(2) **Force ratio**, $R = (F_{min}/F_{max})$

(3) **Waveform profile**:

- Sine wave,
- Triangular wave, and

[‡]The word force, in some definition, can be replaced by stress (WEIBULL, 1961).

- Trapezoidal wave.

(4) **Frequency**, (in Hz), f

(5) **Test mode**:

- Constant load range (ΔF),
- Constant stress-intensity factor range (ΔK), and
- Decreasing ΔK.

An important variable to be considered is the stress intensity factor K. The value of K is a function of the applied stress, the size and the position of the crack(HOSFORD, 2010), (CALLISTER, 2001). Additionally, the geometry of the specimen defines where the cracks are detected. Metallurgical engineers are particularly concerned with the brittle fracture because they can produce the most devastating accidents. The brittle fractures occurs when the applied stress reaches a critical value at the crack tip (CALLISTER, 2001). The fracture toughness can be defined in terms of the stress intensity factor.

The stress intensity factor can be used to predict the **stress state**[§] near the tip of a crack. There are three linearly independent cracking mode in fracture mechanics as shown in Figure 1.4. They are characterized by the load type. Mode I is defined as the tensile mode, where the crack surfaces move directly apart.

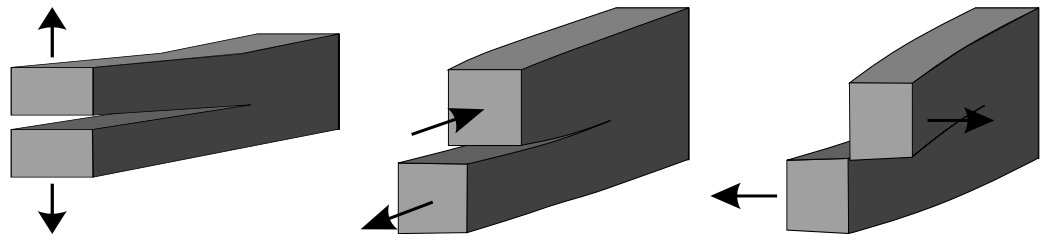

Figure 1.4: Crack loading modes for fracture mechanics: (a) mode I: opening (b) mode II: in-plane shear and (c) mode III: out-of-plane shear. *Source*: adapted from (CALLISTER, 2001), (HOSFORD, 2010).

It was noted that a body under tension, the stress state can be described by semi-infinite elastic solid (HOSFORD, 2010) and the stress intensity factor for mode

[§]Also, known as "stress intensity"

I is defined as

$$K_I = \lim_{r \to 0} \sqrt{2\pi r}\, \sigma_{yy}(r, 0)\,, \tag{1.1}$$

where

r is the coordinate for the stress state near a tip crack, and

σ_{yy} is the stress distribution near the tip crack.

For a standard specimen, the stress intensity factor is calculated as

$$K = \frac{F}{BW^{1/2}}\, g(a/W)\,, \tag{1.2}$$

where

F is the force applied to the specimen [N],

B is the specimen thickness [m],

W is the specimen width [m], and

$g(a/W)$ is the stress intensity factor function.

For a CT specimen (See Figure 1.3 on page 7), the stress intensity factor function is given by

$$g_{\mathrm{CT}}(\alpha) = \frac{(2+\alpha)(-5.6\alpha^4 + 14.72\alpha^3 - 13.32\alpha^2 + 4.64\alpha + 0.886)}{(1-\alpha)^{3/2}} \tag{1.3}$$

where

$\alpha = a/W$.

The expression Eq. (1.3) is valid for $0.2 \leq \alpha \leq 1.0$.

The forces applied to the sample during a fatigue test must be precisely controlled. As defined by ISO:

> " The testing machine shall have smooth start-up and a backlash-free force train if passing through zero force. Cycle to cycle variation of the peak force during precracking shall be less than ±5% and shall be held to within ±2% of the desired peak force during the test. ΔF shall also be maintained to within ±2% of the desired range during test."

(ISO-12108, 2002)

The restrictions according to ASTM E647 (2008) and (ISO-12108, 2002) can be translated in terms of the maximum deviations tolerated as shown in Figure 1.5.

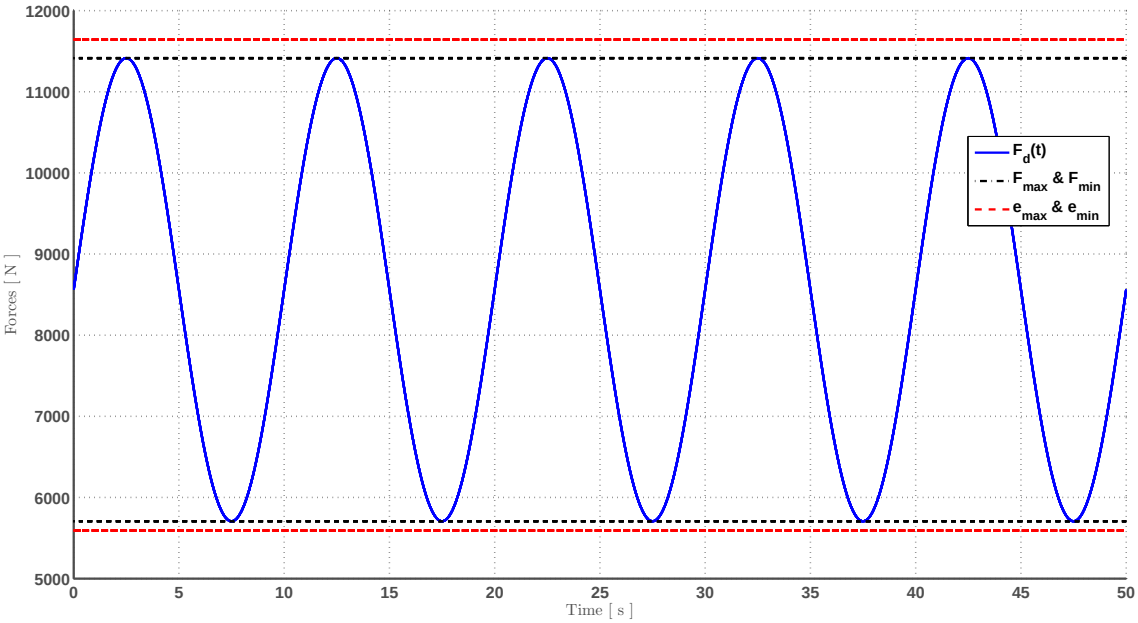

Figure 1.5: Reference force with $\mathrm{R} = 0.5$, $\Delta F = 5707.1\,[\mathrm{N}]$ and $f = 1\,[\mathrm{Hz}]$. The blue solid line represents the reference force calculate for a CT specimen with $B = 10\,[\mathrm{mm}]$, $W = 60\,[\mathrm{mm}]$, an initial crack size $a_i = 16\,[\mathrm{mm}]$ and an initial stress intensity factor range $\Delta K = 12\,[\mathrm{MPa\,m^{1/2}}]$. The black dot-dashed line represents the maximum and minimum force applied at the test specimen and the red dashed is the maximum force deviation that HTM should applied at the specimen.

Larger deviations invalidate the test since they cause a stress concentration, which may modify the plastic regime for the material and change the testing results. According to (CULLEN *et al.*, 1985), an automated testing machine must fulfill some additional requirements :

(1) Implement a user-friendly human-machine interface (HMI) which allows the programming of the entire procedure,

(2) Control the independent variables in a given test,

(3) Monitor and register all test variables for out-of-range or out-of-specification conditions,

(4) Acquire and store all required raw test data,

(5) Detect the end-of-test conditions and stop the test,

(6) Limit raw data register during the test,

(7) Outcome reduced data in a comprehensible format (graphs, tables, etc.),

(8) Store the test results in a database for future reference, and

(9) Provide database management tools to manipulate the stored results.

Note that, the control design plays an important role in the complete system, mainly due to the fact that each test depends on different specimens and requirements(LEE; SRINIVASAN, 1990).

After the test is completed, the information of the material fatigue life is obtained by two plots. Figure 1.6 shows a typical result obtained from a laboratory experiment. In this case, an embedded functionality in the user interface HMI provides the mechanism for data interpolation and also to render the final graphical result. Figure 1.6b shows the distinct regimes of crack growth. HOSFORD (2010) asserts that failure occurs when $K_I = K_{IC}$. After this, the crack growth rate accelerates rapidly.

Generally, fatigue failures can be divided into three distinct stages as illustrated in Fig. 1.6b:

(1) Crack initiation (short cracks) (See Figure 1.3a on page 7),

(2) Crack propagation (long cracks)[¶], and

(3) Fast fracture (final fracture) (See Figure 1.3b on page 7).

Therefore, the fatigue testing system should monitor this variable as well. The most common fatigue test is the one referred to as *Constant Amplitude*.

The stress-intensity factor (K) is a function of specimen's geometry (Eq. (1.2)), the stress applied and the crack length. Based on Eq. (1.3) as the testing evolves, ΔK increases accordingly to the crack length. To illustrate a typical testing result, Figure 1.6a shows a plot of the stress level (S) against the number of cycles. Usually, these tests are heavily time consuming. Depending on the cycle frequency, they can last for months. For example, a fatigue test of 10^9 cycles at a frequency of $50\,[\,\mathrm{Hz}\,]$, done using a traditional HTM would take more than 231 days to finish (MORGAN;

[¶](ASTM E647, 2008) describes test methods for measurement of fatigue growth rates.

MILLIGAN, 1997).

Incremental polynomial method

This method for computing da/dN involves fitting a second-order polynomial to sets of $(2n+1)$ successive data points, where n is usually 1, 2, 3, or 4. The form of the equation for the local fit is as follows (ASTM E647, 2008)

$$\hat{a}_i = b_0 + b_1\left(\frac{N_i - C_1}{C_2}\right) + b_2\left(\frac{N_i - C_1}{C_2}\right)^2 \tag{1.4}$$

where

b_0, b_1, and b_2 are the regression parameters that are determined by the least squares method over the range $a_{i-n} \leq a \leq a_{i+n}$,

$C_1 = 1/2(N_{i-n} + N_{i+n})$ and $C_2 = 1/2(N_{i-n} - N_{i+n})$ are used to scale the input data, thus avoiding numerical difficulties in determining the regression parameters,

$\hat{a}_i$ is the fitted value of crack size at N_i

N_i is the number of cycle.

Then, the crack growth propagation rate at N_i can be obtained from the derivative of the Eq. (1.4) which is given by the following expression:

$$\left(\frac{\mathrm{d}a}{\mathrm{d}N}\right)_{\hat{a}_i} = \frac{b_1}{C_2} + 2b_2(N_i - C_1)/C_2^2\,. \tag{1.5}$$

An example of a desired output data is given in Table B.1. Information on the specimen, loading variables, and environmental conditions should all be listed in the output along with tabulated values of the raw data and processed data. Moreover, the values of total crack size obtained from measurement and from the regression equation (Eq. (1.4)) should also appear. Values of Delta K (ΔK) and da/dN are given in the same units as the input variables.

Paris' Law

Figure 1.7b shows a plot of a typical relationship between the crack growth rate

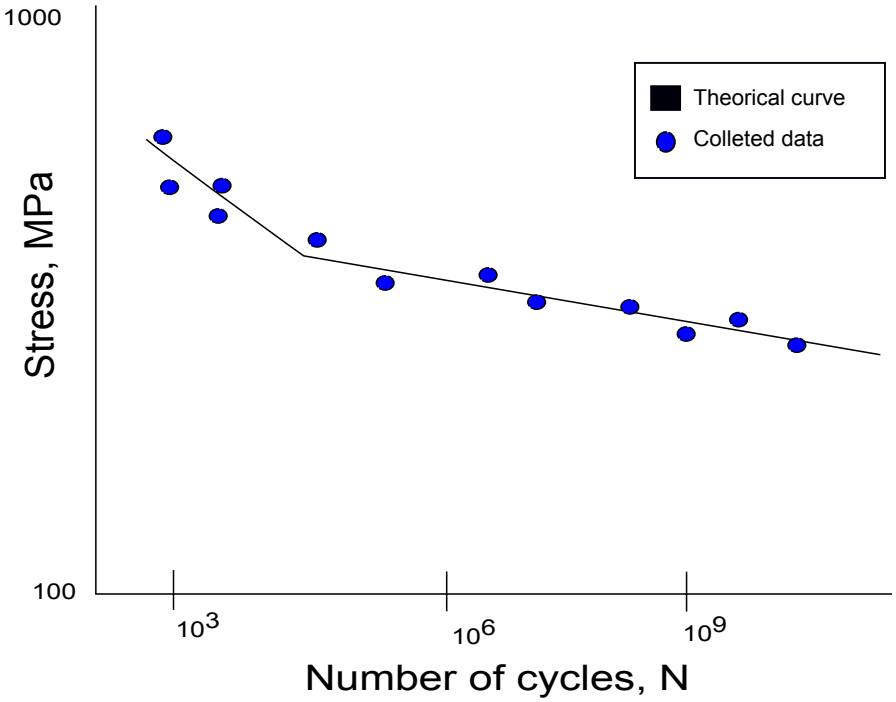

(a)

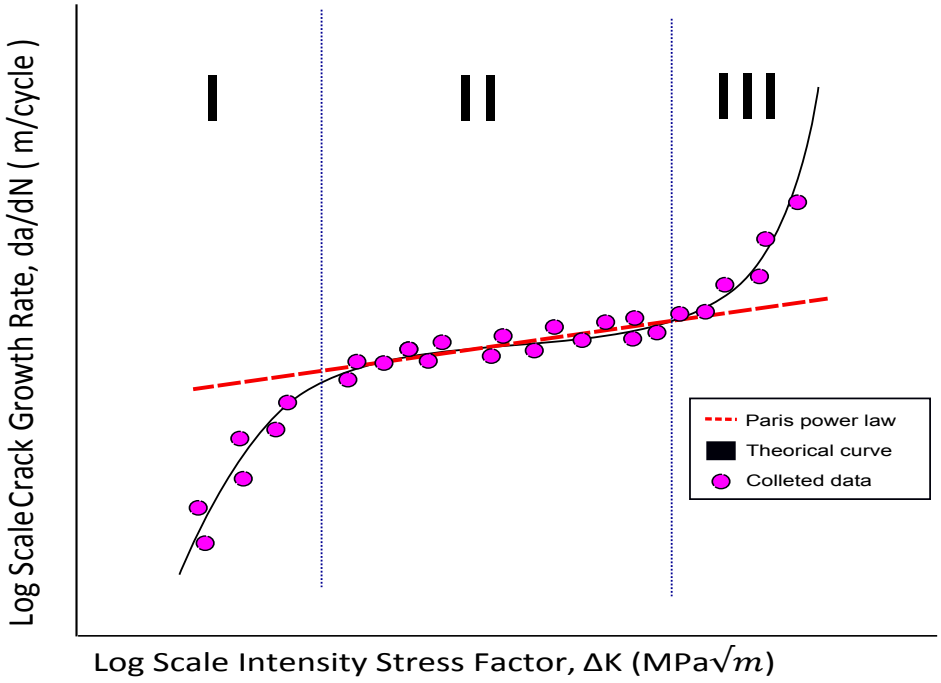

(b)

Figure 1.6: Fatigue life curve and three regions of fatigue crack growth rate: (a) $S \times N$ curve or Wohler curve, (b) Schematic of da/dN and the main regions: (I) crack initiation, (II) crack propagation and (III) fast propagation. *Source*: adapted from (HOSFORD, 2010, Fig. 17.6, pp. 278 and Fig. 17.20, pp. 290), (ASTM E647, 2008), (PEREIRA-DIAS *et al.*, 2013).

da/dN and the range of the stress intensity factor ΔK. The stress intensity factor range ΔK under a fatigue stress regime can be characterized by the well known **Paris' Law**[‖] and described as

$$\frac{\mathrm{d}a}{\mathrm{d}N} = C\Delta K^M \,, \tag{1.6}$$

where

a is the crack length in $[\,\mathrm{mm}\,]$,

C and M are appropriate constants,

N is the number of cycles of load cycles $[\ ]$.

Actuation systems for fatigue testing

In industry, there are three main types of actuation: (1) Servo-hydraulic, (2) Electromagnetic, and (3) Shakers.

The commercially available HTM's vary from small capacities ($\sim 10\,[\,\mathrm{N}\,]$) up to large capacities ($\sim$1000 $[\,\mathrm{kN}\,]$). They can produce small displacements ($\sim 1\,[\,\mu\mathrm{m}\,]$) or large ones ($\sim 0.1\,[\,\mathrm{m}\,]$). A large variety of waveforms, speeds, and frequencies are selectable. Speeds can range from $0.5\,[\,\mu\mathrm{m\,min^{-1}}\,]$ to $20.0\,[\,\mathrm{m\,s^{-1}}\,]$ and frequencies starting at $1 \times 10^{-4}\,[\,\mathrm{Hz}\,]$ to $300.0\,[\,\mathrm{Hz}\,]$.

They set and control the actuator operating modes, as well as the testing conditions such as force amplitudes and mean values. Some variables measured are displacement, distortion, speed, acceleration, pressure inside the cylinder, and so on.

Machines where the hydraulic actuator is operated by a servo-valve electrically controlled is called electro-hydraulic testing machines (EHTMs) (AHN; DINH, 2009), (RABIE, 2009), (SOHL; BOBROW, 1999). Their main advantages are the broad load range and high precision for a wide frequency range. The disadvantages are the costs of installation, maintenance and non-linearities present in each subsystem.

[‖] Also known as **Paris-Erdogan law**.

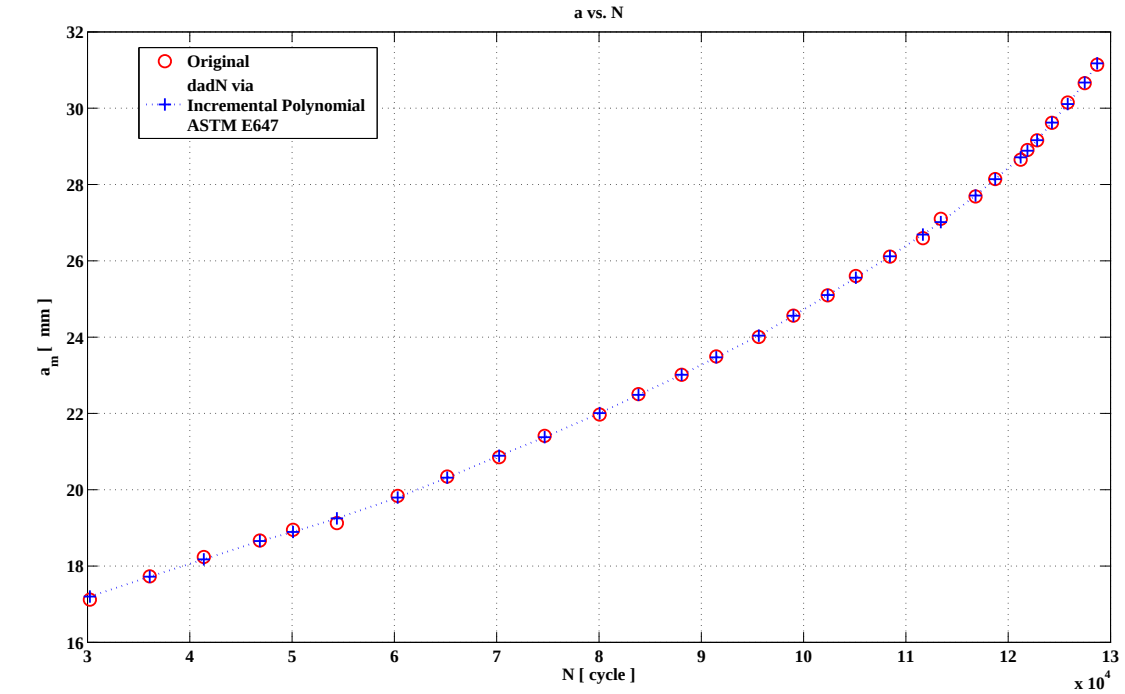

(a)

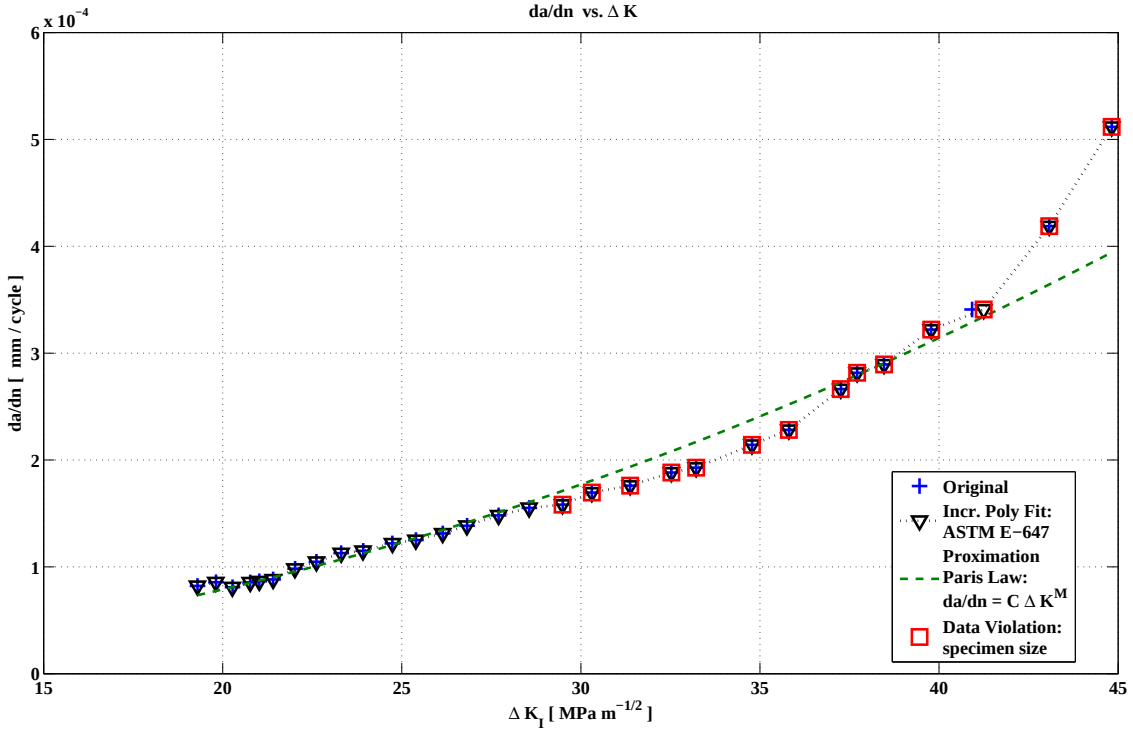

(b)

Figure 1.7: (a) Crack growth rates obtained from adjacent pairs of a vs. N data points. (b) plot of log da/dN *versus* log ΔK. Data points from (ASTM E647, 2008, Table X1.2, p. 32).

1.3.2 Control of hydraulic actuator

Over the years, more advanced HSSs and computers have been developed and applied to HTM's aiming to improve their performance (ASTM E647, 2008), (CULLEN *et al.*, 1985). In (CULLEN *et al.*, 1985) the problem of acquiring and processing HTM data in real-time was considered. A wide range of application and measurement techniques using HTM are found in CULLEN *et al.* (1985).

The development of HSSs have attracted the attention of the control community and generated several industry applications. Although some technologies such as electrical, pneumatics, mechanical, solar, and others are nowadays in the spotlight, it is well known that hydraulic technology plays an important role (BAUER, 2011; JELALI; KROLL, 2003), (ALLEYNE; LIU, 2000), (MERRITT, 1967). Indeed, hydraulic system is attractive mainly due to its good power/mass ratio, its high mechanical stiffness, its fast response during the startup/stop and its fast response for reversions (JELALI; KROLL, 2003).

The hydraulic actuator can be assembled in order to produce linear or rotational displacements (BAUER, 2011), (LINSINGEN, 2001), allowing a wide range of applications, such as: excavator, mining vehicles, flight simulator platforms, Stewart platforms and testing machines. Hydraulic systems have become a natural solution for actuation in testing machines due to their reliable components and unique characteristics which surpass the overall performance of other technologies (BAUER, 2011), (JELALI; KROLL, 2003), (MERRITT, 1967).

As mentioned before, the advantages of the hydraulic servo-systems when compared to electrical servo-systems (for example) are the ability to: generate higher force/torque, higher load stiffness and faster transient response during speed reversal (JELALI; KROLL, 2003). On such conditions, electro-motors tend to overheat (VOSSOUGHI; DONATH, 1995). In addition, it must be highlighted that HSSs are able to operate continually under different required operation conditions (BAUER, 2011), (BESSA *et al.*, 2010a),(JELALI; KROLL, 2003), (SIX *et al.*, 2001), (ALLEYNE; HEDRICK, 1995), (SIROUSPOUR; SALCUDEAN, 2000), (SOHL;

BOBROW, 1999),(MERRITT, 1967).

Hydraulic systems are also attractive for developing high performing applications and high power applications, however, according to (BESSA *et al.*, 2010a), (JELALI; KROLL, 2003), (SIROUSPOUR; SALCUDEAN, 2000), (SOHL; BOBROW, 1999) and (MERRITT, 1967) there are some issues that must be considered, such as:

(1) Hydraulic components have a significant cost when specified to achieve small tolerances,

(2) Hydraulic system has complex nonlinear characteristic which is hard to model and/or control,

(3) In all hydraulic systems, fluid contamination is an important issue and almost impossible to avoid completely,

(4) Near ignitions sources, explosion is not precluded *a priori*, and

(5) An undesirable working environment can arise due to fluid leakage.

Therefore, hydraulic servo-systems implementations may become inadequate when considering low power applications. In spite of the challenges/difficulties concerning hydraulic systems, several results can be found in the literature which seek for improvements in the modeling and/or control of HSSs (BAUER, 2011), (BESSA *et al.*, 2010a), (JELALI; KROLL, 2003), (SIROUSPOUR; SALCUDEAN, 2000) and (SOHL; BOBROW, 1999).

PELLOUX; BROOKS (1964) and CULLEN *et al.* (1985) present a fatigue machine without feedback, i.e., under open-loop control, with a hydraulic actuator. The control system is composed by a hydraulic pressure generator and an electronic rack containing an oscilloscope, a program command unit and a function generator. Conversely, several feedback control strategies were proposed for hydraulic systems (BAUER, 2011), (JELALI; KROLL, 2003) and (MERRITT, 1967), since the early 1960's. Applications using HSSs normally require position control. However, in the context of fatigue testing, force control is also needed (See Figure 1.8 on page 19).

In particular, results for position control can be found in (BESSA *et al.*, 2010a), (GUAN; PAN, 2008), (KIM; LEE, 2006), (SIROUSPOUR; SALCUDEAN, 2000),

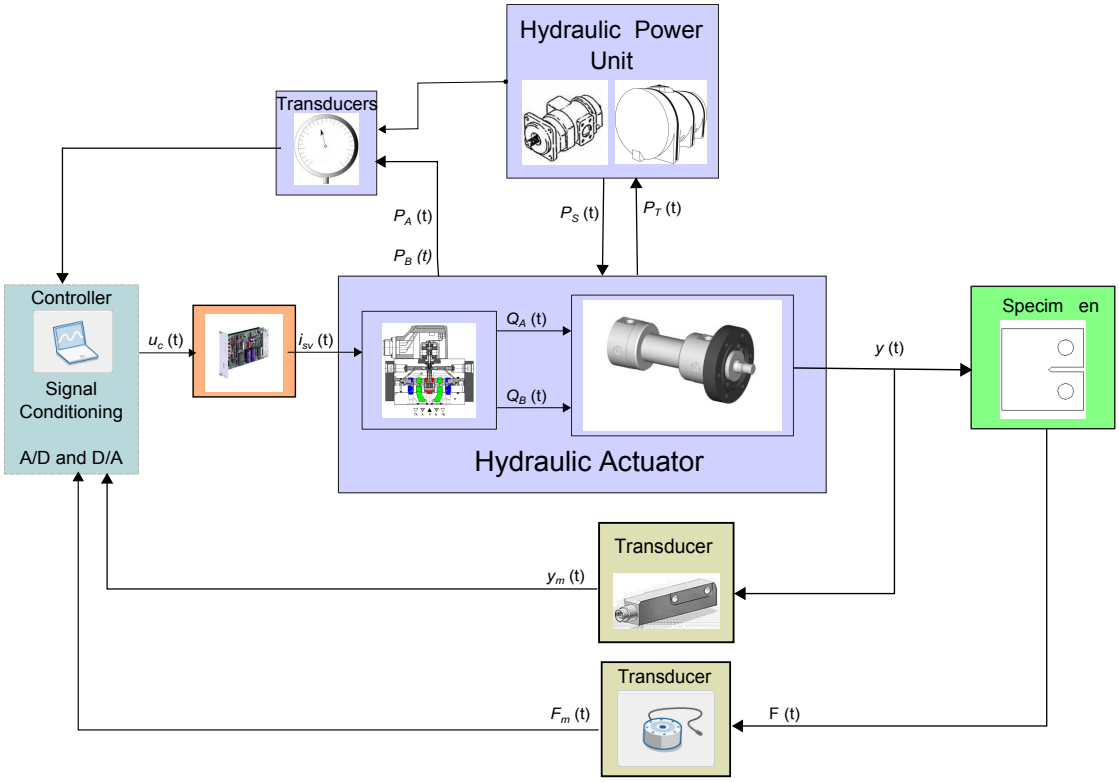

Figure 1.8: Schematic block diagram of hydraulic actuation system for hydraulic actuated fatigue testing machine: position and force control algorithm. In terms of fatigue testing, force control is the main objective because the test mode depends directly to its trajectory generation. The position control has two goals: specimen positioning and safety mechanism.

(VOSSOUGHI; DONATH, 1995), (STOTEN; BENCHOUBANE, 1990) and (MERRITT, 1967). Moreover, results regarding force control can be found in (SÁNCHEZ *et al.*, 2012), (TRAN *et al.*, 2012), (AHN; DINH, 2009), (ALVA, 2008), (SERRANO, 2007), (NIKSEFAT; SEPEHRI, 1999), (KASPRZYCZAK; MACHA, 2008), (JELALI; KROLL, 2003) and (CLARKE, 1997). No comprehensive control strategy dealing with all non-linearities in HTM is found. In general, the non-linearities due to deviation from the operating conditions are considered as plant uncertainties (VOSSOUGHI; DONATH, 1995).

The constructive components are assumed to be perfect built and no leakage is found (BAUER, 2011), (JELALI; KROLL, 2003), (VALDIERO, 2012) and (PLUMMER, 2007). However, friction forces have their importance. They are one of the dominant disturbance in the system. Their effect is usually a positioning error but

can also cause instability. (CANUDAS-DE-WIT *et al.*, 1995),(CANUDAS-DE-WIT; GE, 1997).

The control performance is degraded due to friction effect. (SOHL; BOBROW, 1999). ARMSTRONG-HÉLOUVRY *et al.* (1994) showed the performance reduction due to the non-linearity of the friction. Some effects due to friction include stick-slip, hunting, standstill and quadrature glitch (VALDIERO, 2004). The common friction effects are depicted in Figure 1.9.

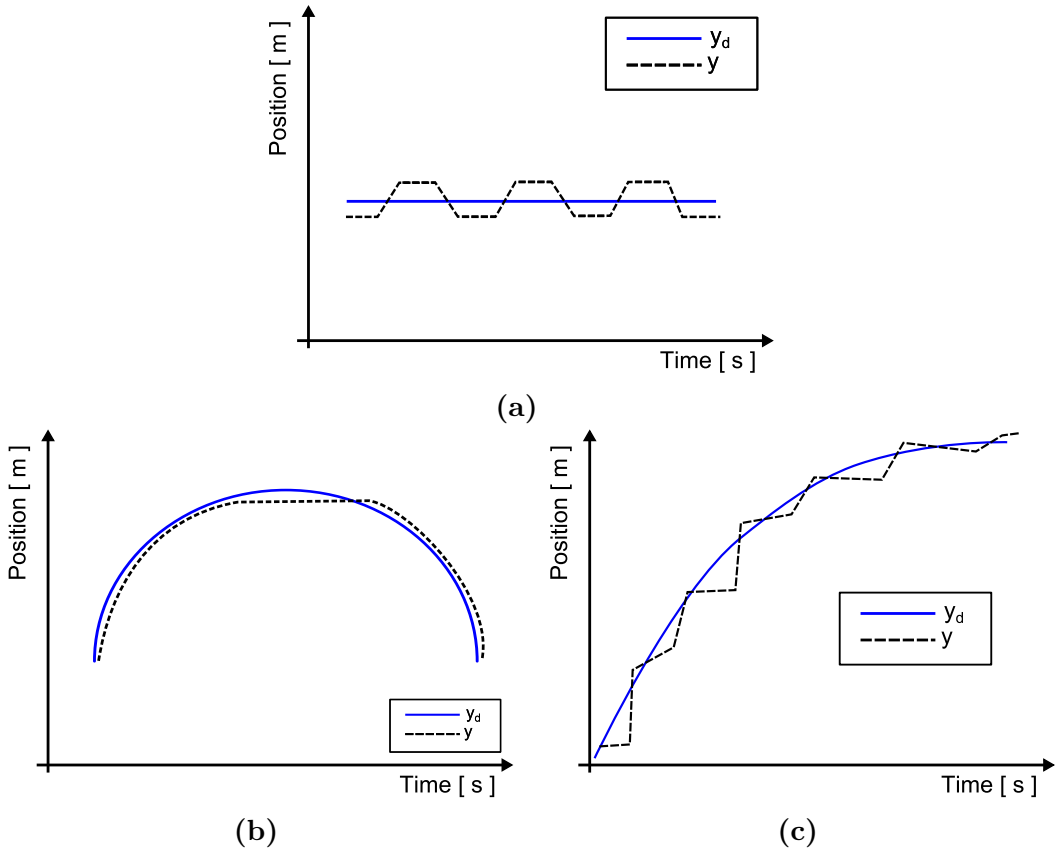

Figure 1.9: Common position degradation effects caused by friction force: (a) hunting, (b) standstill and (c) stick-slip.
Source: adapted from (VALDIERO, 2012).

The hunting effect causes the position to oscillate around desired position with a constant value (VALDIERO, 2012) (Fig. 1.9a). Another effect that may impact controller performance is standstill, because the actuator does not perform well at null velocities. As seen in Figure 1.9c, the effect of stick-slip is caused by a slight holding effect for low velocities.

Output feedback control

Hydraulic servo-system control strategies via output feedback date from the early 67's (MERRITT, 1967), (ANDERSON, 1989). Advanced control techniques have being developed to overcome some difficulties, in particular, regarding force control (AHN; DINH, 2009), (ALVA, 2008),(ALLEYNE; LIU, 2000), (SOHL; BOBROW, 1999), (NIKSEFAT; SEPEHRI, 1999).

For example, in SOHL; BOBROW (1999) it is shown that the local linear approximation model may become unstable, for some initial conditions (or operating point). The practical importance of a proper estimation of the dead-band for the valve is highlighted in (SOHL; BOBROW, 1999), where it is verified that force tracking performance degradation may become significant, for large values of the estimation error. Moreover, the friction force must be considered in order to obtain acceptable tracking accuracy. In SOHL; BOBROW (1999), the proposed control law

$$u = \frac{1}{z}\Big(\dot{F}_{hd} - \kappa_F(F_H - F_{hd}) + g(A_1, A_2, V_1, V_2)\cdot \dot{y}\Big)\,, \tag{1.7}$$

where,

z is a parametric function of hydraulic actuation system,

κ_F is the control gain to be tuned, and

$g(A_1, A_2, V_1, V_2)$ is a function that depends on hydraulic parameters,

assures that the tracking error $\varepsilon = F_H - F_{hd}$ converges exponentially to zero according to

$$\frac{\mathrm{d}\varepsilon}{\mathrm{d}t} = -\kappa_F \varepsilon\,,$$

by using the Lyapunov function $V = (1/2)\varepsilon^2$, where F_{hd} is the desired force trajectory for the hydraulic force F_H, $\kappa_F > 0$ is a design parameter. It was proved that the system is exponential stable (SOHL; BOBROW, 1999). This control law, however, is difficult to implement since it requires several derivatives. Noise is normally found in industrial plants and their effects are amplified in such control laws.

Later on, in KASPRZYCZAK; MACHA (2008), after assuming that both servo-

valve and actuator can be modeled by second order systems, a PID controller was designed and tuned. However, after several tuning process, it was verified that the force transient always contains overshoot. As mentioned before, the overshoot must be avoided for an acceptable fatigue test. On the other hand, some practical hints on how to tune PID controllers for fatigue testing machines was provided. A previous control solution was made using self-tuning approach (LEE; SRINIVASAN, 1990). Differently from KASPRZYCZAK; MACHA (2008), the nonlinearities appears due to:

(1) Servo-valve was not critically centered, but had a small overlap and leakage that should be taken in account,

(2) The hydraulic actuator (HA) leakage effect was significant and hence necessary to model (LEE; SRINIVASAN, 1990).

Backstepping control

According to ALLEYNE; LIU (2000), classical PID controllers cannot overcome some problems related to tracking force (or pressure) in hydraulic systems, mainly due to friction. In order to increase flow rate and response speed, in general, traditional servo-controller requires a high accurate system model.

The problem consists of a double-ended hydraulic cylinder driven by a single-stage, four-way spool valve. The valve dynamics was approximated by a first-order model due to the inner control loop response rate and it was considered to be fast enough.

The Karnopp's friction model was adopted to be used in this study because the "stick" phase occurs when velocity is within small critical velocity range (ALLEYNE; LIU, 2000), (CANUDAS-DE-WIT; GE, 1997). In this sense, a robust backstepping control scheme was developed in ALLEYNE; LIU (2000) for an electro-hydraulic actuator (EHAc), but at a price. High computational effort is required for its implementation.

Quantitative feedback theory for hydraulic actuator

Nonlinear Quantitative feedback theory (QFT) was considered in NIKSEFAT; SEPEHRI (1999) which provides a closed loop control strategy robust with respect to parametric uncertainties. The nonlinear plant is equivalently replaced by a family of linear time invariant (LTI) plants. The key idea is to consider a family of second-order linear transfer functions of the form

$$G_e q(s) = \frac{K_p}{(1 + s/\alpha_1)(1 + s/\alpha_2)}, \tag{1.8}$$

obtained via Golubev's method, to approximate the dynamics from the actuator (piston) displacement (which is assumed proportional to the electrical control signal) to the generated hydraulic force, where the uncertain parameters K_p, α_1, and α_2 belong to some known interval. Three scenarios were considered:

(1) The effect of specimen stiffness variation,

(2) Pump pressure reduction, and

(3) Loading conditions.

These three situation are expected on a fatigue test, due to

(1) Crack growth,

(2) Continuously and long period operations, and

(3) Dynamic force operating point (changing ΔK).

The corresponding linear controller is given by

$$C(s) = \frac{k_1(1 + s/k_2)(1 + s/k_3)}{s(1 + k_4 s + k_5 s^2)}, \tag{1.9}$$

where k_i $(i = 1, \ldots, 5)$ are appropriate constants. The main problem here is that overshoot can appear in the applied force. Therefore, since force overshoot can modify the stress intensity factor (K), the fatigue test result may become questionable (HOSFORD, 2010).

In a similar approach, AHN; DINH (2009) considered a self-tuning QFT. Based on previous work found in (NIKSEFAT; SEPEHRI, 1999), they performed an identi-

fication procedure for a reduce order model assuming that

$$P(s) = \frac{k}{(1+p_1 s)(1+p_2 s)} = \frac{k\omega_p^2}{s^2 + 2\xi_p\omega_p + \omega_p^2}\,, \tag{1.10}$$

where $k \in [3.97, 6.81](N/mV)$, $p_1 \in [0.85, 1.16]$, $p_2 \in [0.85, 1.16]$, $\omega_p = 1/\sqrt{p_1 p_2}(rad/s)$ and $\xi_p = (p_1+p_2)/(2\sqrt{p_1 p_2}) \leq 1$. The self-tuning controller is considered to be of the form $C(s) = k(s+a)/[(s+b)(s+c)] = (ks+ka)/(s+m^2+\omega^2)$. The controller time varying parameters (a, b, c) are defined as follows: $(STQTF)_{t+1} =$ (new set), if the conditions are satisfied, otherwise the previous setting is applied, *i.e.*, $(STQTF)_{t+1} = (STQTF)_t$, where each element comes from the QFT algorithm. The results were compared with:

- Conventional PID controller and
- QFT controller.

For different environment conditions, the self-tuning QFT controller presented better tracking performance, with overshoot $\leq 2\%$.

More recently, (LEDEZMA-PÉREZ, 2012) tackled the problem of force control for hydraulic actuators applying QFT. Two cases were analyzed: (1) static environments and (2) dynamic environments. The force control of static environments can be applied for fatigue testing machines. The main advantage is the estimation of the parametric uncertainties present in hydraulic actuation system.

Cascade control for hydraulic actuator

Adaptive cascade control of HA to compensate unknown dead-zone can be seen in CUNHA (2001). It is assumed that the valve has a dead-zone with unknown parameters. The strategy is to consider the HA as two interconnected subsystems: one hydraulic and one mechanical.

The control objective was to track a position reference. A third-order model for the system was considered. The cascade control algorithm implements two compensations: (1) estimates the desired pressure load, so the desired position trajectory is followed and (2) calculates the control signal u so that the hydraulic

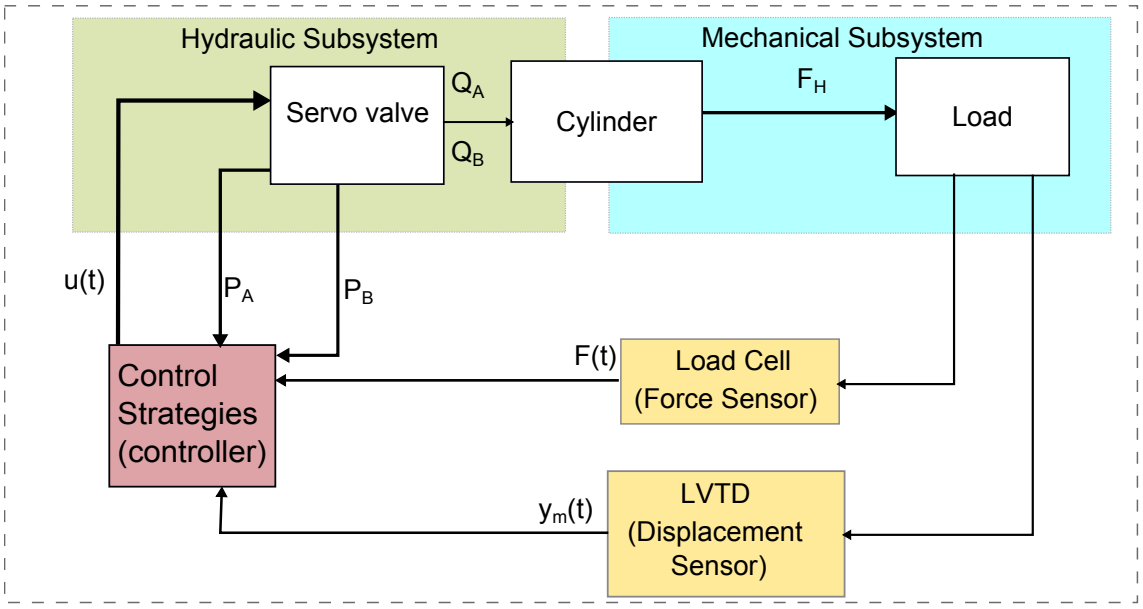

Figure 1.10: Cascade control for hydraulic actuator: interconnected subsystems. Combination of hydraulic control subsystem and mechanical control subsystem. The problem is divided into two parts: (1) control design to compensate the non-linearities of the hydraulic subsystem and (2) control design to compensate the non-linearities of the mechanical subsystem
Source: adapted from (VALDIERO, 2012), (CUNHA; GUENTHER, 2006).

subsystem has a desired pressure load.

An extension for dead-zone compensation is presented in (CUNHA; GUENTHER, 2006).

Using evolutionary algorithms, the optimization of the gains of the adaptive cascade controller was discussed in (COELHO; CUNHA, 2011). Evolutionary algorithms have been proven to be resourceful for solving global optimization problems, specially with nonsmooth objective functions. It is shown that such algorithms are effective to tune the optimization as well as to estimate parametric uncertainties in the mechanical and hydraulic subsystems.

Control design based on expert systems

An adaptive fuzzy sliding mode controller for an electro-hydraulic servo system (EHSS) with unknown dead-zone was designed in (BESSA *et al.*, 2010a) and the closed loop system stability was demonstrated. Some assumptions were made:

(1) The dead-zone is not available to be measured, and

(2) The dead-zone is limited.

The strategy is interesting for fatigue testing because the system has parametric uncertainties, unmodeled dynamics and an unknown dead-zone. Only numerical simulations was conducted, but the results encourage practical control implementations.

All these (hybrid) control schemes try to estimate the system uncertainties. When dealing with friction and hydraulic uncertainties, learning control and neuro-fuzzy learning control (SÁNCHEZ *et al.*, 2012), (ALVA, 2008), and feedback linearization with fuzzy compensation (TANAKA *et al.*, 2012) were applied to overcome uncertainties in order to increase the frequency of the load cycles. In (ALVA, 2008) a comparison was made among PI, PID, and learning controller. A forth order linear model was considered, and a learning method control was applied on a HTM. The results show that no prior knowledge is necessary to improve the learning gain. A comparison between learning control and neuro-fuzzy system is found in (SÁNCHEZ *et al.*, 2012). For the same simulation and experiment conditions, the neuro-fuzzy learning control converges faster than conventional learning control and the difference between them is that the former requires less memory to store the tuning parameters.

1.3.3 Summary

Comprehensive, cost effective material testing has been achieved through hydraulic actuated fatigue testing machine development. Due to the inherent complexity of the fatigue testing machines, the hydraulic actuation system should be appropriately designed to compensate all the nonlinearities.

The problem with uncertainty estimation, such as friction and compressibility of hydraulic fluid (bulk), must be carefully considered. Indeed, in the mentioned references friction is disregarded and the fatigue test degradation is apparent and high frequency tests are precluded.

1.4 Thesis Outline

The rest of this document follows this outline:

- Chapter 2 shows the most relevant aspect of hydraulic actuation and how it can affect the machine performance through a fatigue testing.
- In Chapter 3, the software and hardware requirements were presented and the initial testing platform was implemented. Moreover, the friction force model is identified and the validity of the friction model is tested.
- In Chapter 4, the main control challenge is presented. The specimen stiffness is considered to be time variation for the spring constant and evaluation and a force control is proposed.
- Chapter 5 presents the main conclusion of this study and also leaves some suggestions for further research and implementations.

Chapter 2

Modeling of hydraulic actuation for testing machines

In this chapter the mathematical model for HTM is described which provides a simulation framework for control design and tuning. The most relevant aspects regarding fluid properties and hydraulic components are discussed. Additionally, this chapter aims to provide a survey to the control community w.r.t. hydraulic servo-system (HSS) applications. Furthermore, the main advantages and shortcoming of hydraulic actuation is presented.

The methodology to identify the nonlinear model considered in this work is as follows. First, a theoretical model is presented where each individual components is expressed in a phenomenological description context (basic physical laws). Next, data acquisition is considered to better characterize the relevant system dynamics and non-linearities and to identify the hydraulic parameters. Finally, the model is validated over simulations and its parameters are compared with realistic physical parameters. This approach can be found in (JELALI; KROLL, 2003), see Figure 2.1. Hydraulic actuation transforms hydraulic energy into mechanical energy through an arrangement of interconnected components, based on Pascal's law: (a) hydraulic power supply, (b) control element, (c) conversion element, (d) actuating element and (e) energy limiter. Usually, the input power is electrical (or thermal) and it

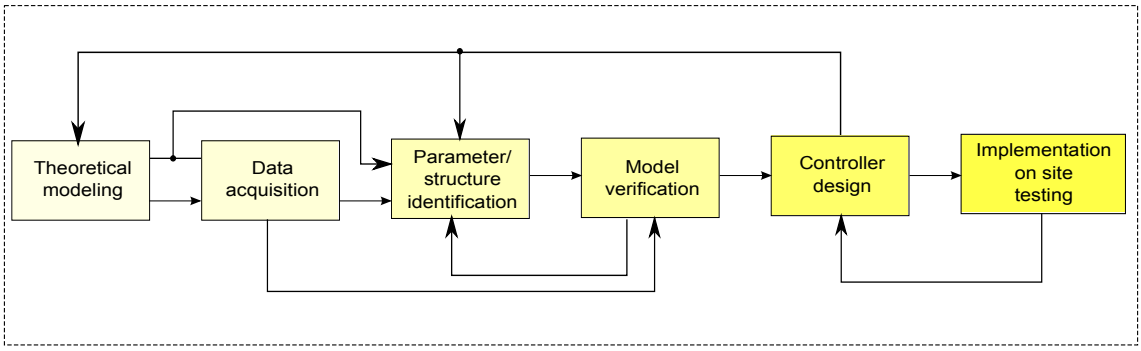

Figure 2.1: Block diagram of the modeling methodology (including control design) proposed by (JELALI; KROLL, 2003).
Source: Adapted from (JELALI; KROLL, 2003).

is converted into mechanical through an electrical (or combustion) motor. In the hydraulic power unit (HPU) occurs the primarly conversion*. Valves are used to: control the direction of the pump flow, to limit the power transmitted and the amount of fluid (consequently, the pressure) introduced into the actuator. The actuator converts the hydraulic power to useful mechanical power for an application. It is clear that, the fluid used needs to be stored and conditioned to ensure the quality of the hydraulic actuator (JELALI; KROLL, 2003) and (LINSINGEN, 2001) (Fig. 2.2).

2.1 Fluid properties

The main purpose of the fluid is to transmit power in a HSS. However, depending on the fluid characteristics (or properties) it can also provide good lubrication and cooling and seal clearances. These properties tend to change as the fluid operates on high pressures and high velocities. Since friction is unavoidable and the resultant heat raises temperature, hence fluid properties are affected (CUNDIFF, 2001).

Most industrial hydraulic actuation systems use petroleum based oils with additives to inhibit foaming and corrosion. The mineral oil is slightly compressible which is a suitable characteristic for high velocities (fast transmitting systems) (CUNHA, 2013). The mineral oil used in HTM is the ISO VG68 oil. The letter VG stands for viscosity grade.Another important property is the cleanness of the hydraulic

*Hydraulic power is defined as, $P_h = Q \cdot P$, where P_h is hydraulic power [kW], Q is flow [$\mathrm{L\,min^{-1}}$] and P is pressure [bar].

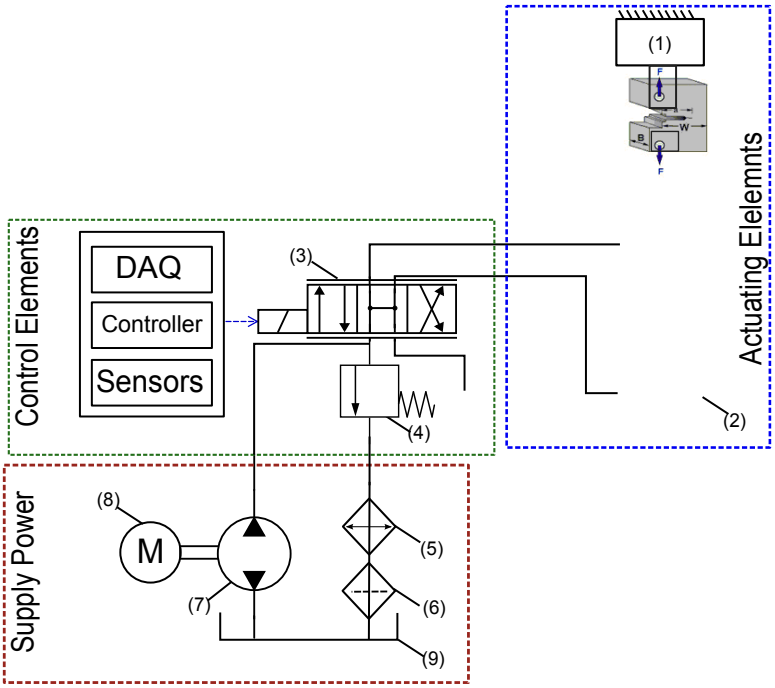

Figure 2.2: Basic hydraulic circuit for HTM with: (1) load cell (connected to specimen); (2) hydraulic single-rod cylinder; (3) 4/3 direction servo-valve; (4) pressure relief valve; (5) cooler; (6) filter; (7) pump (8) electric motor and (9) tank or reservoir.
Source: Adapted from (JELALI; KROLL, 2003).

fluid. The excess of contamination particles can damage the equipment and, in general, the hydraulic control element for this type of application (fatigue tests) is quite expensive.For instance, as described in (BOSCH REXROTH, 2005), the maximum admissible degree of contamination according to ISO 4406 is given by classes 18/16/14. Thus, a 3 [µm] filter inline should be installed. Sometimes oil condition are often overlooked, but in the long run will prevent costly downtime and the replacements of pumps, valves, cylinders and seals.

Finally, an important issue regarding hydraulic actuation system is the temperature. Fluids should be cooled down by dissipation of heat, due to the fact that it helps to prevent leaks, maintains lubrication properties and prevents chemical breakdown. Also, oil viscosity is highly dependent on its temperature (CUNHA, 2013), (JELALI; KROLL, 2003) and (MERRITT, 1967). The viscosity changes affect directly the performance of the closed loop control in hydraulic actuation. At the LNDC a cooler was installed in the hydraulic circuit and the cooler is activated when

temperature rises above 37 [°C]. This assures: (1) fluid integrity, (2) avoidance of components heating up and injuring people with burn and (3) regulation of the fluid temperature (*isothermal*) .

Fluid Compressibility

The compressibility of the fluid is the most important property to be taken in consideration. The degree of oil compressibility is expressed by the bulk modulus (CUNDIFF, 2001). The bulk modulus represents a measure of the fluid's resistance to compressibility. The bulk modulus[†] (β) can be defined as

$$\beta := -V_0 \left(\frac{\partial P}{\partial V} \right)_T , \tag{2.1}$$

or, equivalently,

$$\beta := \frac{-\Delta P}{(\Delta V / V_0)} ,$$

where

β is given in [Pa],

ΔP is the fluid pressure variation [Pa],

ΔV is the fluid volume variation when ΔP is applied [m^3],

V_0 is the original fluid volume [m^3].

The relationship described in Eq. (2.1) is the variation in pressure divided by the corresponding variation in volume at a constant temperature (JELALI; KROLL, 2003). It is called the modulus of elasticity, also known as isothermal bulk modulus of the fluid. A typical oil will decrease about 0.5% in volume for 6.894 [MPa] increase in pressure. For a typical mineral oil, the bulk modulus varies from 1.4 [GPa] to 1.6 [GPa] (CUNHA, 2013). However, the bulk modulus is difficult to estimated since it is susceptible to changes in the temperature, for example. Variations in the bulk modulus can result in actuation delays. An actuator may not move until fluid has

[†]For instance, assume that 172×10^5 [Pa] is applied to a 1.639×10^{-4} [m^3] volume of oil. Then if a variation of 1.639×10^{-5} [m^3] is measured, then the bulk modulus is given by $\beta = -(175 \times 10^5)/(1.4751 \times 10^{-4} - 1.639 \times 10^{-4})/(1.639 \times 10^{-4}) = 172 \times 10^7$ [Pa].

been compressed and the energy stored may cause the actuator to continue moving after its control valve has been closed. In this sense, when the compressibility is significant, it can be modeled as a capacitor in an electrical equivalent.

An empirical formulation for the *effective bulk modulus* β_e is proposed in the form (Eggerth's formula)(JELALI; KROLL, 2003, 35 pp.),

$$\beta_e = \frac{1}{\kappa_1 + \kappa_2 (P/P_0)^{-\lambda}}\,, \tag{2.2}$$

where

κ_1, κ_2 and λ are appropriate constants,

P_0 is atmospheric pressure ($1\,[\,\text{bar}\,]$),

P is the pressure applied to the fluid $[\,\text{Pa}\,]$.

The effect bulk modulus for HTM was estimated to be $\beta_e = 1200\,[\,\text{MPa}\,]$. In (SOHL; BOBROW, 1999) an experimental procedure is proposed to determine the bulk modulus.

2.2 Control element: valve

Valves are considered as essential control elements to achieve high tracking precision in force or position control. They are the hydraulic component responsible of controlling hydraulic power provided by the hydraulic power unit (HPU). Major hydraulic components manufactures offer valves that are proportional to the input signal. Usually, valves are classified as: spool valve position (directional valves), pressure valves or flow valves (JELALI; KROLL, 2003).

Note that, the valves are controlled by a low power signal which commands a high hydraulic power. This low power signal can be of mechanical, pneumatic, hydraulic or electrical nature. Modern valves are controlled by electrical signal: current or voltage (PEREIRA, 2006), (PEREIRA-DIAS *et al.*, 2014). In HTM, a spool valve (SV) is controlled usually by a current signal and the fluid flows into the actuators generating the necessary force to be applied over the specimen. Most of spool valves

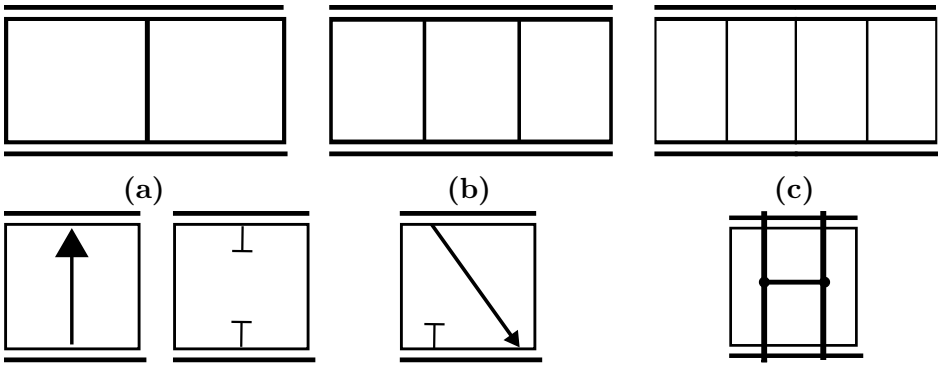

Figure 2.3: Classification of a spool valve: number of switching position (a) two positions, (b) three positions and (c) four positions; number of ports: (d) two ports, (e) three ports and (f) four ports.

are classified by (JELALI; KROLL, 2003) (See Figure 2.3 on page 33):

(1) number of ports through which the fluid can enter or leave;

(2) number of switch positions;

(3) the valve actuation method which causes the valve mechanism to move into an alternative position and

(4) the center type (open, closed, critical) corresponding to the valve spool in the neutral position: over-lapping (positive), zero-lapping (ideal) and under-lapping (negative) (RABIE, 2009).

These constructive characteristics define the valve curve response (PEREIRA, 2006). In fact, the type of the center defines the internal leakage of the valve, consequently the behavior of the actuation system. In Figures (2.4) and (2.5) it is characterized three types of center.

Closed center valves consists of a valve that the spool land overlaps the edge of the port. In this case, at the null position, the flow is completely blocked. These type of valves are not commonly used in critical HSSs because of the negative effect of the resulting dead-band. An experimental method is proposed in (VALDIERO, 2012) to compensate and identify the dead-band for a robotic application. Once the dead-band is determined, the control signal applied to the valve could be calculated

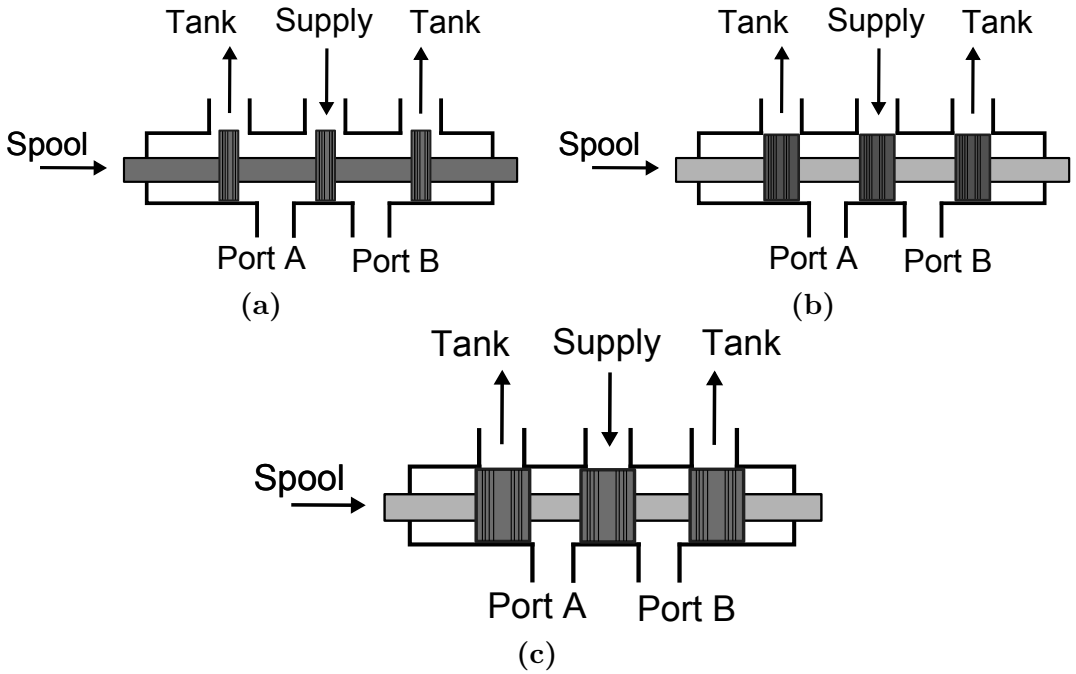

Figure 2.4: Classification of a spool valve according to the center type: (a) negative overlap (sub-critical), (b) zero-lapping (critical) , (c) positive overlap (super-critical).

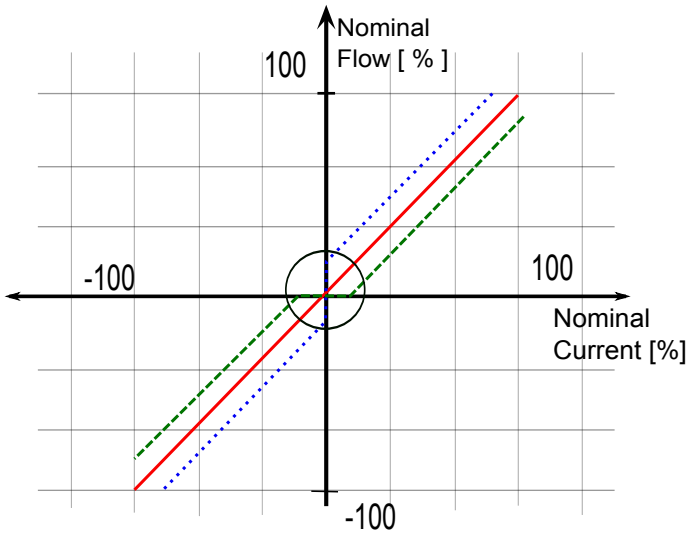

Figure 2.5: Flow characteristics depending on the spool valve center type (BOSCH REXROTH, 2005). In Fig. 2.4b the under-lapped spool land does not cover the whole port orifice and the flow characteristics is presented as a blue dotted line in (d). In Fig. 2.4a the spool land fit just right the edge of the ports red solid line and in Fig. 2.4c the spool is over-sized and a dead-band is present around the null spool position (green dashed line).

with compensation. However, the dead-band is in general unknown. In this sense, control strategies to compensate the unknown dead-band can be found in (CUNHA, 2005), (BESSA *et al.*, 2010b), (BESSA *et al.*, 2010a), (COELHO; CUNHA, 2011).

Critical center spool valves are the most popular configuration found to achieve high performance SV. These valves are suitable for position control in hydraulic servo systems because they deliver smooth control flow to the actuator. Additionally, they give higher pressure which increases actuation stiffness (RABIE, 2009).

Moreover, open center spool valves does not fully cover the corresponding control port in the null position. When the valve is at null position, the flow provided by the supply port is distributed across each control port to the return port. These valves may be used to achieve a suitable pressure gain and to achieve better stability and higher stiffness at null position. Under-lap can be helpful because the increased flow versus port pressure characteristic in the null region gives a natural damping effect.

For HTM the SVs available are of under-lap spool valves type.

2.2.1 Servo Valve

In general, HTM uses servo valves manufactured by *Bosch Rexroth Ltda* (BOSCH REXROTH, 2005) (See Figure 2.6 on page 36). These valves have four ports (A, B, P, T) and are driven by a pilot-stage. The port A and the port B are connected directly to the chambers A and B of the actuator, respectively. The port P connects the valve to the HPU and the port T connects the valve to the tank or reservoir.

The pressure at the valve ports A, B, P and T are denoted as P_A, P_B, P_s and P_T, respectively (Figures (2.6a) and (2.6c)). A hydraulic schematic for the valve is shown in Figure 2.6c.

These valves have many attributes that make them suitable for fatigue testing machines, such as: high bandwidth, low hysteresis, low response sensitivity and no pollution of the solenoid gaps by the hydraulic fluid. However, an effective fluid filtration system is required to prevent faults and to increase the hydraulic components life cycle (BOSCH REXROTH, 2005). A simple linear relationship

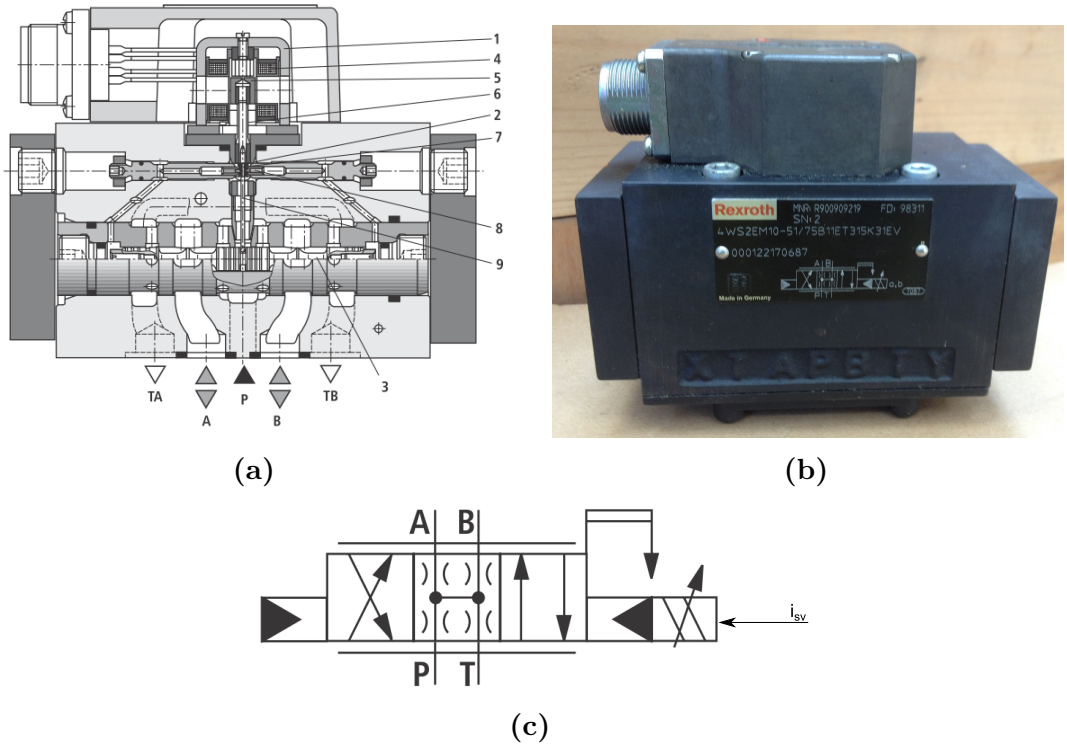

(a) **(b)**

(c)

Figure 2.6: Directional servo-valve in four-way design: (a) two-stage flapper-nozzle servo valve (SV) (BOSCH REXROTH, 2005) with [1] torque-motor; [2] hydraulic amplifier; [3] control spool; [4] solenoid; [5] armature; [6] flexible tube; [6] flapper plate and [8] control nozzles, (b) servo-valve used in HTM, (c) hydraulic block diagram of the directional servo-valve in 4-way design with mechanical return and without integrated electronics (ISO-1291-1, 2012). (*Courtesy of Bosch Rexroth AG*).

between the input voltage (u_c) and the current (i_{sv}) applied at the coils of the SV is considered:

$$i_{sv} = k_{vt}\, u_c\,, \tag{2.3}$$

where

k_{vt} is the amplifier analog gain $[\,\mathrm{A\,V^{-1}}\,]$.

2.2.2 Spool Valve Dynamics

The spool valves considered here have two stages of power amplification (JELALI; KROLL, 2003), so they are named "two stage spool valves". These valves consists of three main parts: the electrical torque motor, the hydraulic amplifier and the valve

spool assembly. In these SVs, the motor torque is commanded by an electrical current resulting in the flapper plate movement from its central position. The first stage is the so called flapper-nozzle system which allows the spool motion by adjusting the flapper via a low power electrical signal[‡]. The second stage relates the small spool motions ([µm]) into a large fluid flow through the spool ports.

The two control nozzles provoke a differential pressure across the front faces of the spool. Thus, the spool position changes and the valves ports open or close (CUNHA, 2013), (BOSCH REXROTH, 2005). At the same time, one port is connected to HPU and the other is connected to the return flow port. This valve has a mechanical return, which is a bending spring connected to the flapper plate. The position of the control spool is changed until feedback torque across the bending spring and the electromagnetic torque are balanced. Thus, the differential pressure at the flapper-nozzle becomes zero. The valve dynamics is illustrated in Figure 2.7 and is given by a second order linear system (CUNHA, 2001), in general.

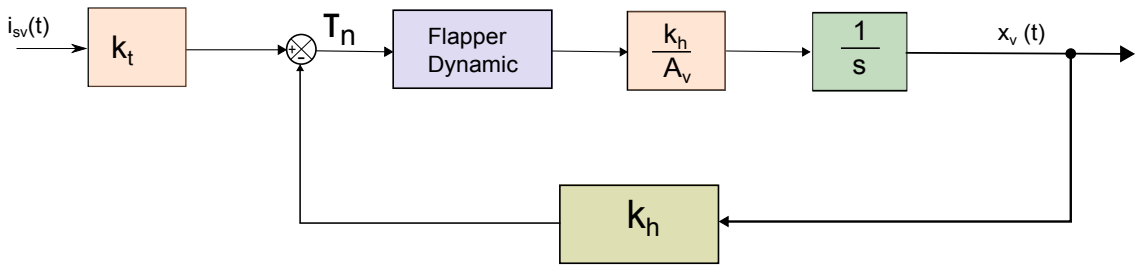

Figure 2.7: Spool Valve Dynamics: block diagram.
Source: adapted from (CUNHA, 2001).

The relationship between the electrical input signal (i_{sv}) and spool displacement (x_v) can be described as follows (CUNHA, 2001):

$$\tau_n = k_t i_{sv} - k_w x_v \,, \tag{2.4}$$

where

τ_n is the induced motor torque [N m],

k_t is the torque constant [N m A^{-1}],

[‡]The spool is the mobile part located in the valve housing (CUNHA, 2013).

k_w is the spring coefficient [N].

The flapper position dynamics is given by the following second order linear ODE

$$\ddot{x}_n + 2\xi_n\omega_n\dot{x}_n + \omega_n^2 x_n = \left(\frac{\omega_n^2}{k_n}\right)\tau_n\,, \tag{2.5}$$

where

x_n is the flapper plate position [m],

ξ_n and ω_n are the damping coefficient and natural frequency, respectively.

Finally, relationship between the flapper position (x_n) and the spool velocity ($\dot{x}_v$) is described by

$$k_h x_n = A_v \dot{x}_v \tag{2.6}$$

where

k_h is the gain of the hydraulic amplifier [$\mathrm{m\,s^{-1}}$],

A_v is the area of the spool extremity [$\mathrm{m^2}$].

Now, from (2.3), (2.5) and (2.6), the flapper-nozzle system of the spool-valve can be described by the third order transfer function (CUNHA, 2001):

$$G_n(s) = \frac{X_v(\mathrm{s})}{I_{sv}(\mathrm{s})} = \frac{\left(\dfrac{k_h\omega_n^2}{A_v k_n}\right)k_t}{\mathrm{s}^3 + 2\xi_n\omega_n\mathrm{s}^2 + \omega_n^2\mathrm{s} + (k_w k_h\omega_n^2/A_v k_n)}\,. \tag{2.7}$$

However, there are some nonlinearities associated with these type of valve that must be taken into account, e.g., the saturation of flapper position and friction (Coulomb) forces on the valve spool.

The third order system Eq. (2.7) could have its parameters identified by the frequency response given in Figure 2.8a.

First Order Approximation

From Figure 2.8b, it is apparent that the transfer function Eq. (2.7) can be approximated by a first order transfer function. Indeed, this approximation was considered by many authors (CUNHA, 2001), (VALDIERO, 2012), (FILHO, 2009).

In fact, the dominant spool valve dynamics can represented by the following first order system:

$$\dot{x}_v = \frac{-1}{\tau_v} x_v + \frac{k_{em}}{\tau_v} i_{sv} \tag{2.8}$$

where

τ_v is the valve time constant and k_{em} is an appropriate constant which relates the input for HTM' SV to the position of the spool in the steady-state.

Static Approximation

Additionally, there is a lack of mechanical details about the internal parts of the valve (CUNHA, 2013). This issue can be overcame by neglecting the valve time constant and the following static relationship between the spool position (x_v) the valve current input (i_{sv}) holds

$$x_v = (1/k_s)\ i_{sv}\,, \tag{2.9}$$

where

k_s is the gain of the spool, $[\,\mathrm{A\,m^{-1}}\,]$.

In this case, from Eq. (2.9) and Eq. (2.3), the spool displacement x_v satisfies

$$x_v = k_v u_c\,, \tag{2.10}$$

where

k_v is the combined assembly servo-valve and electronic analog amplifier gain $[\,\mathrm{m\,V^{-1}}\,]$.

Without lost of generality, it is assumed that $k_v = 1$, i.e., the spool position is given by $x_v = u_v$.

2.2.3 Flow Equations

The fluid flow magnitude Q through an orifice is a function of the differential pressure ΔP (assumed positive) across the orifice and can be written as

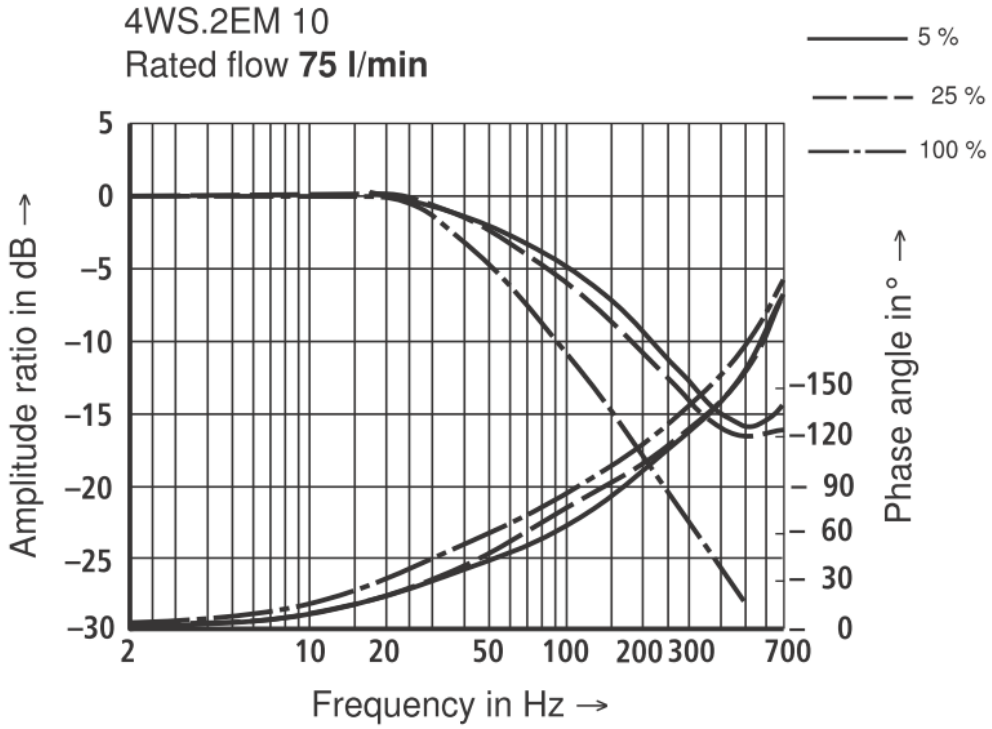

(a)

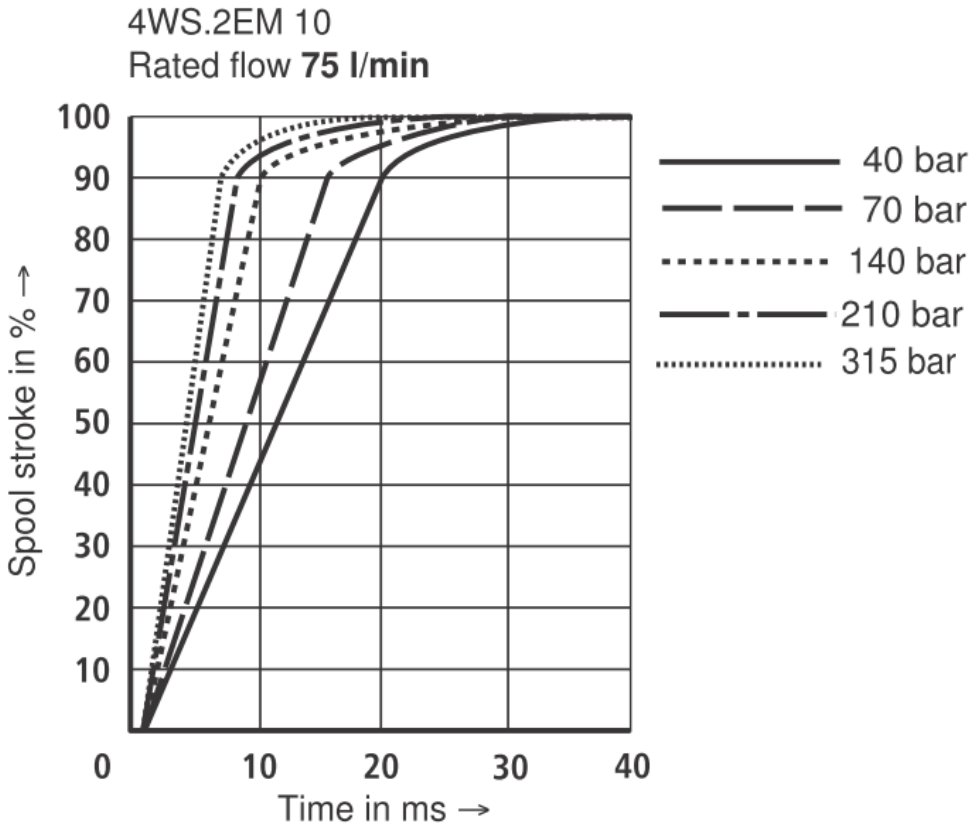

(b)

Figure 2.8: SV frequency and time responses: (a) frequency response (pressure rating 315 bar) without flow and (b) time response without flow. *Source*: Extracted from (BOSCH REXROTH, 2005). (*Courtesy of Bosch Rexroth AG*).

$$Q = c_d a(u_v)\sqrt{\frac{2\Delta P}{\rho}} \tag{2.11}$$

where,

c_d is the discharge coefficient, $\approx (\ 0.6,\ \ 0.8\ )$ (MERRITT, 1967),

ρ is the fluid density,

$a(u_v)$ is the orifice adjustable area,

u_v is the spool position.

As previously discussed, the valve position controls the magnitude and direction of the flow. By considering that the relationship between the spool position and the adjustable area is linear

$$a(u_v) = w u_v \tag{2.12}$$

with

w being the area gradient $[\,\mathrm{m}^2\,\mathrm{V}^{-1}\,]$,

the flow magnitude can be rewritten as

$$\begin{aligned} Q &= c_d w u_v \sqrt{\frac{2\Delta P}{\rho}} \\ &= c_d w u_v \sqrt{\frac{2}{\rho}}\sqrt{\Delta P} \\ &= k_{sv} u_v \sqrt{\Delta P} \end{aligned} \tag{2.13}$$

where

$k_{sv} := c_d w \sqrt{\frac{2}{\rho}}$ is defined as the spool valve gain.

In order to consider the flow direction in Eq. (2.13), the sign of u_v and the sign of the differential pressure ΔP must be taken into account. In fact, the flow equation

that describes flow through valve orifices Q can be expressed as

$$Q = Q(u_v, \Delta P) = k_{sv} u_v \sqrt{|\Delta P|}\, \mathrm{sgn}\,(\Delta P)\,. \tag{2.14}$$

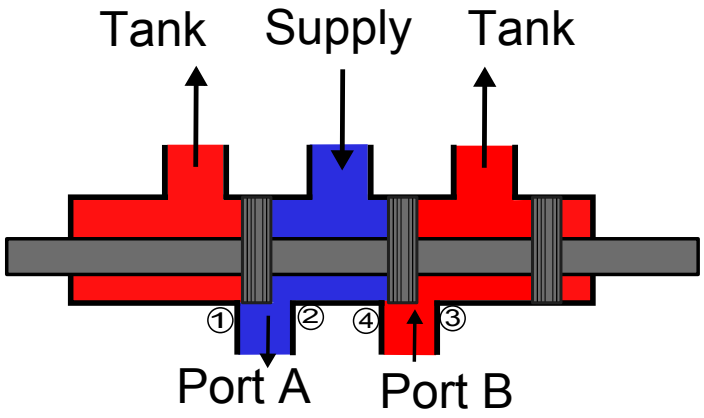

Figure 2.9: Sub-critical four ports/three switching position spool valve.
Source: adapted from (JELALI; KROLL, 2003).

In particular, for a four-way spool valve with a sub-critical center as shown in Figures 2.4a and 2.9, the flows through ports A and B are given by

$$\begin{aligned} Q_A = {} & k_{v1}\ \mathrm{sg}\,(x_{u1} + x_v)\ \mathrm{sgn}\,(P_S - P_A)\sqrt{|P_S - P_A|} \\ & - k_{v2}\ \mathrm{sg}\,(x_{u2} - x_v)\ \mathrm{sgn}\,(P_A - P_T)\sqrt{|P_A - P_T|} \end{aligned} \tag{2.15}$$

$$\begin{aligned} Q_B = {} & k_{v3}\ \mathrm{sg}\,(x_{u3} - x_v)\ \mathrm{sgn}\,(P_S - P_B)\sqrt{|P_S - P_B|} \\ & - k_{v4}\ \mathrm{sg}\,(x_{u4} + x_v)\ \mathrm{sgn}\,(P_B - P_T)\sqrt{|P_B - P_T|} \end{aligned} \tag{2.16}$$

where

k_{vi} $(i = 1, \ldots, 4)$ are the discharge coefficients of the valve orifices (also known as valve constants).

x_{uj} $(j = 1, \ldots, 4)$ are underlaps of the valve orifices, which are assumed equal if all orifices have identical geometry.

The `sg` can be defined as

$$\mathrm{sg}\,(u) = \begin{cases} u & \text{para} \quad u \geq 0 \\ 0 & \text{para} \quad u < 0 \end{cases}\,. \tag{2.17}$$

2.3 Hydraulic actuator

The hydraulic actuator (the cylinder) converts hydraulic power into mechanical power, which can be implemented via a hydraulic motor, hydraulic rotary actuators (RABIE, 2009) or cylinders. In this work, a hydraulic cylinder performs linear motion applying an axial force to the specimen. The hydraulic cylinder consists mainly of two parts: a hollow cylindrical body and a piston. The piston is attached to the load. For HTM the load is the specimen to be tested. There are essentially two kind of linear cylinders: cylinders with rods at both end (so called, symmetric or double-rod cylinders) and cylinder with only one rod (named asymmetric or single-rod cylinders) as shown in Figure 2.10 (CUNHA, 2013). A typical hydraulic single-rod cylinders has a larger extending force than retracting force because of the area difference between full bore and annulus sides of the piston.

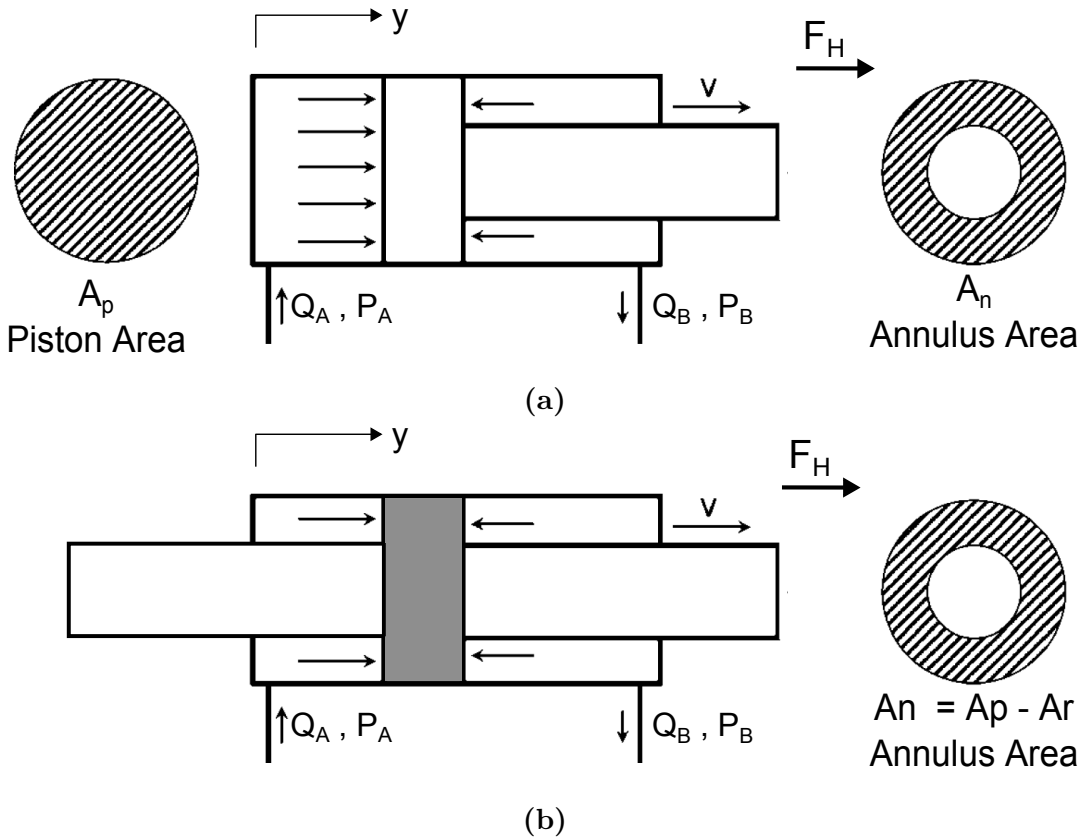

Figure 2.10: Functional scheme of a hydraulic cylinder: (a) asymmetrical cylinder (b) symmetrical cylinder
Source: adapted from (RABIE, 2009).

The HTM uses a double-rod cylinder to move the specimen. In these type of

cylinders the effective chamber areas are equal and it can be written as,

$$\begin{aligned} A_n &= A_p - A_r \\ &= \left(\frac{\pi\phi_p^2}{4}\right) - \left(\frac{\pi\phi_r^2}{4}\right) \\ &= \frac{\pi}{4}\left(\phi_p^2 - \phi_r^2\right) \end{aligned} \tag{2.18}$$

where,

ϕ_p is the piston diameter [m],

ϕ_r is the piston rod diameter [m].

The hydraulic force (F_H) can be described by the following relationships, in absence of friction and leakage:

$$F_H = P_A A_p - P_B A_n \,, \tag{2.19}$$

where

A_p is the piston area [m^2],

A_n is the annulus area, i.e., the effective area of the rod side of the cylinder [m^2],

P_A is the pressure applied at the piston side [Pa],

P_B is the pressure applied at the rod side [Pa].

The HTM valves are assembled on a manifold located directly on the cylinder body and the valve ports A and B are connected to cylinder ports. Placing SV as close as possible reduces the compliance of the system and the non-linearities brought by the flexible houses, depicted in Figure 2.11.

Neglecting internal and external leakages, the chamber pressure dynamics is a well-know expression proposed by (MERRITT, 1967) and can be obtained by applying the conversation principle to each individual chamber, as follows

$$\dot{P}_a = \frac{\beta_e}{V_A}\left[Q_A - A_p\frac{\mathrm{d}y}{\mathrm{d}t}\right] \,, \tag{2.20a}$$

$$\dot{P}_b = \frac{\beta_e}{V_B}\left[-Q_B + A_n\frac{\mathrm{d}y}{\mathrm{d}t}\right] \,. \tag{2.20b}$$

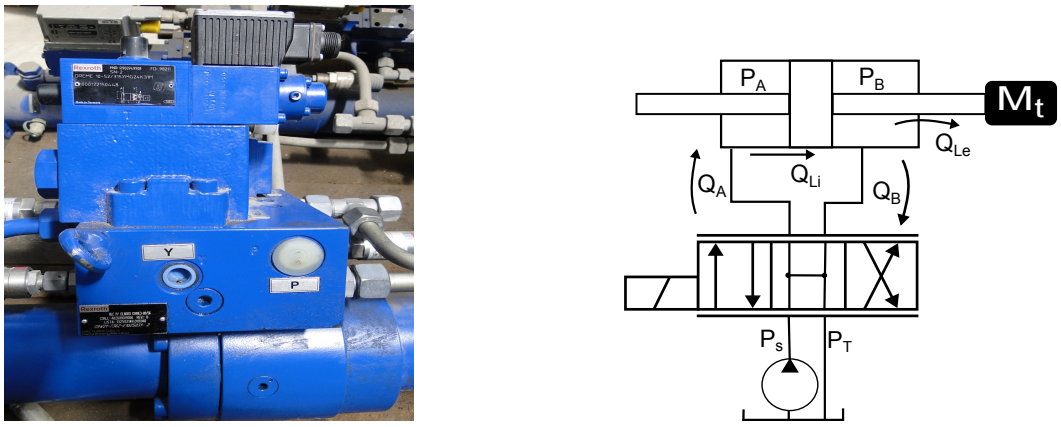

(a) (b)

Figure 2.11: Schematics of the valve-cylinder. *Source*: adapted from (JELALI; KROLL, 2003).

where

V_A is the chamber A volume $[\,\mathrm{m}^3\,]$,

V_B is the chamber B volume $[\,\mathrm{m}^3\,]$.

The chamber volumes can vary according to piston position y and the volume inside of each chamber can be modeled as,

$$V_A = V_{A0} + A_n y\,, \tag{2.21}$$

and

$$V_B = V_{B0} + A_n(L - y)\,, \tag{2.22}$$

where

V_{A0} is the initial volume inside of chamber A plus pipeline volume $[\,\mathrm{m}^3\,]$,

V_{B0} is the initial volume inside of chamber B plus pipeline volume $[\,\mathrm{m}^3\,]$,

L is the cylinder stroke $[\,\mathrm{m}\,]$.

2.3.1 Hydraulic force: symmetrical cylinder

For symmetrical cylinders, the hydraulic force F_H can be written as

$$F_H = A_n P_A - A_n P_B = A_n(P_A - P_B)\,, \tag{2.23}$$

where

A_n is piston area ,

P_A is the fluid pressure in the cylinder chamber A [Pa] ,

P_B is the fluid pressure in the cylinder chamber B [Pa] ,

A_n is the annular surface area of the piston [m^2] .

In terms of the *load pressure* $P_L := (P_A - P_B)$, the hydraulic force Eq. (2.23) can be rewritten as

$$F_H = A_n P_L \, . \tag{2.24}$$

From Eq. (2.20a), Eq. (2.20b) and Eq. (2.23), the time derivative of the hydraulic force satisfies

$$\dot{F}_H = A_n \left(\dot{P}_L \right) = A_n \beta_e \left(\frac{1}{V_A} \left(Q_A - A_n \dot{y} \right) - \frac{1}{V_B} \left(-Q_B + A_n \dot{y} \right) \right) \, . \tag{2.25}$$

2.3.2 Friction force

The hydraulic cylinders must be sealed in order to avoid internal leakage. Therefore, friction forces are relevant in hydraulic actuation systems (CANUDAS-DE-WIT; GE, 1997), (VALDIERO, 2012). Some effects due to friction are: stick-slip, hunting, standstill and quadrature glitch (VALDIERO, 2012). In this work, a standard friction model is used to describe this effect over HTM: the Stribeck friction model. The friction force model proposed by Stribeck is a static function of velocity and can be written as

$$F_f = B_v \dot{y} + \operatorname{sgn}(\dot{y}) \left(F_{co} + F_s e^{-|\dot{y}|/C_s} \right) \tag{2.26}$$

where

B_v is the viscous friction coefficient [$N\,s\,m^{-1}$] ,

F_{co} is the Coulomb friction coefficient [N] ,

F_s is the static friction coefficient [N] ,

C_s is known as the Stribeck velocity [$m\,s^{-1}$]

Figure 2.12 illustrates these three main characteristics: static friction F_s, viscous friction F_f and Coulomb friction F_{co}.

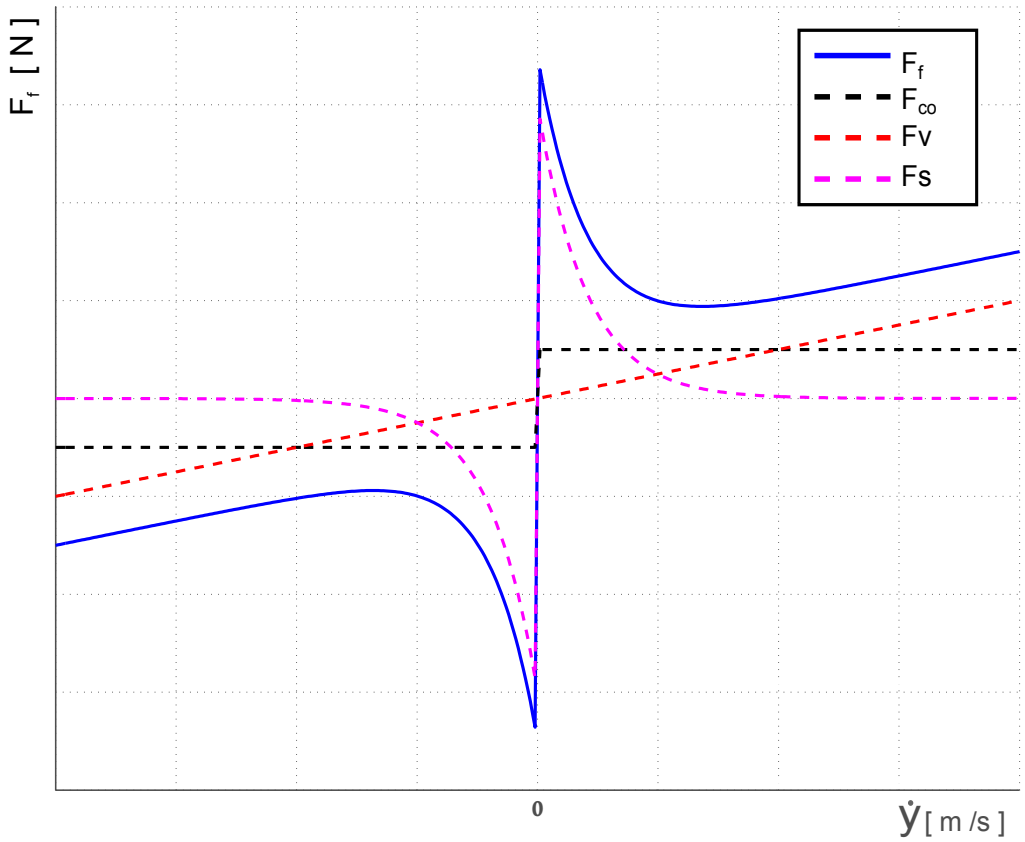

Figure 2.12: Stribeck Friction Force Curve: velocity dependent friction force. The magenta dashed line describes the behavior of static friction which decays faster w.r.t. $|\dot{y}|$ by reducing the so called Stribeck velocity. The red dashed line represents the behavior of viscous friction dissipation term while the Coulomb friction behavior is represented by the black dashed line. The combined behavior, i.e., the total friction force F_f is represented by the blue solid line.
Source: adapted from (PEREIRA-DIAS *et al.*, 2014), (PEREIRA-DIAS *et al.*, 2013).

2.3.3 Piston motion equation

It is well known that, from the Newton's Second Law applied to the piston, the piston position dynamics is described by

$$F_H - F_g - F_f = M_t \ddot{y}\,, \tag{2.27}$$

where

M_t is the total mass, i.e., the piston mass M_t plus the hydraulic fluid mass (M_f) in the cylinder chambers [kg],

F_H is the hydraulic force [N],

F_g is the gravitational force [N],

F_f is the total friction force [N].

The forces acting on the piston are depicted in Figure 2.13.

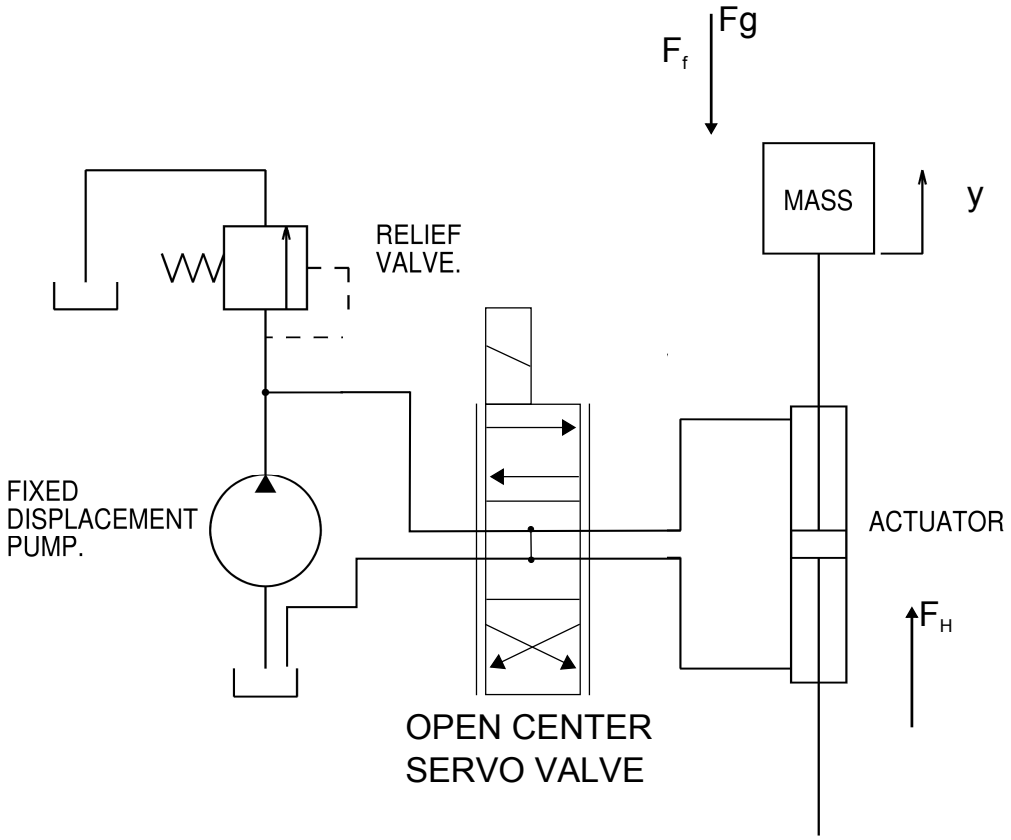

Figure 2.13: Servovalve actuation system and forces acting on the piston. *Source*: adapted from (AKERS *et al.*, 2006).

2.4 HTM mathematical model

From Eq. (2.2), Eq. (2.10),Eq. (2.20a), Eq. (2.20b),Eq. (2.26) and Eq. (2.27), defining the state vector $\mathbf{x} = \begin{bmatrix} P_A & P_B & y & \dot{y} \end{bmatrix}^{\mathsf{T}}$, and neglecting (internal and external) leakages and the spool valve dynamics, the HTM can be described by the following fourth-order nonlinear system: where Δx_1 e Δx_2 are defined as:

$$\begin{cases} \dot{x}_1 = \dfrac{\beta_e}{V_{A0} + A_n x_3} \left(K_{va} u_c \sqrt{\Delta x_1} - A_n x_4 \right) & \text{(2.28a)} \\ \dot{x}_2 = \dfrac{\beta_e}{V_{B0} + A_n (L - x_3)} \left(K_{vb} u_c \sqrt{\Delta x_2} + A_n x_4 \right) & \text{(2.28b)} \\ \dot{x}_3 = x_4 & \text{(2.28c)} \\ \dot{x}_4 = \dfrac{1}{M_t} \left(A_p (x_1 - \alpha x_2) - B_v x_4 - F_s - F_{co} - F_g \right) . & \text{(2.28d)} \end{cases}$$

$$\sqrt{\Delta x_1} = \begin{cases} \sqrt{P_s - x_1} & , u_c < 0 \\ \sqrt{x_1 - P_T} & , u_c > 0 \end{cases} \tag{2.29}$$

and

$$\sqrt{\Delta x_2} = \begin{cases} \sqrt{x_2 - P_T} & , u_c < 0 \\ \sqrt{P_s - x_2} & , u_c > 0 \end{cases} , \tag{2.30}$$

respectively. As mentioned before, a precise model of the servo-valve is difficult to obtain since many non-linear dynamic effects are apparent, such as: dead-band, saturation, hysteresis, and so on (PEREIRA-DIAS *et al.*, 2013). When the control objective is to increase flow rate and response speed to obtain large deflection at higher frequencies, pipeline dynamics should also be taken into account (Fig. 2.14) (MORGAN; MILLIGAN, 1997). It should be mentioned that disturbances may appear in different parts of the HTM system and the load (the specimen) is unknown and time varying (WANG, 2012).

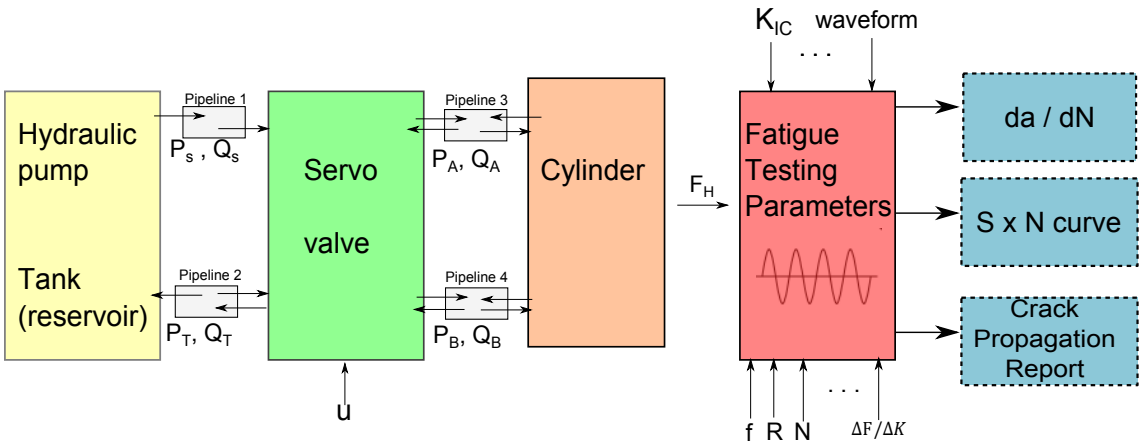

Figure 2.14: Hydraulic actuation system for HTM presented in subsystem schema.
Source: adapted from (PEREIRA-DIAS *et al.*, 2013).

2.5 Summary

This chapter has described the model of the hydraulic actuation system for HTM. This model has provided the basic understanding behavior for each component and what should be excepted for test-bench development, identification procedure, simulation and control design.

Chapter 3

Identification and experimental results

This chapter addresses some aspects of the parameter identification process for the HTM, where the main advantages of applying a gray-box identification procedure is discussed.

In Chapter 2, a HTM dynamic model was described which includes the most relevant phenomena (hydraulic and mechanical) and corresponding parameters. The nominal values of some of these parameters can be obtained from data-sheets provided by the manufacturers. For others, however, a good estimation may be difficult to obtain since usually they depend on details regarding the internal parts of the hydraulic components which are not available (CUNHA, 2013). Therefore, experimental identification is required (RODERMOND, 2006).

3.1 Experimental setup for the HTM

Figure 3.1 depicts the overall control system architecture for the HTM. The communication between the real-time (RT) controller and the user interface is implemented via Ethernet protocol. The RT controller is responsible to handle the control tasks. Moreover, this controller confers a reliable embedded solution for stand-alone applications.

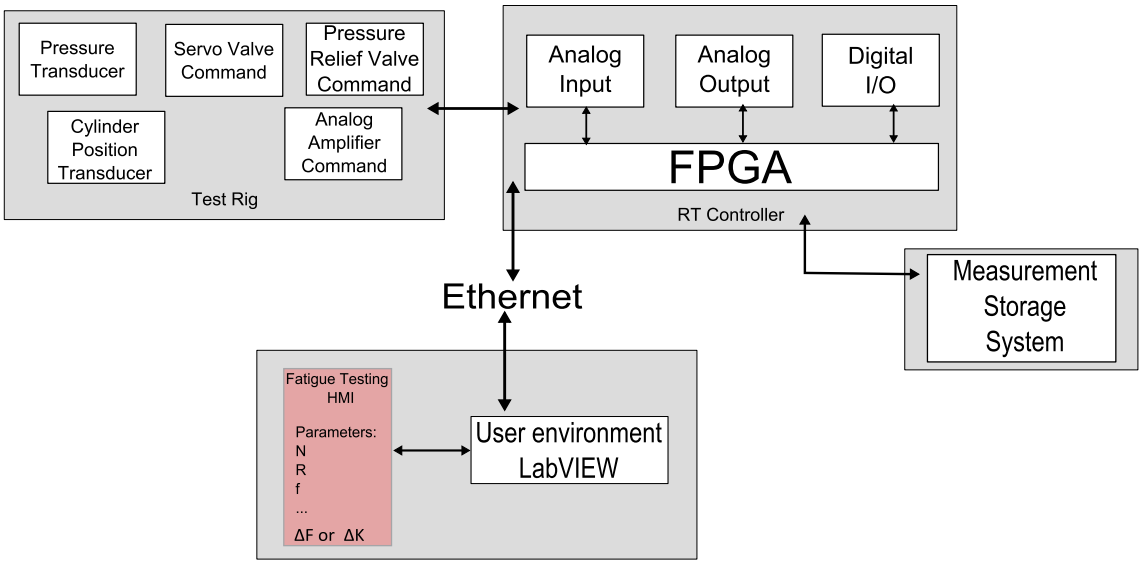

Figure 3.1: Basic control system architecture for the hydraulic actuated fatigue testing machine (HTM). The RT controller handles the Input-output (I/O) modules.

All the hardware specifications are listed in Table 3.1.

Table 3.1: Hardware Specification

MODULE	DESCRIPTION
Hydraulic	
Hydraulic Cylinder	Symmetric cylinder, Bosch Rexroth – Model: CGH2MF3/80/56/200
Servo-Valve	Bosch Rexroth – Model: 4W2S2M10-51/75B11ET315K31EV
Pressure Relief Valve	Bosch Rexroth – Model: DRE(M)E 10
Measurements	
Pressure Transducer	Bosch Rexroth – Model: HEDE 10A1-2x/400K41G24/1/V
Load Cell	HBM U10M
Cylinder Position Transducer	BALLUFF MICROPULSE : BTL5-H110-M0200-B-S94

The analog input module (**NI 9215**) is connected to the electronic pressure transducers and the uncertainty in the corresponding voltage can be calculated from the transducer datasheet. Three of four channels are used to acquire the pressures

Table 3.2: Technical Details of NI Modular I/Os

MODULE	DESCRIPTION
CompactRIO 9104	is a RT embedded industrial controller that consists of a real-time controller, reconfigurable I/O modules (RIO) and field-programmable gate array (FPGA) module. It has eight slots with three mega gates.
NI 9215	Analog Input Module with 4-channels and a range from $\pm 10\,[\,\mathrm{V}\,]$. It has a 16-Bit resolution at 100 $[\,\mathrm{kS/s}\,]$.
NI 9263	Analog Output Module with 4-channels and a range from $\pm 10\,[\,\mathrm{V}\,]$. It has a 16-Bit resolution at 100 $[\,\mathrm{kS/s}\,]$.
NI 9481	Electromechanical Relay Module with 4-channels.
NI 9853	High-Speed CAN Module with 2-channels and ability to transmit/receive 100 percent bus load at 1 $[\,\mathrm{Mbit/s}\,]$.

inside chambers A and B and the pressure available in the HPU. The analog output module (**NI 9263**) generates two (voltage) signals: one to set the supply pressure and other to drive the SV. First, supply pressure is controlled by the relief pressure proportional valve and a proportional voltage signal defines the available pressure P_s. Then, the second channel of the module (**NI 9263**) commands the directional SV.

This SV does not work alone, the input voltage is connected to an analog electronic amplifier. This amplifier converts the input voltage into a current signal. However, this operation is allowed only if the analog electronic amplifier is enabled by a $24\,[\,\mathrm{V}\,]$ signal. This enable signal is generate by the module (**NI 9481**).

Finally, the displacement transducer requires a CANOpen interface which is connected to the module (**NI 9853**). It should be highlighted that the displacement transducer has two types of data frames: one for position and other for velocity.

As seen in Figure 3.2, the initial interface for hardware testing was developed. It has all the functionality required to command each individual component. All the acquired data can be stored. Moreover, shown in Figure 3.3, the identification software front panel is depicted. This software was developed to facilitate the identification procedure. Four tests were designed to be tested: (1) open-loop response test to a constant voltage input, (2) open-loop response test applying sine

and square waves voltage input, (3) closed-loop response (regulation) and (4) closed loop response (tracking problem).

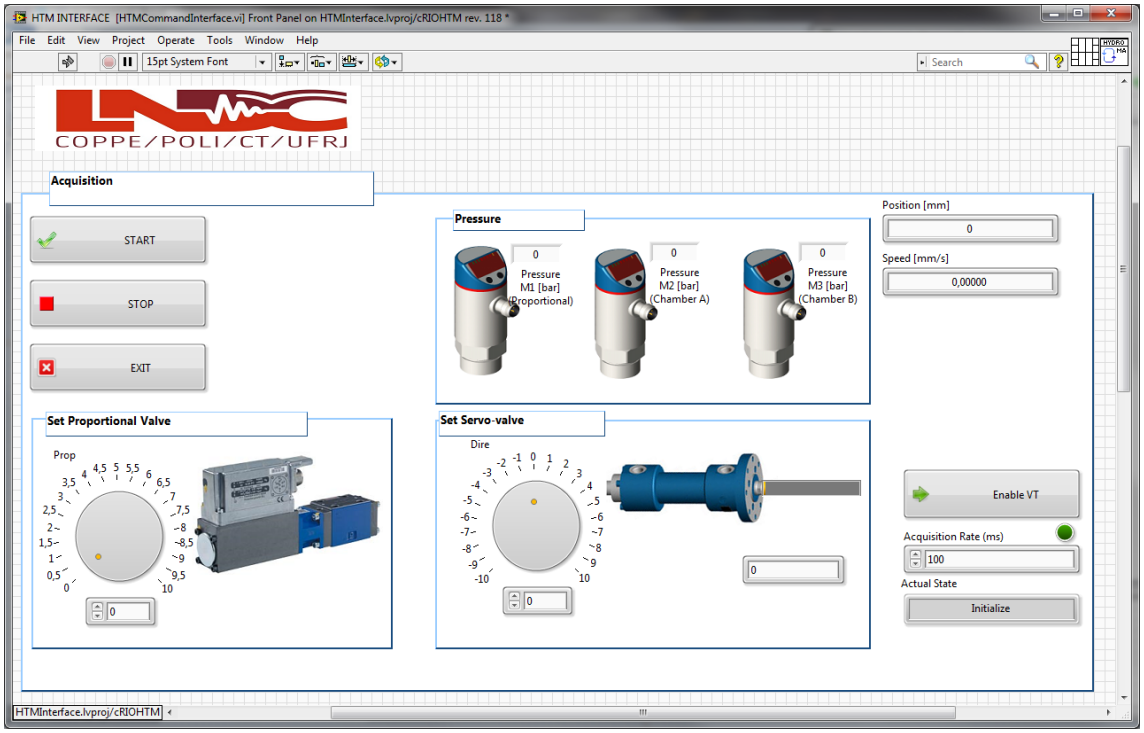

Figure 3.2: User interface for initial hydraulic actuation system

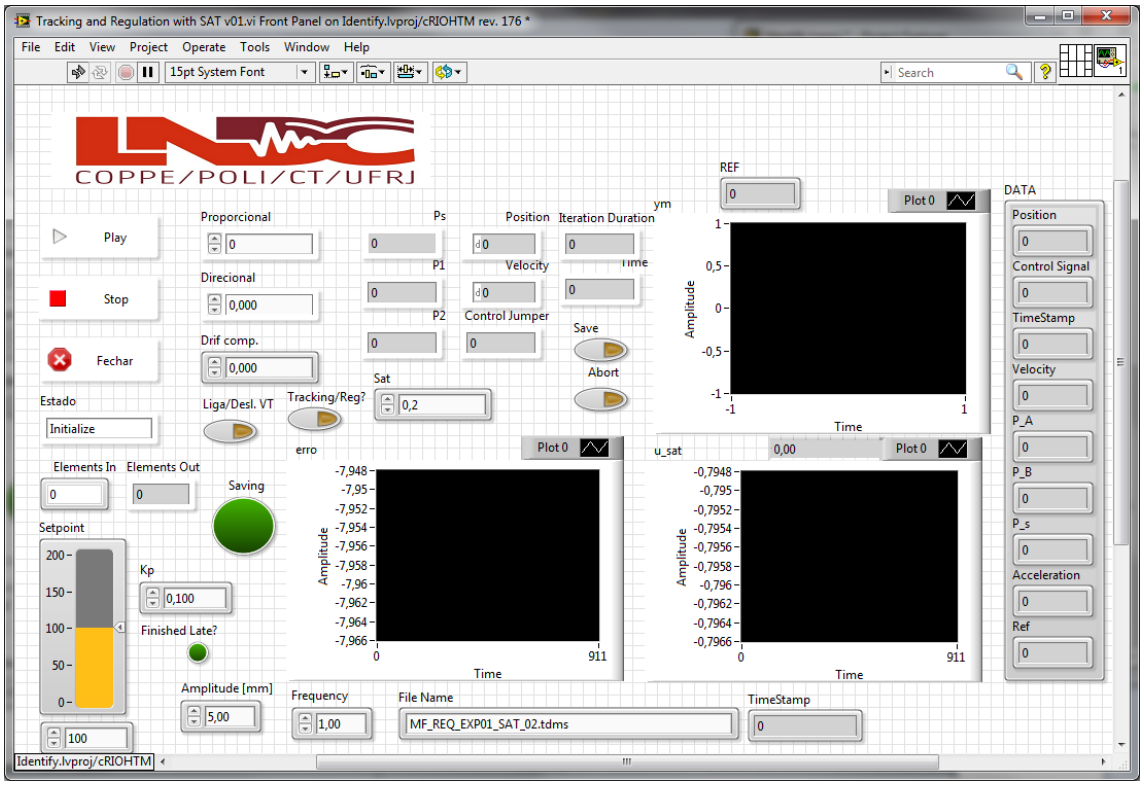

Figure 3.3: Re-design of user interface for identification and control of HTM

3.2 Identification procedure

The main subsystems of a HTM are represented in Figure 3.4, including the relevant physical variables which are used to estimate the unknown hydraulic parameters. The whole system can be considered as a single-input single-output (SISO) nonlinear plant where u_c (voltage related to the valve opening) is the control input and y (piston displacement) or F (force applied to the specimen) is the plant output, both assumed available for feedback. The force applied to the specimen F is only available after the specimen was properly fixed in the grips and connect to a load cell.

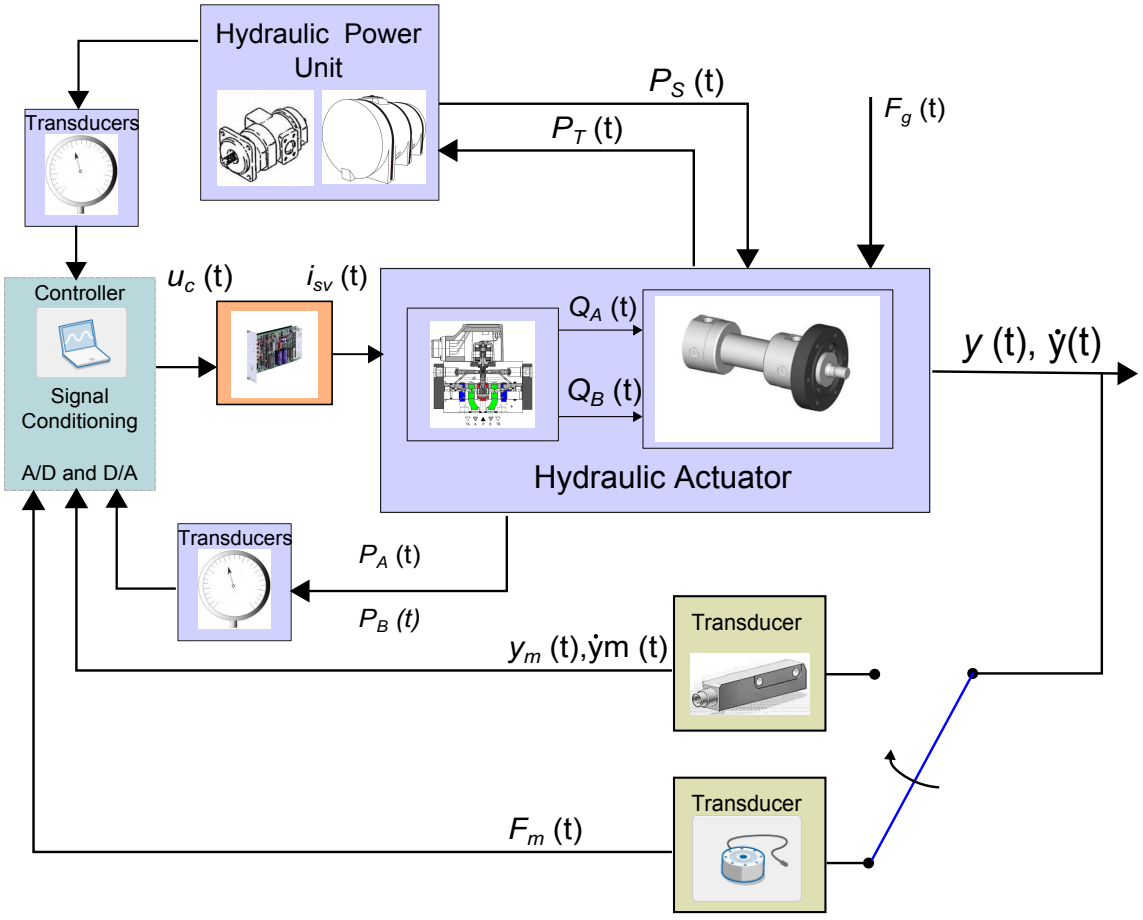

Figure 3.4: Block diagram of the hydraulic actuated fatigue testing machine. The piston position and velocity are represented by $y(t)$ and $\dot{y}(t)$, respectively. The hydraulic force F_H is a function of the chambers pressures P_A and P_B. The external forces is expressed by gravitational force F_g. The total friction force F_f is considered an internal disturbance.

In this work, the identification procedure is based on the following general recommendation (AGUIRRE, 2007), (JELALI; KROLL, 2003):

(1) Planning the experiments in order to select the relevant signals and record the data set for identification;

(2) Selection of an appropriate mathematical model based on a prior knowledgement of the system;

(3) Performing the experiments and data acquisition;

(4) Selection of a mathematical tool for identification;

(5) Validation of the identified model.

As seen in Figure 3.4, position and force must be available for fatigue testing. However, the force transducer was not installed. Therefore, only position and velocity of the piston were used as feedback information for identification procedures.

3.3 Mechanical system model

Since the cylinder presents a symmetric geometry, the hydraulic force induced in the cylinder is proportional to the pressure difference P_L and is given by

$$F_H = A_n \, P_L = A_n (P_A - P_B) \,, \tag{3.1}$$

where,

A_n is the annular area $[\,\mathrm{m}^2\,]$,

P_A is the pressure in the cylinder chamber A $[\,\mathrm{Pa}\,]$, and

P_B is the pressure in the cylinder chamber B $[\,\mathrm{Pa}\,]$.

The cylinders are designed to work with fluids under high pressures. Hence, the piston must be properly sealed in order to avoid internal leakage between chambers. Seals are also needed to prevent external leakage. Therefore, friction is a phenomenon naturally presented in hydraulic actuation systems which interferes in control performance. (RODERMOND, 2006).

The friction forces work as a natural damping effect and introduce a non-linearity into the system (CUNHA, 2013). On the other hand, the fluid power waste is proportional to friction force in hydraulic actuators, *i.e.*, the greater the friction, the

smaller the power transformed in work.

In hydraulic control literature, friction force is usually modeled as a combination of three main components, described as (JELALI; KROLL, 2003):

- Viscous friction force (F_v): it is the linear part of the total friction force being proportional to the piston velocity magnitude.
- Coulomb friction force (F_{co}): it acts as a constant opposing force during the piston motion and may lead to stick-slip phenomena at low speeds (JELALI; KROLL, 2003).
- Static friction force (F_s): this term acts mainly at low speed and decays exponentially to zero as the piston velocity increases. At higher piston velocity, the static force term can be neglected in the total friction force.

The total friction force F_f is a function of the piston velocity $\dot{y}$ and is given by

$$\begin{aligned} F_f(\dot{y}) &= F_v(\dot{y}) + F_{co}(\dot{y}) + F_s(\dot{y}) \\ &= B_v\dot{y} + \operatorname{sign}(\dot{y})\left(B_{co} + B_s \exp\left(-|\dot{y}|/C_s\right)\right), \end{aligned} \tag{3.2}$$

where

B_v is the viscous friction coefficient $[\,\mathrm{N\,s\,m^{-1}}\,]$,

B_{co} is the Coulomb friction coefficient $[\,\mathrm{N}\,]$,

B_s is the static friction coefficient $[\,\mathrm{N}\,]$, and

C_s is known as Stribeck velocity $[\,\mathrm{m\,s^{-1}}\,]$.

In hydraulic control literature (JELALI; KROLL, 2003), (ARMSTRONG-HÉLOUVRY *et al.*, 1994), the friction force F_f is characterized by the well-known curve named "Stribeck Friction Force Curve*"shown in Figure 3.5. Here onwards, the Stribeck friction force model is assumed and the parameters B_v, B_{co}, B_s and C_s are to be identified from experimental data. From Newton's second law, it is well known that

$$F_H - F_f - F_{ext} = M_t\,\ddot{y}\,,$$

*In a more general case, the friction force does not depend only on the piston velocity $\dot{y}$ but also on the pressure difference P_L across the piston. Moreover, the friction force can also be affected by the piston position y and the fluid temperature.

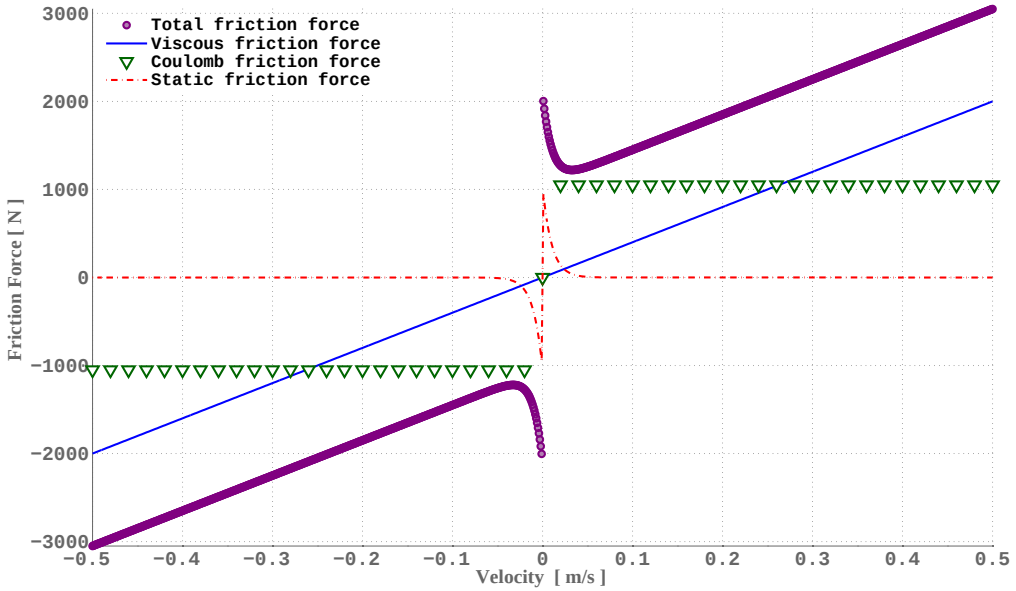

Figure 3.5: Stribeck Friction Force Curve: velocity dependent friction force.

where F_{ext} is the external force (N) and M_t is the total equivalent mass (kg) corresponding to the piston, hydraulic fluid in the chambers and in the pipelines. Hence, one can write:

$$M_t\,\ddot{y} + F_f = F_H - F_{ext} = (F_A - F_B) - F_{ext}\,, \tag{3.3}$$

where,

$F_A = P_A A_n$ is the force applied on the piston surface inside chamber A [N] and

$F_B = P_B A_n$ is the force applied on the piston surface inside chamber B [N].

By considering that the external force is due only to the gravitational force F_g, *i.e.*, no load is attached to the actuator, the hydraulic force is expressed as

$$F_H = M_t\,\ddot{y} + F_f + F_g\,. \tag{3.4}$$

The friction force can be estimated, as mentioned before, when the piston is moving at a constant velocity ($\ddot{y}(t) = 0$). In this case, the friction force is denoted by F_f^* and the following relationship holds

$$F_f = F_H - F_g = F_f^*\,, \tag{3.5}$$

$$F_f^* = A_n\,(P_A - P_B) - M_t\,g\,.$$

The piston mass M_p can be obtained from the manufacturer and the hydraulic fluid mass (M_f) in the chambers can be calculated (which can be neglected if compared to the piston mass). Thus, the total mass M_t is known. Now, the hydraulic force F_H can be estimated since the pressures in the chambers P_A and P_B are measured and the effective area A_n can be obtained from the piston manufacturer. Hence, the friction force F_f^* can be estimated from Eq. (3.5).

Several experiments were conducted and the pressure data at constant piston velocity ($\ddot{y} = 0$) were collected and the friction force F_f^* were estimated, resulting in the Stribeck Friction Force Curve depicted in Figure 3.6. By including the values at low piston acceleration ($\ddot{y} \approx 0$), the Stribeck Friction Force Curve is modified as in Figure 3.7. The constant velocity for each individual experiment is also summarized

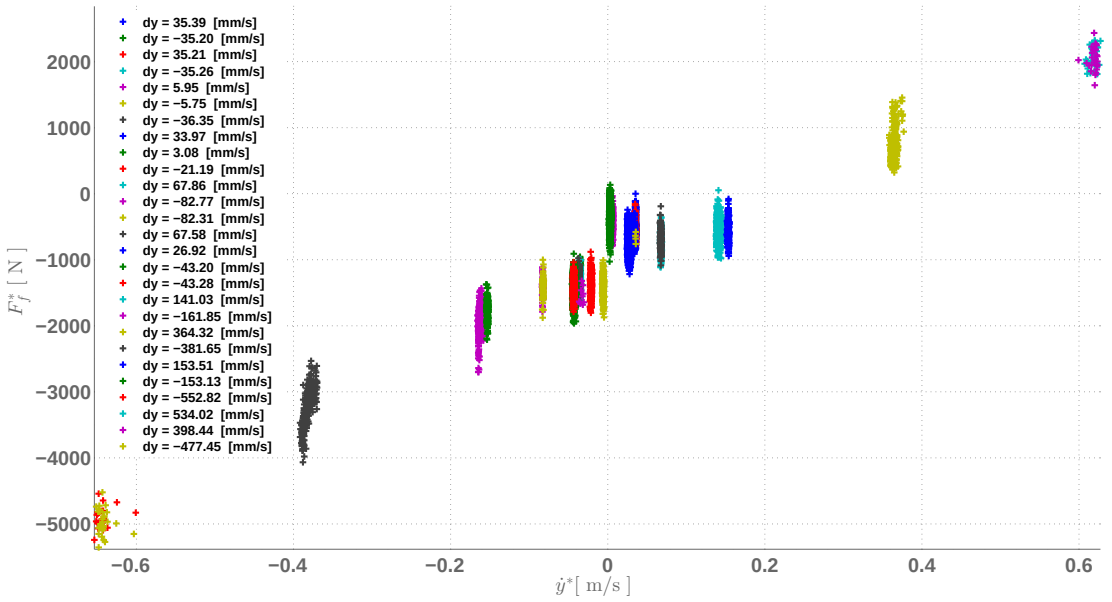

Figure 3.6: Estimated friction force $F_f{}^*$ for constant piston velocities $\dot{y}^*$ in the range $\pm$ 0.6 [$\mathrm{m\,s^{-1}}$].

in Table 3.3. The following experiments were considered:

- Sinusoidal and square reference signals were applied under proportional closed loop control (tracking).
- Additionally, constant input reference signal was also considered in closed-loop

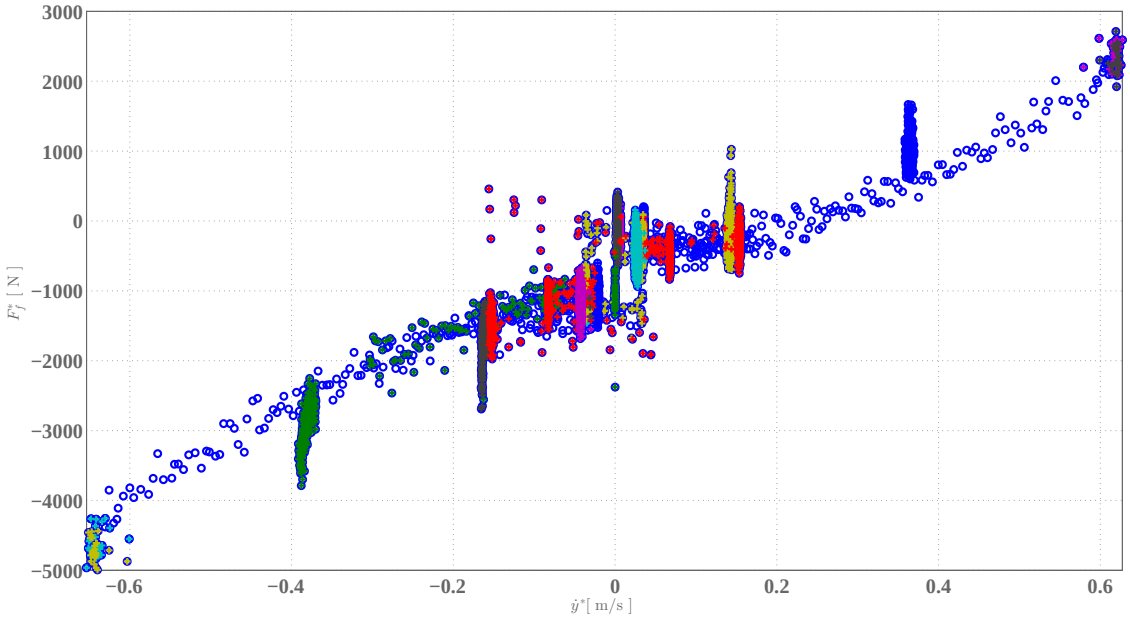

Figure 3.7: Estimated friction force $F_f{}^*$ for constant piston velocities $\dot{y}^*$ ($\ddot{y} = 0$) and for small acceleration ($\ddot{y} \approx 0$), in the range $\pm$ 0.6 [$\mathrm{m\,s^{-1}}$].

Table 3.3: Measured constant velocities for friction force identification

Experiment #	Input Signal u_c^* [V]	Measured Velocity $\dot{y}^*$ [$\mathrm{mm\,s^{-1}}$]
1	0.389	$\approx$ −36
2	-0.611	$\approx$ 35
3	-0.115 $\pm$ .2	$\approx$ $\pm$6
4	-0.115 $\pm$ .5	$\approx$ $\pm$28
5	$\pm$ 1.0	$\approx$ $\pm$66
6	$\pm$ 2.0	$\approx$ $\pm$128
7	$\pm$ 10.0	$\approx$ $\pm$600
8	1.5	$\approx$ 128
9	$\pm$ 5.0	$\approx$ $\pm$369

with proportional control (regulation).

- Experiments were also conducted in open-loop. One representative example of such experiments is illustrated in Figure 3.8, where the main acquired data is shown: piston position y, piston velocity $\dot{y}$ and pressures P_A and P_B. In this experiment, the piston was positioned around 100 [mm] by adjusting manually the input signal. Then, a square wave input signal was applied with constant amplitude and frequency.

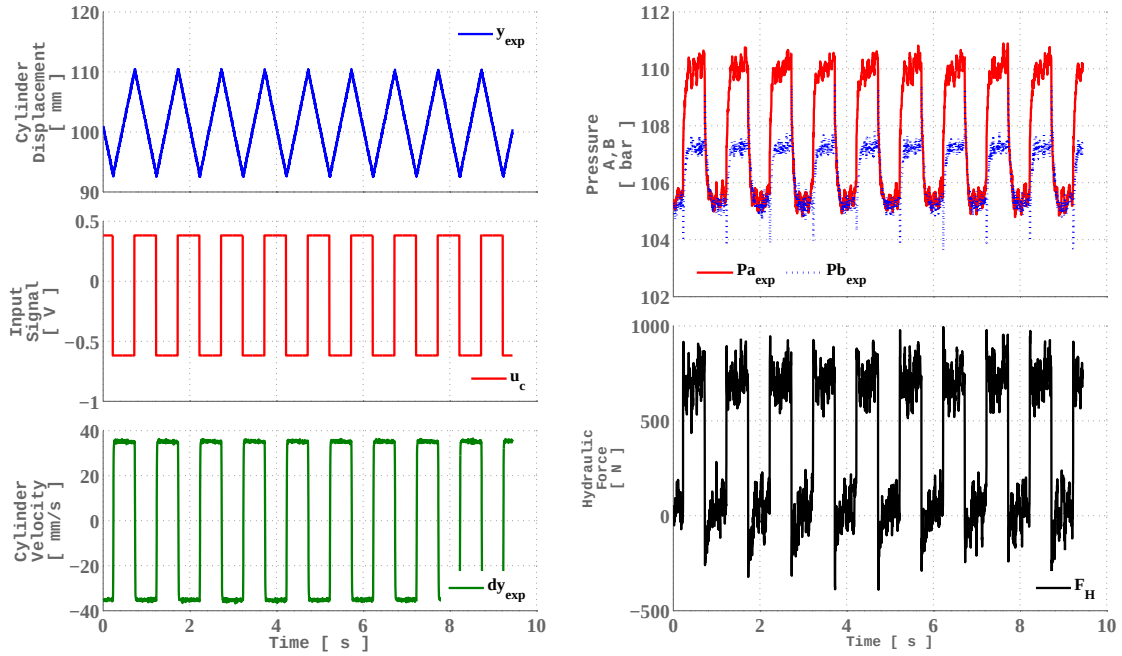

Figure 3.8: One representative data set of the experiments performed. An open-loop experiment: the resulting cylinder position (*upper-left corner*), input signal (mid-left), cylinder velocity (bottom-left corner), the pressures in chambers A and B (upper-right corner) and the hydraulic force calculated as $F_H = A_n(P_A - P_B)$ (bottom-right corner). A square wave input signal was applied (mid-left).

The values of the input signal u_c^* and the corresponding measured piston (constant) velocity $\dot{y}^*$ used to generate the Stribeck Friction Force Curve depicted in Figure 3.6 is given in Table 3.3. Note that, a linear relationship can be observed between u_c^* and $\dot{y}^*$, *i.e.*,

$$\dot{y}^* \approx -0.07 u_c^* \,,$$

indicating that the I/O relationship between u and $\dot{y}$ can be represented by a simple integrator. Indeed, by noting from Fig. 3.8 that the time varying behavior of the piston position has a triangular wave form while the control input signal has a square wave form, one can say that the hydraulic actuation system acts like an integrator. The frequency response can be estimated in closed loop (Figure 3.9) by using the data shown in Figure 3.10. The proportional control gain $K_p = 100$

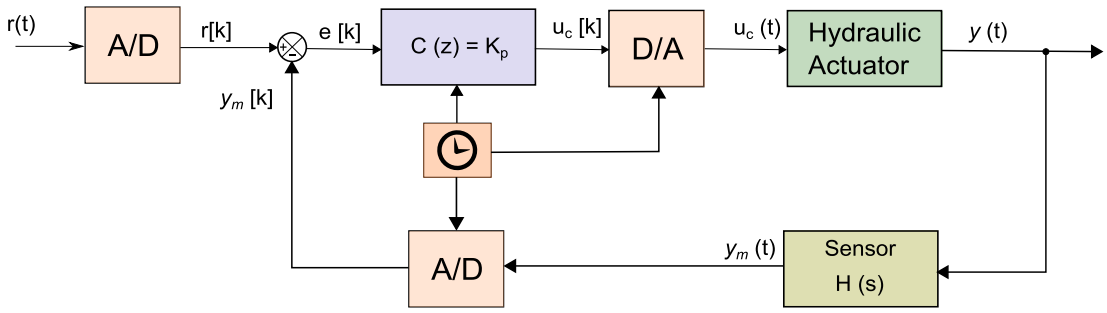

Figure 3.9: Block diagram of a standard proportional control of HTM. In this experiment, a sampling period (T_s) of 2 [ms] is employed.

was implemented during this experiment and the integrator gain was calculated. Therefore, the positioning HSS acts as an integrator (mainly at low frequency) and the hydraulic actuation system for position control can be modeled by the transfer function

$$G_{ol}(\mathrm{s}) = \frac{Y(\mathrm{s})}{U_c(\mathrm{s})} = \frac{K}{\mathrm{s}}, \tag{3.6}$$

where,

$K = -0.07$ is the identified integrator gain.

In must be highlighted that, as frequency increases, the performance of a proportional control is not satisfactory for hydraulic actuation control of HTM. Moreover, friction forces and uncertainties may also reduce the closed loop performance. In general, the disturbances at high frequency cannot be ignored and, for precision tracking at high frequency, the valve dynamics should be taken into account (YAO *et al.*, 2013), (FLOHIL, 2012), (TRAN *et al.*, 2012), (VALDIERO, 2012), (ROMANO; GARCIA, 2008), (OLSSON *et al.*, 1998).

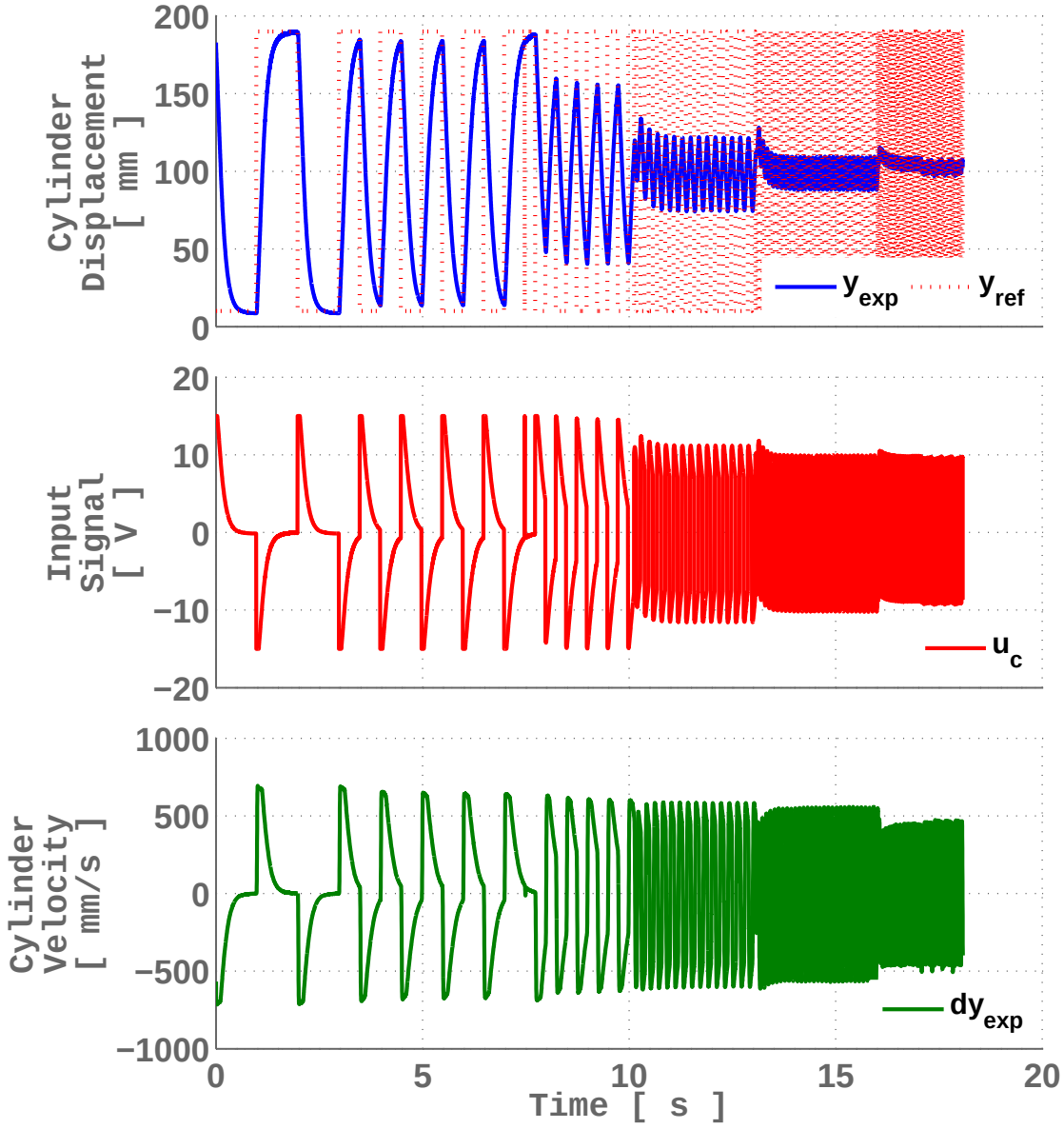

Figure 3.10: HSS closed loop frequency response: cylinder position (*top*), input signal (*middle*) and cylinder velocity (*bottom*). The blue solid line represents the actual piston position y while the red dotted line the desired position y_d.

3.4 Friction force parameters identification

From the Stribeck Friction Force Curve depicted in Figure 3.6, it is possible to estimate the parameters of Eq. (3.2) using well known identification algorithms as, for example: (1) Linear Least-Squares and (2) Non-Linear Least-Squares, via MATLAB®'s Optimization Toolbox.

The friction force model was introduced in Eq. (3.2) and the parameters to be identified can be defined in the vector $\mathbf{\Theta} = \begin{pmatrix} B_v^* & B_c^* & B_s^* & C_s^* \end{pmatrix}^\intercal$. However, to obtain the friction model for simulation and control design, different identification approaches have been implemented in MATLAB®. For simplicity, the leakage flows, the fluid mass and the SV were neglected. Additionally, the bulk modulus is considered to be constant at both sides of the piston. Four different approaches were considered.

(1) The friction force is assumed to be governed only by the viscous friction term (SCHWARTZ, 2004), (PEREIRA, 2006) (See Figure 3.11 on page 68).

(2) The friction force is identified by a second order polynomial equation (See Figure 3.12 on page 70) in $\dot{y}$. This strategy can also be founded in (SZPAK, 2008).

(3) The Stribeck velocity C_s is obtained by inspection and the remaining parameters are estimated (See Figure 3.13 on page 73) (VALDIERO, 2012) via LS.

(4) A smoothed version for the sign function $\text{sign}(\cdot)$ is introduced and the four parameters are estimated (See Figure 3.13c on page 73).

The results obtained using the LS method suggested the existence of an uncalibrated pressure sensor. This was confirmed by means of a calibrated manometer. An extra parameter was introduced to estimate the offset presented in the data set and then used to corrected it.

3.4.1 Linear fitting

The model for the friction force is presented in Eq. (3.2). The corresponding friction force F_f^* for the constant velocity case ($\ddot{y} \approx 0$) is given by Eq. (3.5) and repeated

here for convenience,

$$F_f^* = F_H - F_g\,, \tag{3.7}$$

where F_H and $F_g = M_t\, g$.

By considering that the viscous friction is the dominant term in F_f given in Eq. (3.2), a linear curve fitting should be sufficient to model a first simple model.

Thus, neglecting the static friction term F_s and the Coulomb friction term, the following linear system is obtained from the measurements.

$$\begin{pmatrix} \dot{y}^*[1] & 1 \\ \dot{y}^*[2] & 1 \\ \vdots & \\ \dot{y}^*[n] & 1 \end{pmatrix} \begin{pmatrix} B_v^* \\ p^* \end{pmatrix} = \begin{pmatrix} (A_n(\, P_A[1] - P_B[1]\,) - M_t\, g) \\ (A_n(\, P_A[2] - P_B[2]\,) - M_t\, g) \\ \vdots \\ (A_n(\, P_A[n] - P_B[n]\,) - M_t\, g) \end{pmatrix}, \tag{3.8}$$

Now, defining A and b such that Eq. (3.8) is rewritten as

$$\mathbf{A\Theta} = \mathbf{b}\,, \tag{3.9}$$

with $\mathbf{\Theta} = \begin{pmatrix} B_v^* & p^* \end{pmatrix}^\intercal$, can be obtained via least squares (LS), given by

$$\mathbf{\Theta}^\intercal = (A^\intercal A)^{-1} A^\intercal b\,.$$

Remark. *In fact, it was verified that there exists an offset of* 4.0 ± 0.5 *[*bar*] in the pressure measured by the transducer connected to the chamber A of the cylinder. This was at first detected by the LS fitting and then confirmed by comparison with an external calibrated manometer.*

The selection of the data set is crucial to identification. In some cases, the piston acceleration should be considered (JELALI; KROLL, 2003). Then, the system defined in Eq. (3.8) can be modified to fit the friction force $F_f^* = B_v^* \dot{y}^*$ to the force $F_H - F_g - M_t\, \ddot{y}$, resulting in the following linear system after a simple algebraic

manipulation

$$\begin{pmatrix} \ddot{y}^*[1] & \dot{y}^*[1] & 1 \\ \ddot{y}^*[2] & \dot{y}^*[2] & 1 \\ \vdots & & \\ \ddot{y}^*[n] & \dot{y}^*[n] & 1 \end{pmatrix} \begin{pmatrix} B_v^* \\ B_v^* \\ p^* \end{pmatrix} = \begin{pmatrix} (A_n(\, P_A[1] - P_B[1]\,) - M_t\, g) \\ (A_n(\, P_A[2] - P_B[2]\,) - M_t\, g) \\ \vdots \\ (A_n(\, P_A[n] - P_B[n]\,) - M_t\, g) \end{pmatrix}, \tag{3.10}$$

with $\mathbf{\Theta}$ redefined as $\mathbf{\Theta} = \begin{pmatrix} B_v^* & B_v^* & p^* \end{pmatrix}^\intercal$. By considering the first approach, from Eq. (3.8) one obtains the estimate ${B_v}^* = 5551.90\,[\,\mathrm{N\,s\,m^{-1}}\,]$. For the second approach, one obtains the estimation of ${B_v}^* = 5266.952\,[\,\mathrm{N\,s\,m^{-1}}\,]$ and ${M_t}^* = 53.780\,[\,\mathrm{kg}\,]$, from Eq. (3.10). Note that, the total mass estimate is similar to the value provided by the manufacturer data-sheet ($M_p = 52.0\,[\,\mathrm{kg}\,]$).

The curve fitting is shown in Fig. 3.11 and the corresponding coefficient of determination[†] (R^2) is equal to 0.73. The NLS method was also employed for comparison. In this case, the identification problem is formulated as the following optimization problem:

$$\min_{\mathbf{\Theta}} \sum_{k=1}^{n} \Big(F_f^*[k] + M_t \ddot{y}[k] - (F_H[k] - F_g[k]) \Big)^2, \tag{3.11}$$

with $\mathbf{\Theta}$ redefined as $\mathbf{\Theta} = \begin{pmatrix} M_t^* & B_v^* & p^* \end{pmatrix}^T$.

The result shows that the curve does not pass through the origin which indicates that there is a problem in the data set (as mentioned before, the chamber A transducer is uncalibrated). The Coulomb friction term and static friction term could be considered in order to obtain a better fitting, since these terms better describe the friction force behavior at low velocity.

[†]Coefficient of determination indicates how well data points fit the predicted model and it is also known as "R squared". It is given by the formula $R^2 \equiv 1 - \frac{SS_{\mathrm{res}}}{SS_{\mathrm{tot}}}.$, where $SS_{\mathrm{tot}} = \sum_i (y_i - \bar{y})^2$, is the total sum of squares (proportional to the sample variance); $SS_{\mathrm{reg}} = \sum_i (f_i - \bar{y})^2$, is the regression sum of squares and $SS_{\mathrm{res}} = \sum_i (y_i - f_i)^2$, is the sum of squares of residuals.

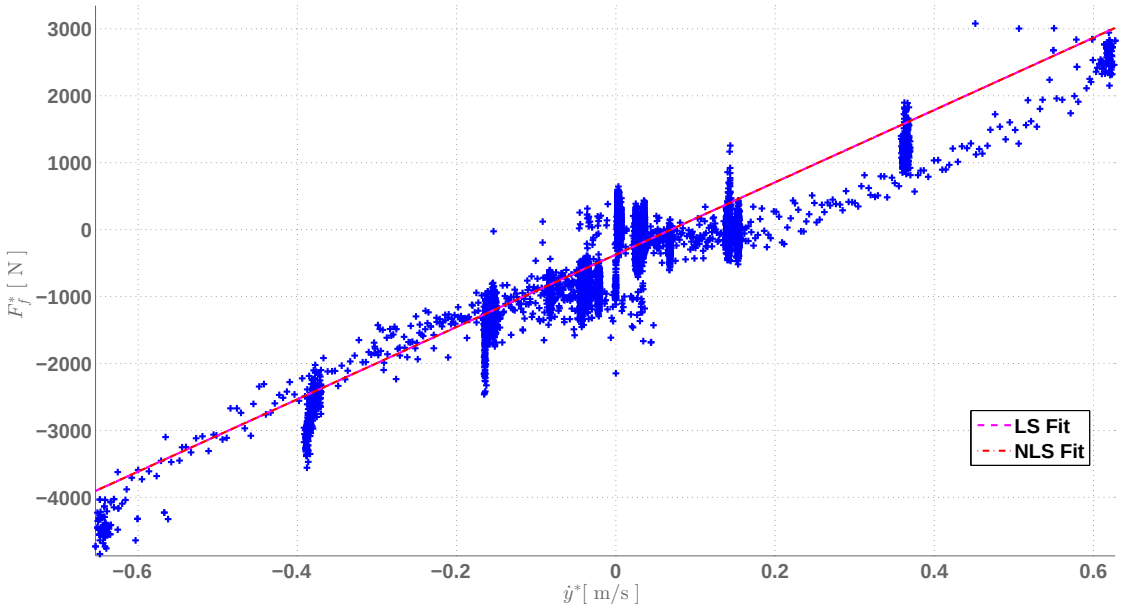

Figure 3.11: Friction force identification considering only the presence of the viscous term.

3.4.2 Polynomial fitting

The friction models proposed above cannot capture the asymmetry of the friction force (JELALI; KROLL, 2003). To overcome this issue, Eq. (3.2) is rewritten as

$$F_f^*(\dot{y}) = \begin{cases} B_v^{+*}\dot{y}^* + \left(F_{co}^{+*} + F_s^{+*}\exp\left(-|\dot{y}^*|/C_s^{+*}\right)\right), & \text{if } \dot{y}^* \geq 0\,, \\ \\ B_v^{-*}\dot{y}^* - \left(F_{co}^{-*} + F_s^{-*}\exp\left(-|\dot{y}^*|/C_s^{-*}\right)\right), & \text{if } \dot{y}^* < 0\,. \end{cases} \tag{3.12}$$

By disregarding the acceleration ($\ddot{y} = 0$) and using the second order approximation for the Mclaurin series of the Stribeck term, the following linear systems is obtained:

$$\begin{pmatrix} \dot{y}^{2*}[1] & \dot{y}^*[1] & 1 \\ \dot{y}^{2*}[2] & \dot{y}^*[2] & 1 \\ \vdots & \vdots & \vdots \\ \dot{y}^{2*}[n] & \dot{y}^*[n] & 1 \end{pmatrix} \begin{pmatrix} p_1^* \\ p_2^* \\ p_3^* \end{pmatrix} = \begin{pmatrix} (A_n(P_A[1] - P_B[1]) - M_t\, g) \\ (A_n(P_A[2] - P_B[2]) - M_t\, g) \\ \vdots \\ (A_n(P_A[n] - P_B[n]) - M_t\, g) \end{pmatrix}. \tag{3.13}$$

Now, re-defining $\mathbf{A}$ and $\mathbf{b}$ such that Eq. (3.13) is rewritten as

$$\mathbf{A}_2\boldsymbol{\Theta}_2 = \mathbf{b}\,. \tag{3.14}$$

with $\boldsymbol{\Theta}_2 = \begin{pmatrix} p_1^* & p_2^* & p_3^* \end{pmatrix}^\intercal$, the LS problem can be solved, for example via MATLAB®which has polynomial curve fitting that finds the coefficients of a polynomial. The result is shown in Figure 3.12. Thus, the viscous friction coefficient ${B_v}^*$ is estimated as $\approx -1.255\,[\,\mathrm{N\,m\,s^{-1}}\,]$ for positive velocities (R^2 is equal to 0.6128) and it is estimated as $\approx 3497.9\,[\,\mathrm{N\,m\,s^{-1}}\,]$ for the negative velocity (R^2 equals to 0.830). The overall estimation (for positive and negative velocities) of the viscous friction coefficient is estimated as $\approx 5530.944\,[\,\mathrm{N\,m\,s^{-1}}\,]$, which is closer to the linear solution presented before.

The same procedure was applied by (SZPAK, 2008) to estimate friction parameters. Different polynomial models were tested and the second order had the better performance. However, another phenomenon was observed in that experiment, the so called "stick-slip phenomenon" at low frequencies (SZPAK, 2008). The stick-slip can be heard from hydraulic cylinders and it is characterized by jerking motion. This problem invalidated the collected data at low frequencies in the experiments described in (SZPAK, 2008), resulting in a poor estimation of the static and Coulomb friction parameters. Conversely, this phenomenon was not observed in the experiments performed here, thus, the low velocities data is useful for identification of the static and Coulomb friction parameters.

Remark. *A non-linear least squares (LS) curve fitting with constrains* [‡] *was applied to find the parameters with a specified input bounds. Hence, the lower bound was defined, so that all the coefficients of the polynomial fitting would have positive values. A comparison between LS and NLS approaches shows that both deliver the same solution for the linear fitting. Additionally, the LS approach results in a inconsistent negative coefficient for positive velocities.*

[‡]The MATLAB®'s algorithm `lsqnonlin` solves nonlinear least-squares curve fitting problems with optional lower and upper bounds. The "Trust-Region Method" was chosen to solve this bounded nonlinear optimization problem.

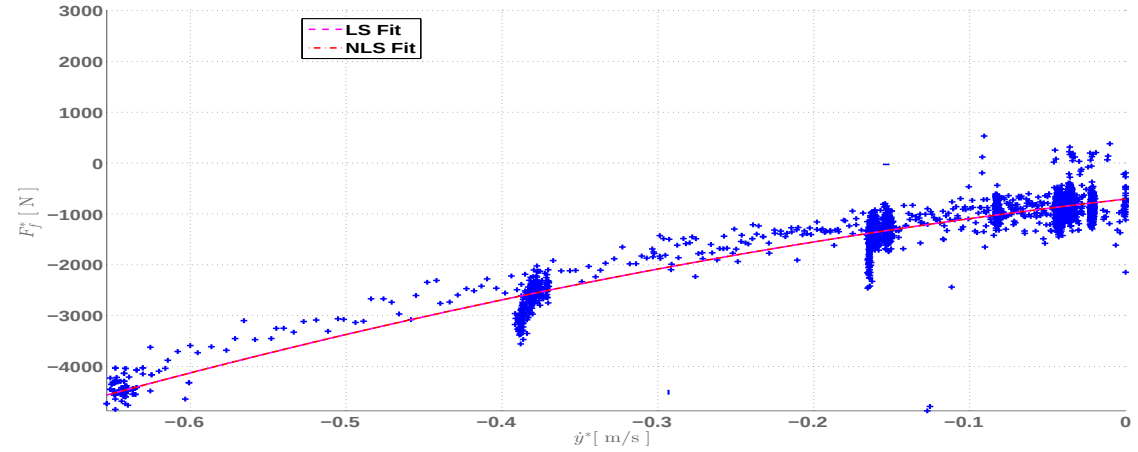

(a)

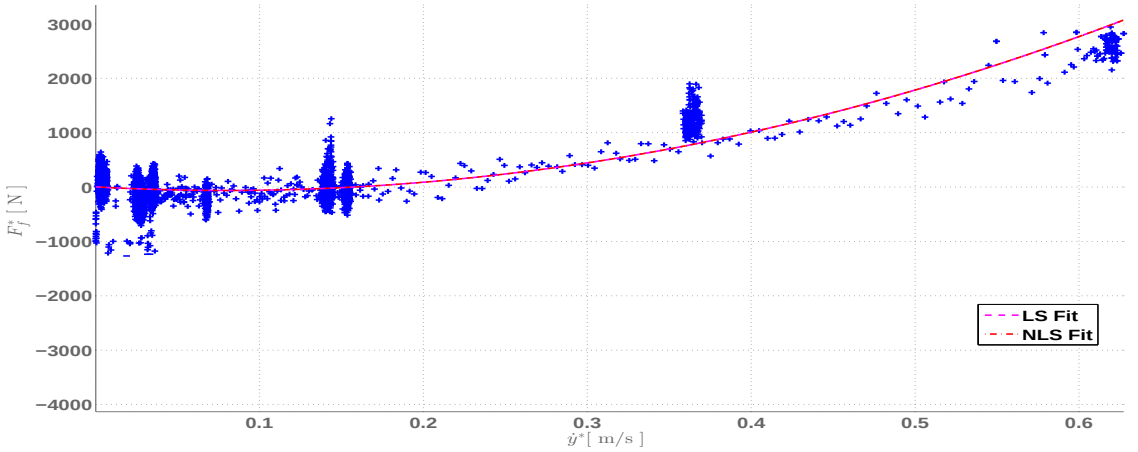

(b)

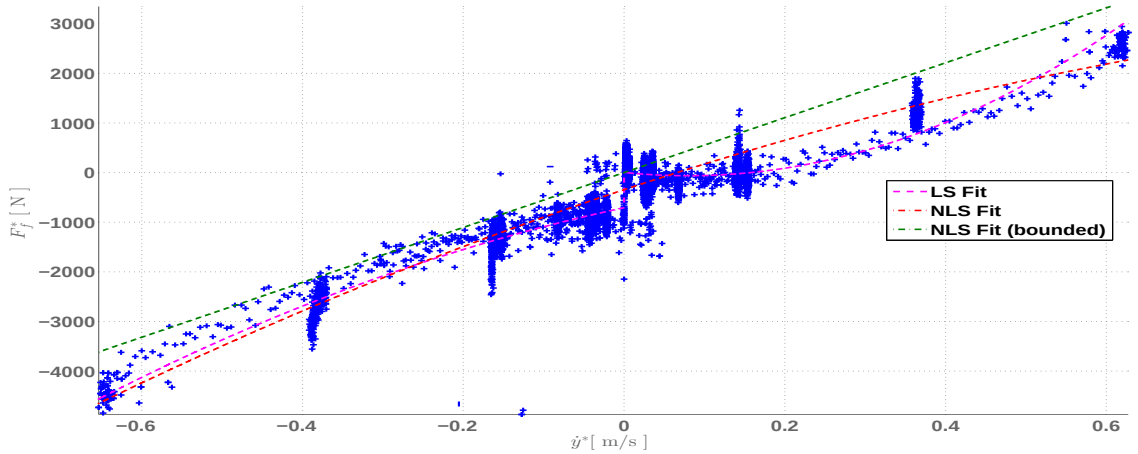

(c)

Figure 3.12: Friction force for viscous coefficient - second order polynomial curve fitting. The red dash-dotted line represents the LS fitting: (a) negative velocities $\dot{y}^* < 0$, (b) positive velocities $\dot{y}^* > 0$, (c) overall fit for the total velocity range. The dash-dotted magenta represents the NLS fit with no constraints and the dash-dotted green line shows the NLS fit with bound constraints. The friction force identification via polynomial fitting shows the existence of a non-symmetric behavior w.r.t. the vertical axis.

3.4.3 Stribeck friction model fitting

As mentioned before, the static and the Coulomb friction parameters are required to be estimated. The previous models used do not capture the lower velocity behavior, which may be relevant for the hydraulic control system. The fitting between the friction force given in Eq. (3.2) and the force $F_H - F_g$ can be rewritten more conveniently in a matrix form as follows. Define the $N \times M$ regression matrix (JELALI; KROLL, 2003)

$$\boldsymbol{\phi} = \begin{pmatrix} \dot{y}^*[1] & \text{sign}\,(\dot{y}^*[1]) & \text{sign}\,(\dot{y}^*[1])\exp(-|\dot{y}^*[1]|/C_s) & 1 \\ \dot{y}^*[2] & \text{sign}\,(\dot{y}^*[2]) & \text{sign}\,(\dot{y}^*[2])\exp(-|\dot{y}^*[2]|/C_s) & 1 \\ \vdots & \vdots & \vdots & \vdots \\ \dot{y}^*[n] & \text{sign}\,(\dot{y}^*[n]) & \text{sign}\,(\dot{y}^*[n])\exp(-|\dot{y}^*[n]|/C_s) & 1 \end{pmatrix} \tag{3.15}$$

and the column vectors

$$\mathbf{b} = \begin{pmatrix} (A_n(P_A[1] - P_B[1]) - M_t \cdot g) \\ (A_n(P_A[2] - P_B[2]) - M_t \cdot g) \\ \vdots \\ (A_n(P_A[n] - P_B[n]) - M_t \cdot g) \end{pmatrix}, \quad \boldsymbol{\Theta} = \begin{pmatrix} B_v^* \\ B_{co}^* \\ B_s^* \\ p^* \end{pmatrix}. \tag{3.16}$$

Thus, one can write

$$\boldsymbol{\phi}\boldsymbol{\Theta} = \mathbf{b}\,, \tag{3.17}$$

which has the well known LS solution

$$\hat{\Theta} = \left(\boldsymbol{\phi}^\intercal \boldsymbol{\phi}\right)^{-1} \boldsymbol{\phi}^\intercal \mathbf{b}\,. \tag{3.18}$$

Initially, the identification process considered the original formulation of the Stribeck friction curve, which includes a sign function, as mentioned before (See Figure 3.13a on page 73). The sign function introduces a non-smooth model for identification, possibly causing numerical problems. In order to avoid numerical problems in the identification algorithm, the following smoothed version of the sign function is

introduced:

$$\text{sig}\,(\dot{y}) = \dot{y}/(|\dot{y}| + \epsilon)\,, \tag{3.19}$$

where

ϵ is a small design constant.

The introduction of this function does not change the friction force behavior. In fact, it still captures the friction force behavior at low velocity (See Figure 3.13b on page 73).

An similar approach is described in (MAKKAR *et al.*, 2005), (JELALI; KROLL, 2003), while an alternative friction model is proposed by (MAKKAR *et al.*, 2005) to describe the friction force as a continuous function. This alternative model is related with the Stribeck model and retains similar properties. However, this model has overparameterization (six parameter to be identified) and relationship between MAKKAR *et al.* (2005)'s model and Stribeck's model is not easy to obtain. Here onwards, the friction force model described in Eq. (3.2) is slightly modified to include the smoothed sign function. Applying the algorithms above proposed, the additional coefficient p_4^* was estimated to be 4.14×10^5. The magnitude of this term corroborates with the uncalibrated pressure transducer, which was measured via a calibrated manometer an offset of 4.0 $\pm$0.5 [bar] in the pressure transducer connected to the chamber A . The fitting results are depicted in Figure 3.13.

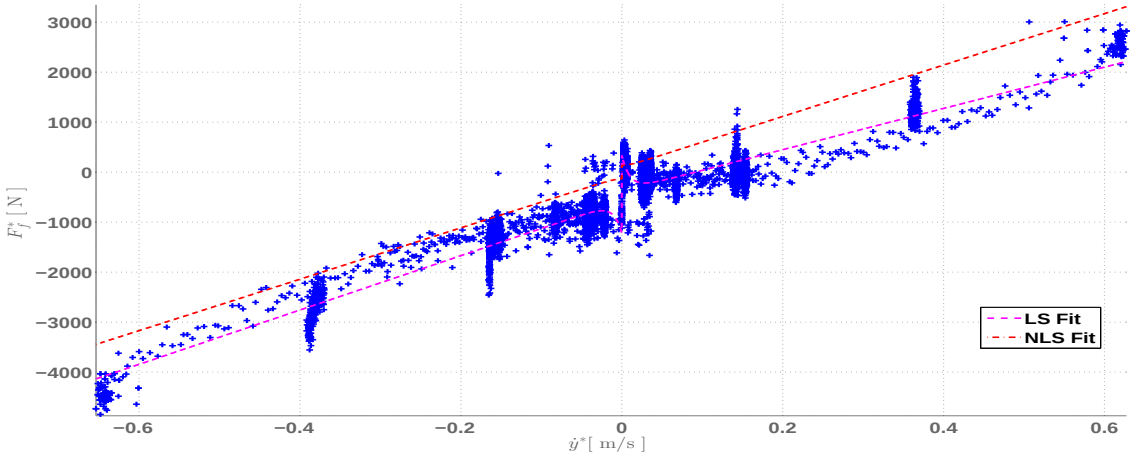

(a)

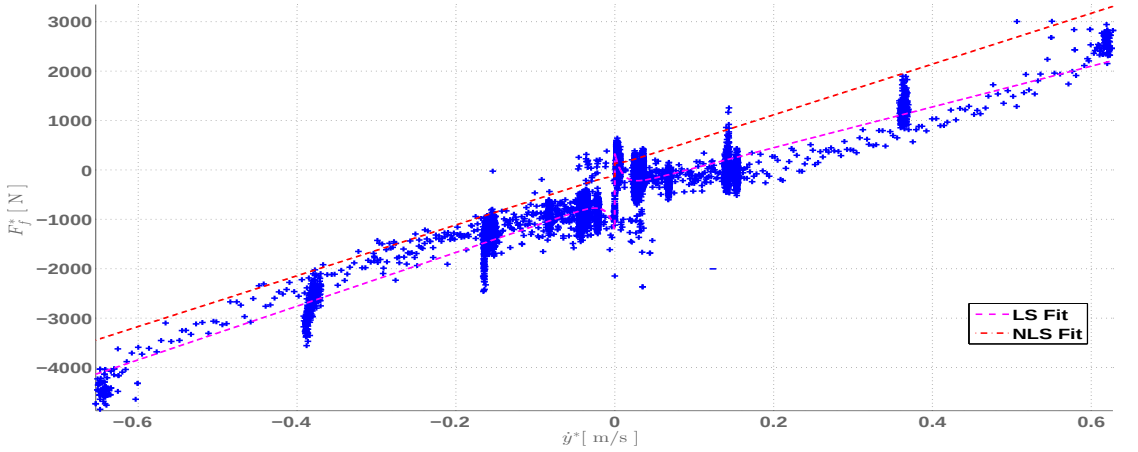

(b)

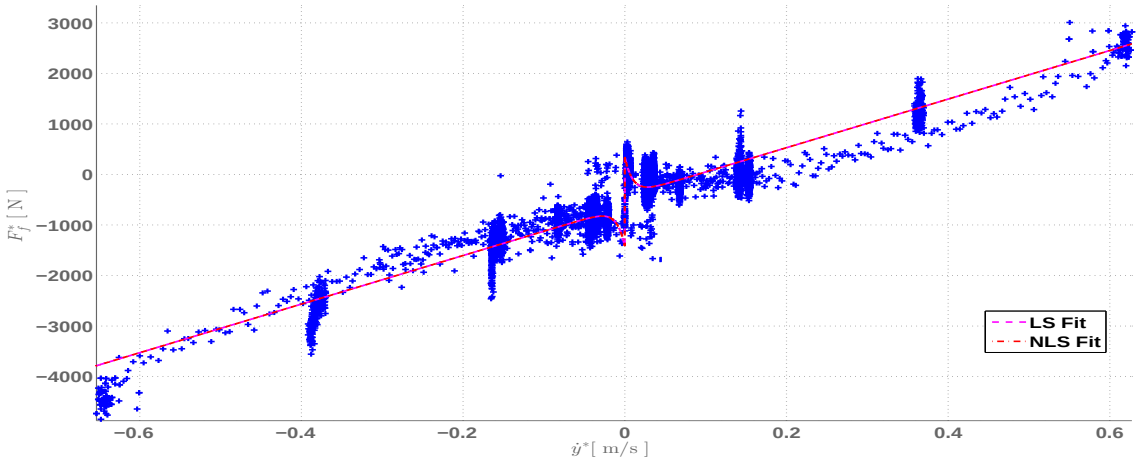

(c)

Figure 3.13: Friction force identification considering the Stribeck term: (a) with original sign function $\operatorname{sign}(\cdot)$, (b) with the smoothed version of the sign function $\operatorname{sig}(\cdot)$ and (c) with pressure A calibration (the data set is shifted to the origin).

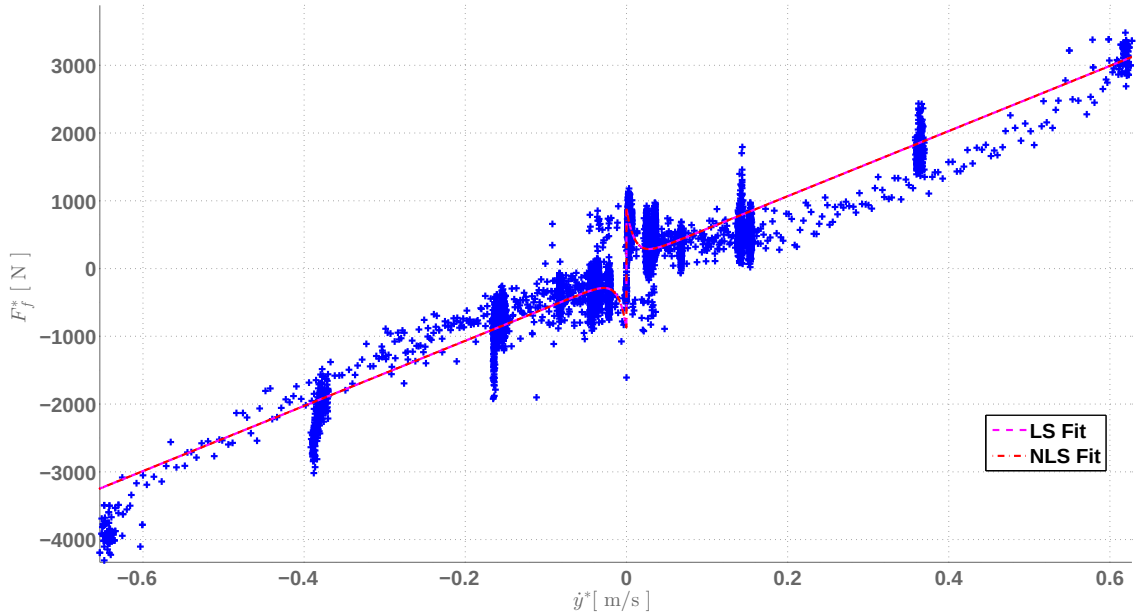

Figure 3.14: Stribeck Fitted Curve with Calibrated Pressure. Both algorithms applied in this estimation have produced the same result. The viscous friction coefficient B_v is 4.541×10^3 [N s m^{-1}]. The static friction B_s coefficient is 136.50 [N] while the Coulomb friction coefficient isB_{co} 760.05 [N].

The friction force estimation results are summarized in Table 3.4.

Table 3.4: Estimated friction force parameters

Model #	B_v $[\,\mathrm{N\,s\,m^{-1}}\,]$	B_s $[\,\mathrm{N}\,]$	B_{co} $[\,\mathrm{N}\,]$	C_s $[\,\mathrm{m\,s^{-1}}\,]$
Linear (LS & NLS)	5551.90	X	X	X
Poly2^{+} (LS)	-1255	532.0		X
Poly2^{-} (LS)	3498	-202.72		X
Poly2 (NLS)	5530.94	178.02		X
sign (LS)	5008.51	103.36	775.3	0.01
(NLS)	5450.34	43.51	-423.98	0.0006
sgn (LS)	4999.51	106.31	624.86	0.01
(NLS)	5008.51	103.96	819.86	0.01
sig $/\nu$ (LS & NLS)	5017.35	102.61	792.33	0.01

Note: "X" denotes a not estimated value, the superscript + (−) indicates positive (negative) velocities and (LS) and (LS) denotes the estimation technique applied. The symbol ν represents the calibration term for the chamber A pressure sensor and it was estimated to be $4.14 \times 10^5\,[\,\mathrm{Pa}\,]$.

3.4.4 Friction force model validation

The friction force estimation based on the Stribeck curve (See Figure 3.5 on page 59) is obtained by estimating the coefficients B_v, F_{co}, F_s in Eq. (3.2) via LS (similar values for NLS) and with C_s chosen by inspection. The estimated parameter values are :

- Viscous friction coefficient (B_v): 4541.64 $[\,\mathrm{N\,s\,m^{-1}}\,]$
- Coulomb friction coefficient (B_{co}): 760.05 $[\,\mathrm{N}\,]$
- Static friction coefficient (B_s): 136.50 $[\,\mathrm{N}\,]$
- Stribeck velocity coefficient (C_s): 0.01 $[\,\mathrm{m\,s^{-1}}\,]$
- Constant smoothing factor for the sig function (ϵ): 1×10^{-3} $[\,\mathrm{m\,s^{-1}}\,]$.

Hence, the friction force is estimated as

$$F_f^*(\dot{y}) = 5017.35\dot{y} + \operatorname{sign}(\dot{y})\Big(792.33 + 102.61\exp\Big(-|\dot{y}|/0.01\Big)\Big)\,. \tag{3.20}$$

Disregarding the acceleration ($\ddot{y} = 0$), one has that the friction force satisfies

$$F_f = F_H - F_g\,.$$

Experimental validation of the friction force identification is conducted by comparison along time and for different experiments. Additionally, the friction force is obtained from Eq. (3.20), denoted by F_f^*, with the friction force obtained from $F_f = F_H - F_g$. Figures 3.15 to 3.18 illustrate the time behavior of the estimated friction force F_f^*, i.e, obtained with approximately constant velocities ($\ddot{y} \approx 0$) based on the Stribeck curve (See Figure 3.5 on page 59), and the estimated friction force obtained from the estimated version obtained along time, i.e., by disregarding the acceleration values.

From these figures it is evident that the identification carried out provides a reasonable model for the friction force.

In Figure 3.15, the friction model is validated in an open loop experiment, where a square wave signal (1 [Hz]) is applied in the control input (valve voltage). The estimated friction force varies from $-500\,\mathrm{N}$ to $600\,\mathrm{N}$ as shown in Figure 3.15a. It is apparent that, neglecting the noise presented in the acquired data, the identification of the friction force is satisfactory. The corresponding hydraulic force is illustrated in Figure 3.15b.

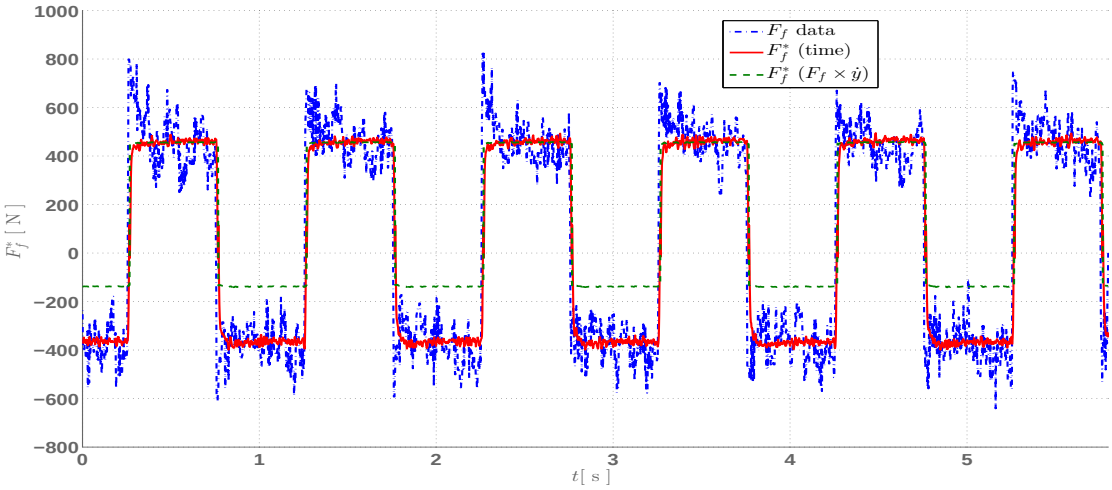

(a)

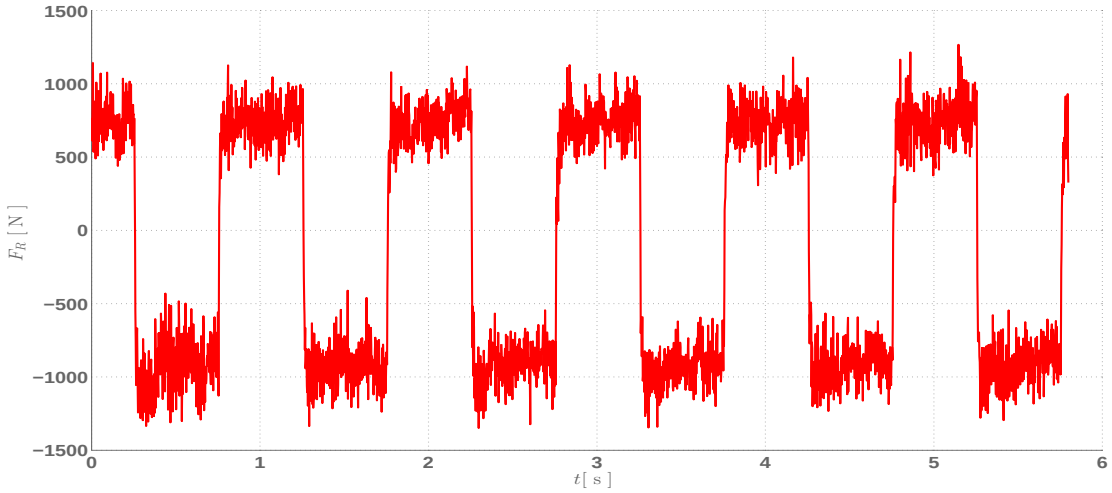

(b)

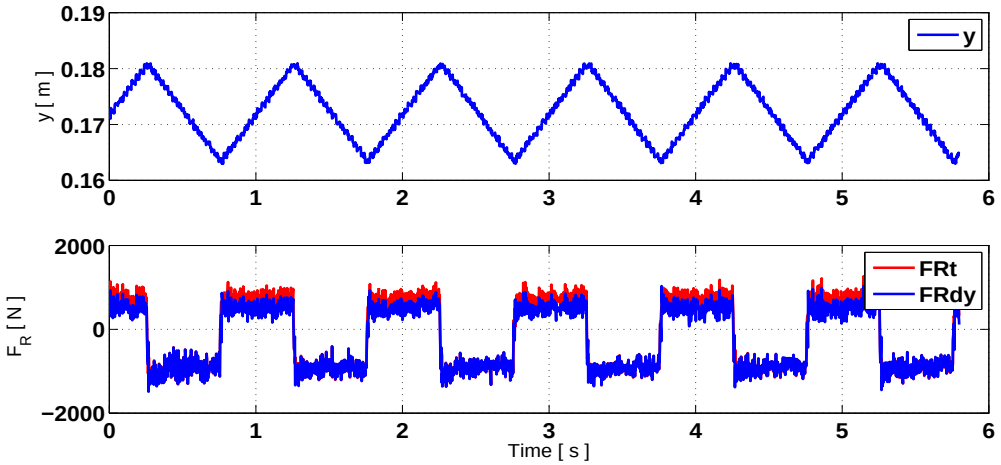

(c)

Figure 3.15: Friction force validation in an open loop experiment (valve voltage being a square wave with frequency of 1 [Hz]): (a) friction force: the blue dashed line represents the friction force $F_f = F_H - F_g$, the red solid line shows the friction force estimated F_f^* based on the experimental data and the green dot-dashed line the friction force based on obtained values. (b) depicts the total force (resulting) (F_R) to move the piston. (c) piston position and force (resulting) (F_R).

This procedure was applied to three different testing conditions presented in fatigue-corrosion tests. These experiments are depicted from Figure 3.16 to Figure 3.18. First, an open loop experiment is considered, with a square wave input voltage with frequency equal to $\pm 0.2\,[\,\mathrm{Hz}\,]$. In this case, the piston moves at constant speed until it reaches the maximum stroke length, then the piston returns back to the original position. Second, a 1 [Hz] square wave is applied (See Figure 3.17 on page 81) as the desired position trajectory, under closed loop control. Finally, the closed loop frequency response w.r.t. a $1\,[\,\mathrm{Hz}\,]$ sine wave reference signal is considered.

This procedure allowed the identification of the friction force parameters based on Eq. (3.2). The different conditions examined above present a better understanding of which friction term is more relevant for the hydraulic actuation system in fatigue testing.

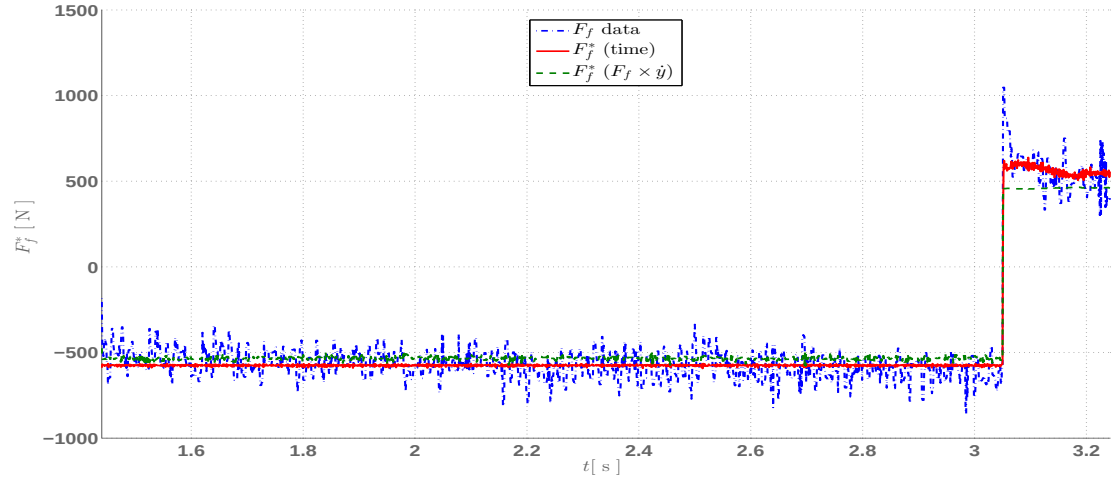

(a)

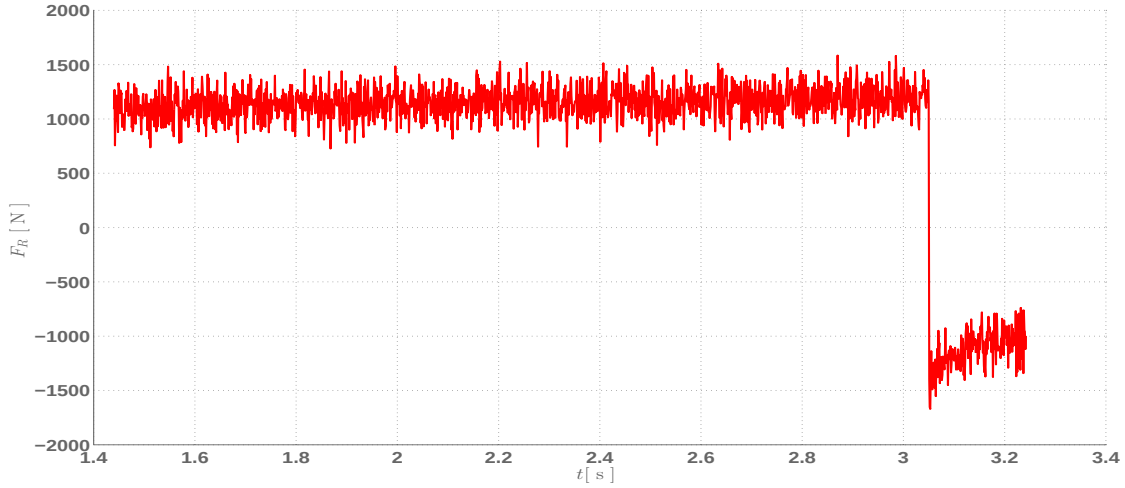

(b)

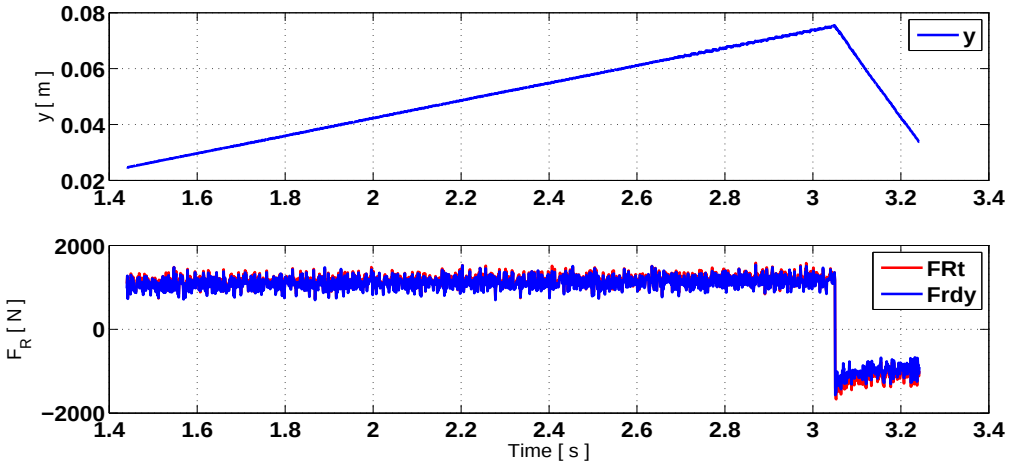

(c)

Figure 3.16: Measured and estimated friction force of the open loop system for a constant input voltage: (a) friction force: the blue dashed line represents the friction force, the red solid line shows the friction force estimated F_f^* based on the experimental data and the green dot-dashed line the friction force based on obtained values. (b) depicts the total force (resulting) (F_R) to move the piston. (c) piston position (y) and force (resulting) (F_R).

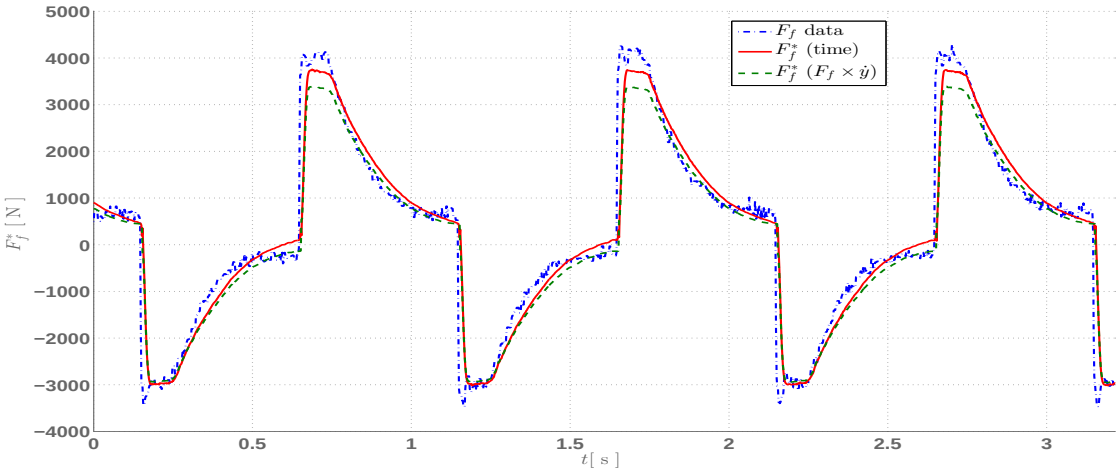

(a)

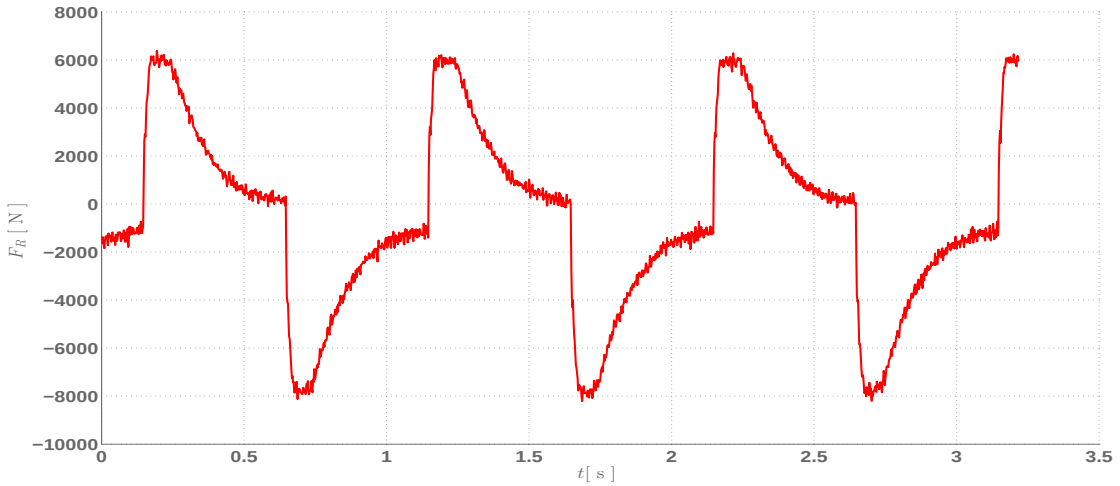

(b)

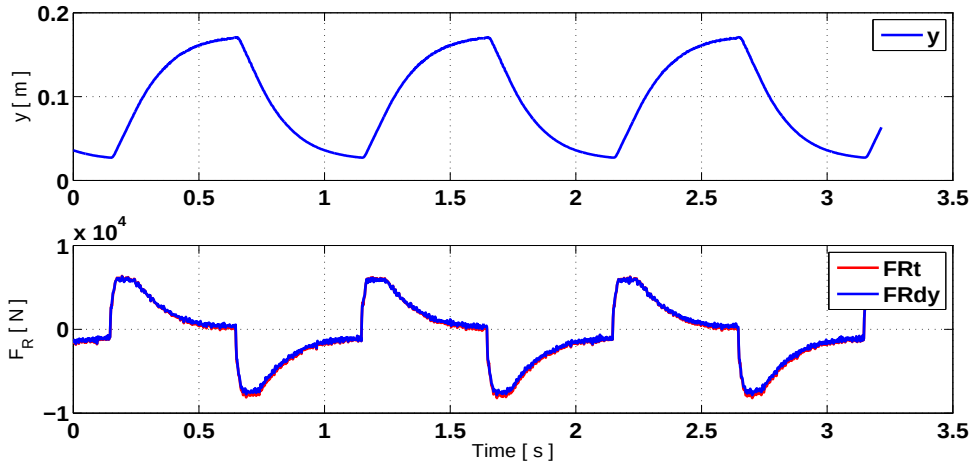

(c)

Figure 3.17: Friction force in a open loop experiment with square wave input voltage with frequency is equal to 1 [Hz]. (a) friction force: the blue dashed line represents friction force obtained from $F_H - F_g$, the red solid line shows the friction force estimation based on the experimental data without considering $\ddot{y} \approx 0$ and the green dot-dashed lined depict the friction force based on Stribeck curve, i.e., with $\ddot{y} \approx 0$. (b) depicts the force $F_H - F_g$. (c) piston displacement.

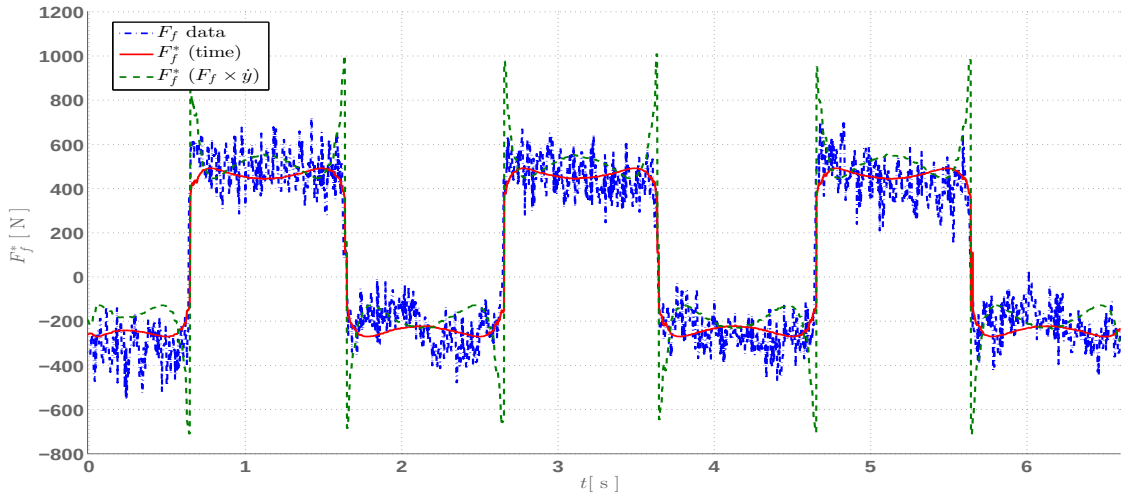

(a)

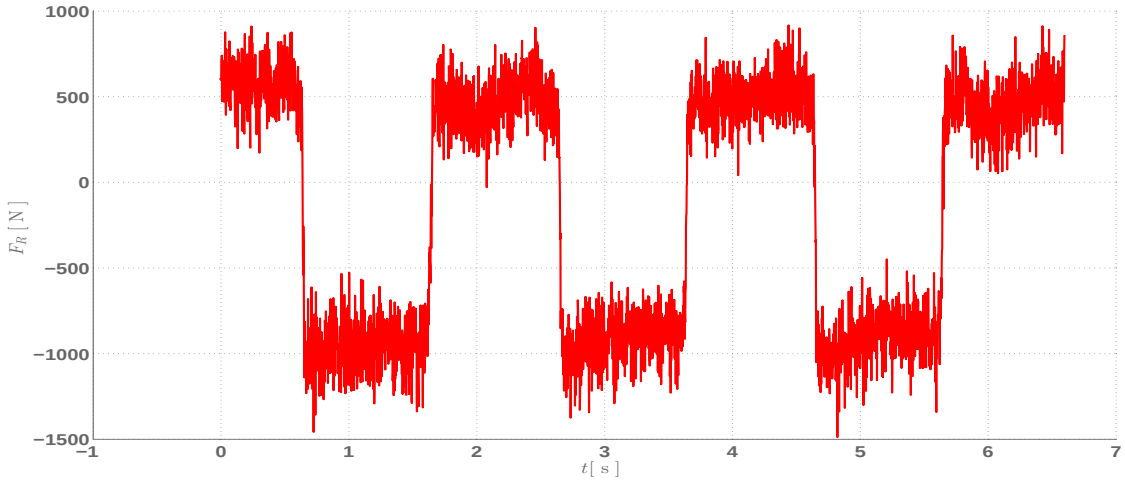

(b)

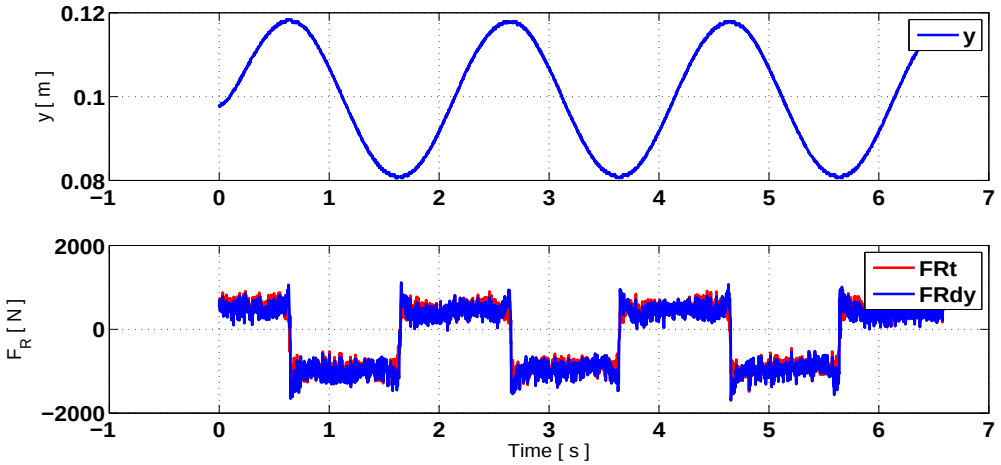

(c)

Figure 3.18: Friction force in an open loop experiment with sine wave input voltage with frequency is equal to $1\,[\mathrm{Hz}]$. (a) friction force: the blue dashed line represents friction force obtained from $F_H - F_g$, the red solid line shows the friction force estimation based on the experimental data without considering $\ddot{y} \approx 0$ and the green dot-dashed lined depicts the friction force based on Stribeck curve, i.e., with $\ddot{y} \approx 0$. (b) depicts the force $F_H - F_g$. (c) piston displacement.

3.5 Velocity gain identification

The piston velocity $\dot{y}$ depends on the position x_v of the spool valve and depends on the valve opening. Increasing x_v results in a large flow into chambers of the hydraulic actuator. If the non-linearities present in the valve are neglected then, assuming a linear relation between the applied voltage u_c and the spool displacement x_v, then the so called *velocity gain* can be determined. The velocity gain can be defined as the relationship between the spool displacement x_v and the piston velocity $\dot{y}$ (RODERMOND, 2006). In fact, one can write

$$\dot{y} = k_{vel} x_v = k_{vel} u_c \,, \tag{3.21}$$

where

k_{vel} is the velocity gain defined as $k_{vel} = Q_N / A_n$, $[\,\mathrm{V\,m\,s^{-1}}\,]$

with Q_N being the nominal flow rate of the valve $[\,\mathrm{L\,min^{-1}}\,]$.

The relationship given in Eq. (3.21) can be validated via simple experiments and linear regression, since the position transducer can provide two measurements: actual piston position and velocity. This feature made easier the velocity gain estimation.

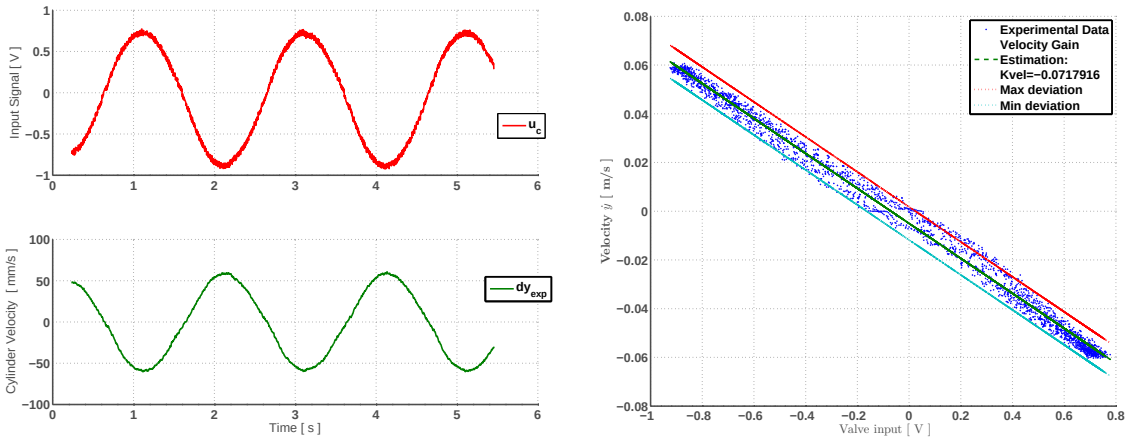

(a) **(b)**

Figure 3.19: Velocity gain identification: (a) the piston actual velocity (lower) and the input signal (upper) and (b) first order least square fitting for the velocity gain estimation.

This procedure was repeated for different reference signals illustrated in Table 3.5. The velocity gain k_{vel} is represented by the slope of the curve given in Figure 3.19a, which is equal to $-7.179\,16 \times 10^{-2}\,[\,\mathrm{V\,m\,s^{-1}}\,]$. According to Eq. (3.21) this curve should pass through the origin. However, an offset is apparent. This offset could be related to the leakage in the valve. The valve is of open-center type and according to the manufacturers' specification there is a zero flow defined as (BOSCH REXROTH, 2005),

$$Q_{V,L} = \sqrt{P_s/(70[\,\mathrm{bar}\,])}1.5[\,\mathrm{L\,min^{-1}}\,]\,, \tag{3.22}$$

where

P_s is the supply pressure given by the HPU.

The estimated velocities gains for different testing sets are presented in the Table 3.5. It was analyzed four situation: (1) the overall value of the velocity gain (considering high and low frequency); (2) open loop square wave; (3) open loop sine wave, and (4) closed loop proportional control. Finally, the estimation of the velocity gain was carried out from two tests: at high frequency and at low frequency.

Table 3.5: Mean values of Velocity Gain

	Theoretical Value	High Frequency $\lvert k_{vel}\rvert$	Low Frequency $\lvert k_{vel}\rvert$
Overall	4.8761×10^{-2}	4.3105×10^{-2}	6.6327×10^{-2}
Square wave		4.6344×10^{-2}	6.5596×10^{-2}
Sine wave		3.6485×10^{-2}	6.7152×10^{-2}
Proportional Control		4.2777×10^{-2}	6.6731×10^{-2}

The experiments indicate that the actuator has better tracking performance for low frequency than for high frequency. A statistical analysis is shown in Figure 3.20. High frequency tests have a larger range, however show a lower median value and the presence of outliers. In contrast, for low frequency tests the standard deviation is closer to the mean value of the velocity gain.

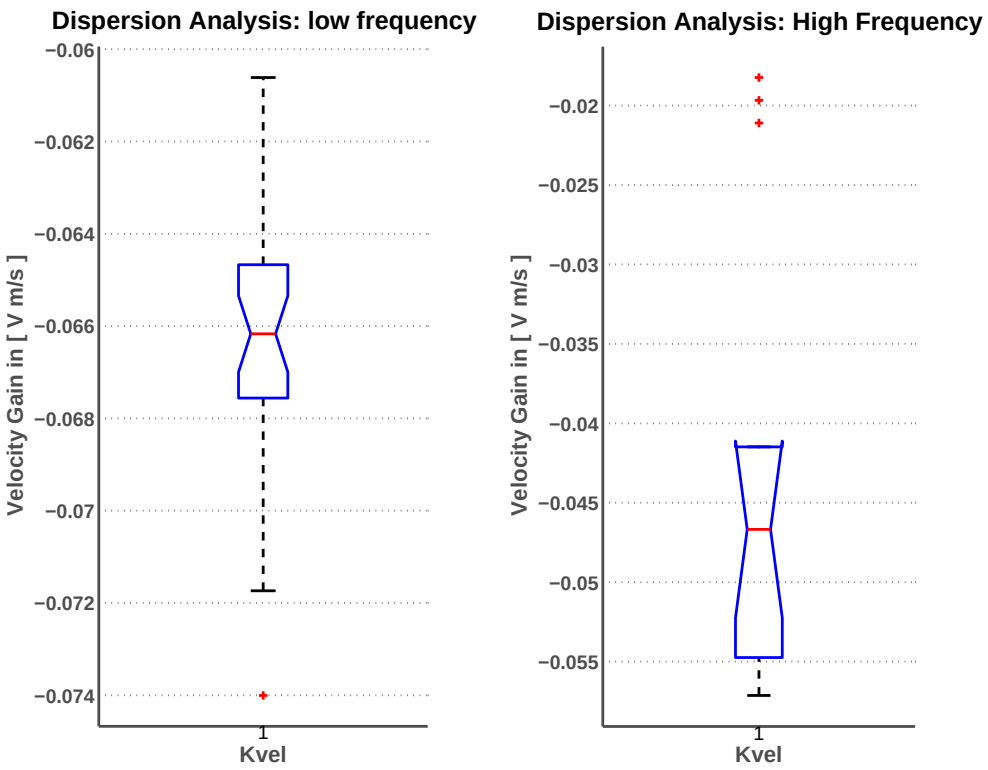

Figure 3.20: Statistics Analysis of Velocity Gain Estimation.

Chapter 4

HTM control

The main control challenge in HTM is the equivalent specimen stiffness constant (K_{sp}), which is time varying due to the crack propagation growth. This time varying behavior corresponds to a non-linear relationship between position and force. However, the nonlinear effect appears only at lower load levels due to the *crack closure*[*].

In this sense, two important variables to be considered are: the stress intensity factor K and the stress ratio R. As described briefly in the Introduction, the stress intensity factor range (ΔK) for all standard specimen configurations under Mode I conditions is given by the following relationship (HOSFORD, 2010), (CALLISTER, 2001)

$$\Delta K = \frac{\Delta F}{B W^{1/2}}\, g(a/W)\,, \tag{4.1}$$

where

ΔF is the force range applied to the specimen [N],

B is the specimen thickness [m],

a is the crack length [m],

W is the specimen width [m], and

$g(a/W)$ is an appropriate function[†].

[*]Crack closure is a phenomenon which the crack remains in a closed position even though the tensile force is applied on the test specimen (ANDERSON, 2005).

[†]Function of the specimen geometry.

For a CT specimen (See Figure 1.3 on page 7) and $\alpha := a/W$, one has that

$$g(\alpha) = \frac{(2+\alpha)(-5.6\alpha^4 + 14.72\alpha^3 - 13.32\alpha^2 + 4.64\alpha + 0.886)}{(1-\alpha)^{3/2}} \tag{4.2}$$

holds for $0.2 \leq \alpha \leq 1.0$.

Therefore, from (4.1) it is apparent that ΔK is a function of the crack propagation. The crack propagation a can be obtained experimentally by adjusting a polynomial to the points given in Table B.1 (2^{nd} and 3^{rd} columns), see Figure 4.1a. Applying finite difference w.r.t. N, one can directly compute da/dN. Here, however, a more elaborate method (named "Incremental Polynomial Method") is used. Moreover, ΔK can be computed using the data in Table B.1 (5^{th} column in Table B.1) and applying Eq. (4.1).

In Figure 4.1b, a typical relationship between the crack growth rate da/dN and ΔK is depicted. It must be highlighted that the Paris' law describes the linear interval of the curve $\Delta K \times da/dN$ illustrated in Figure 4.1b.

Under a fatigue stress regime, ΔK can be characterized by the well known **Paris' Law**[‡] which is described as

$$\frac{\mathrm{d}a}{\mathrm{d}N} = C\Delta K^M\,, \tag{4.3}$$

where

a is the crack length in [mm],

C and M are appropriate constants, and

N is the number of load cycles.

The relationship between *fracture toughness*[§] (K) and the crack size (a) is described by

$$K = Y\sigma\sqrt{\pi a}$$

where

[‡]Also known as **Paris-Erdogan law**.

[§]Fracture toughness is a property which describes quantitatively the ability of a material to resist fracture (ANDERSON, 2005).

Y is the geometry correction factor, and

σ is the stress applied at the specimen [MPa].

Then, a quantitative estimation of *residual life* (number N_f of load cycles before reaching the critical stress intensity factor) for a crack can be determined as follows.

By using experimental data, the fatigue residual life of a specific material can be estimated. Indeed, by separating the variables and rearranging the Pariślaw one can write (ANDERSON, 2005),

$$\frac{\mathrm{d}a}{\mathrm{d}N} = C\Delta K^M = C\left(Y\Delta\sigma\sqrt{\pi a}\right)^M$$

$$\therefore \quad N_f = \int_0^{N_f} \mathrm{d}N = \int_{a_0}^{a_f} \frac{\mathrm{d}a}{CY^M\left(\Delta\sigma\right)^M\left(\pi a\right)^{M/2}}\,. \tag{4.4}$$

The stress/force ratio (R) is the ratio between the minimum and maximum values of K (or F) in a load cycle, depending on the fatigue test mode (constant intensity stress factor or constant load force). From Table B.1 one has that

$$R = \frac{F_{min}}{F_{max}} = 0.8\,,$$

and, since

$$\Delta F = F_{max} - F_{min} = 4.4 \times 10^3 [\,\mathrm{N}\,]\,,$$

then $F_{max} = 2.22 \times 10^4\,[\,\mathrm{N}\,]$ and $F_{min} = 1.78 \times 10^4\,[\,\mathrm{N}\,]$.

As discussed in (SHIH; WEI, 1973), no crack closure was observed for stress ration greater than 0.3 in titanium alloy. Note that, in the present case $R = 0.8$, thus no crack closure is expected. Moreover, the crack opening can be indirect estimated based on experimental measurement of specimen compliance variation (SARZOSA *et al.*, 2013) as depicted in Figure 4.2.

In fact, from (ASTM E1820, 2008, A12.2, p. 32), the compliance[¶] C of a specimen

[¶]Compliance, $C := v/F$, is the ratio of displacement(v) to force increment (F).

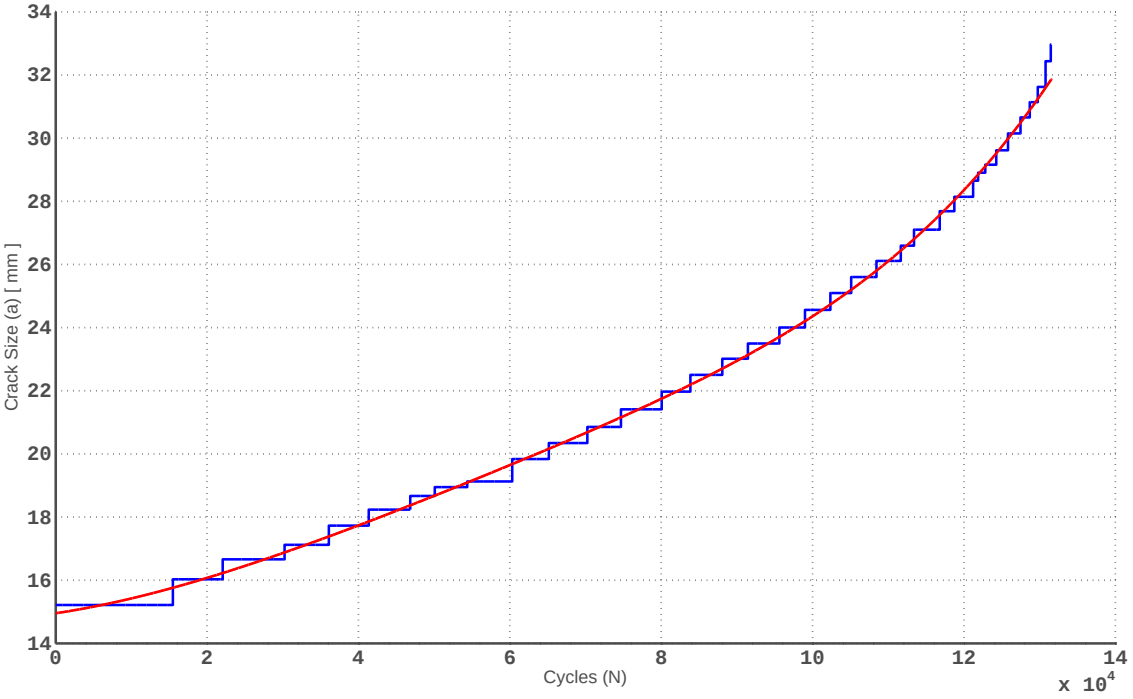

(a)

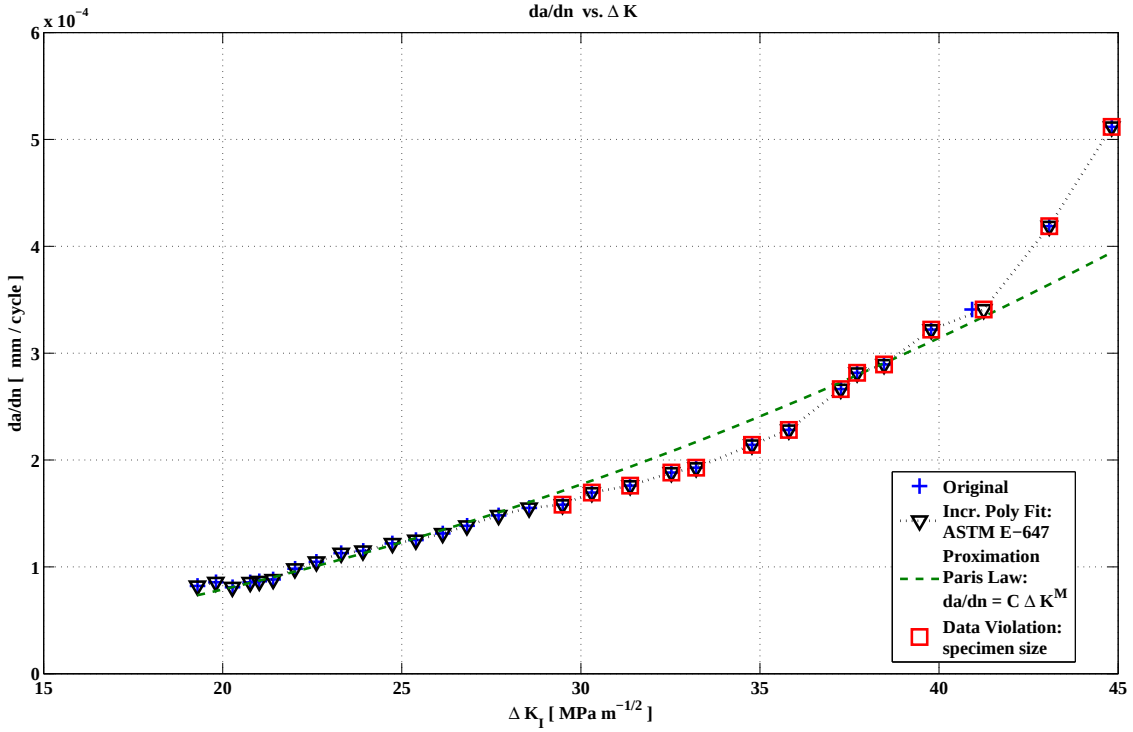

(b)

Figure 4.1: Experimental data: (a) $a \times N$, (b) da/dN *versus* ΔK.

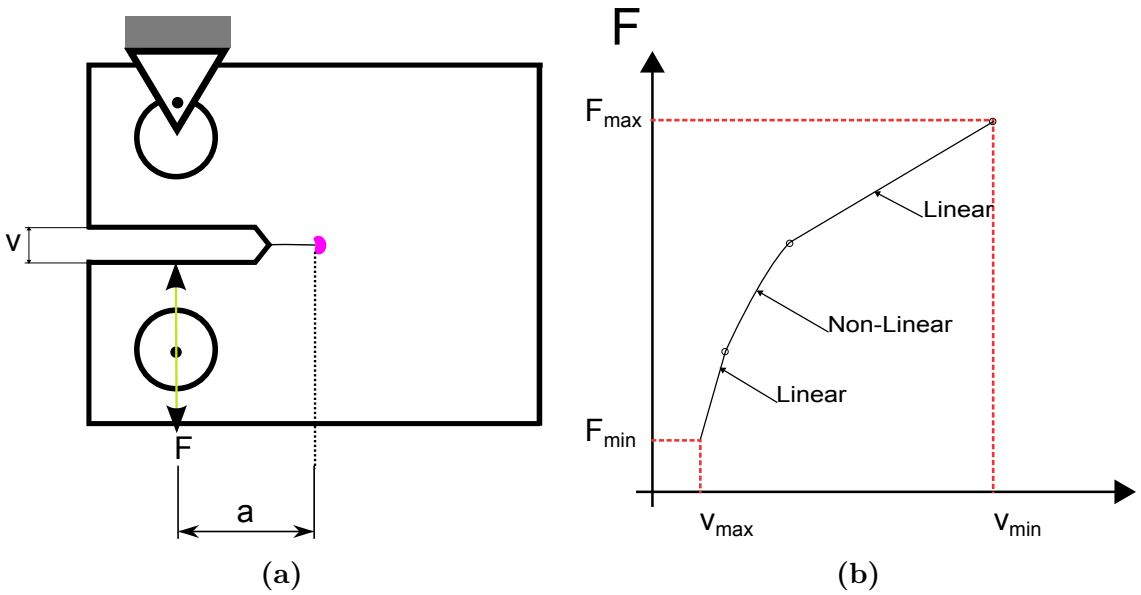

Figure 4.2: Schematics of closure effects of cyclic load versus crack opening displacement for a CT specimen: (a) crack closure measurement location on CT specimen. (b) load-displament menasurement with crack mouth opening displacement (CMOD) and its distinct regions depending on the measured compliance.
Source: adapted from (SARZOSA *et al.*, 2013).

is given by the following function of the crack length:

$$C := \frac{v}{F} = \frac{Y^2}{B_e E'} h(\alpha)\,, \tag{4.5}$$

where

v is the total displacement measured by clip gauges or other devices spanning the crack faces [m],

F is the force applied to the specimen [m],

Y is the location of the clip-gauge [m],

B_e is the effective thickness of the specimen [m],

$E' := E/(1-\nu^2)$ is the effective Young's modulus.

For a CT specimen, the function $h(\alpha)$ is given by

$$h(\alpha) = (2.163 + 12.219\alpha - 20.065\alpha^2 - 0.9925\alpha^3 + 20.609\alpha^4 - 9.9314\alpha^5)\,. \tag{4.6}$$

In fact, by using the experimental data from Table B.1, Eq. (4.5) and Eq. (4.6), the specimen stiffness constant can be estimated as depicted in Figure 4.3.

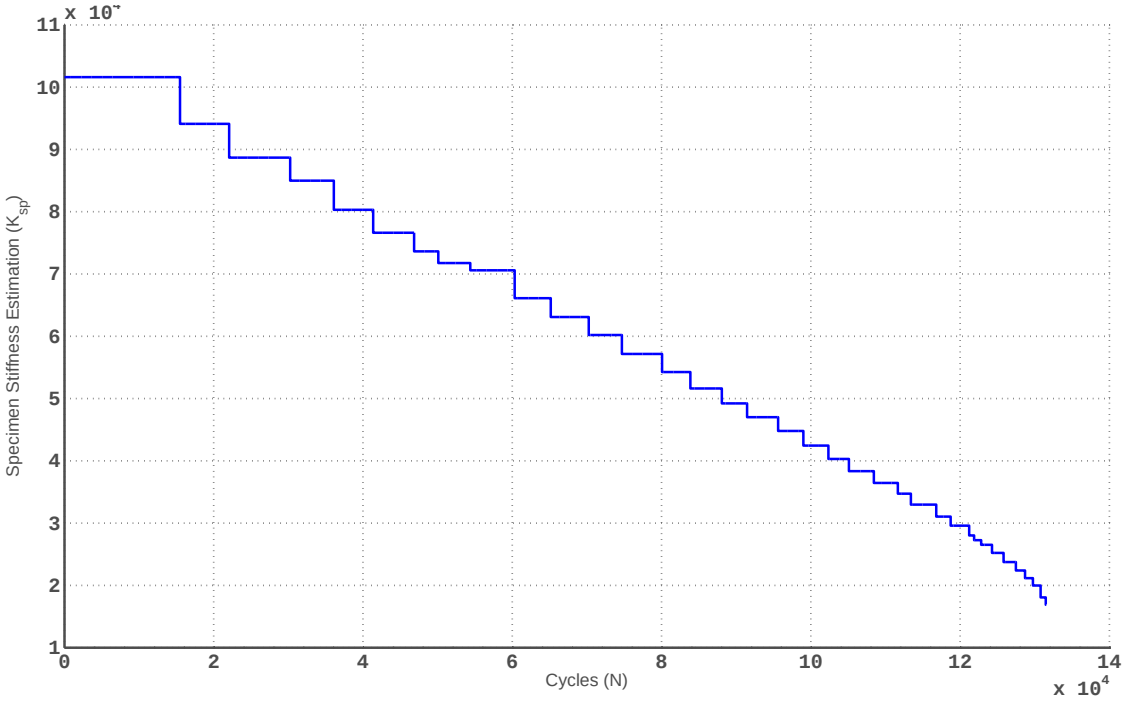

Figure 4.3: Time varying equivalent specimen stiffness constant estimation (K_{sp}) based on compliance.

The nominal value of K_{sp} is given by

$$K_{sp}^{nom} := \frac{1}{C(\alpha)}\bigg|_{\alpha=a_0/W} = 1.04 \times 10^5 \, [\mathrm{N\,mm^{-1}}].$$

Figure 4.3 suggests that C varies with time in a similar fashion as a grows, depicted in Figure 4.1a. The time varying curve of the K_{sp} shown in Figure 4.3 is considered for simulation. Finally, here onwards the crack is considered to be fully open and the specimen compliance remains constant and the crack closure in fatigue is neglected without the lost of generality.

4.1 Preliminary results

In order to illustrate that K_{sp} may causes closed-loop performance degradation in fatigue tests, a simple proportional controller is considered (see Figure 4.4). First,

recall that the plant dynamics (from the control input to the piston position) is a simple integrator Eq. (3.6).

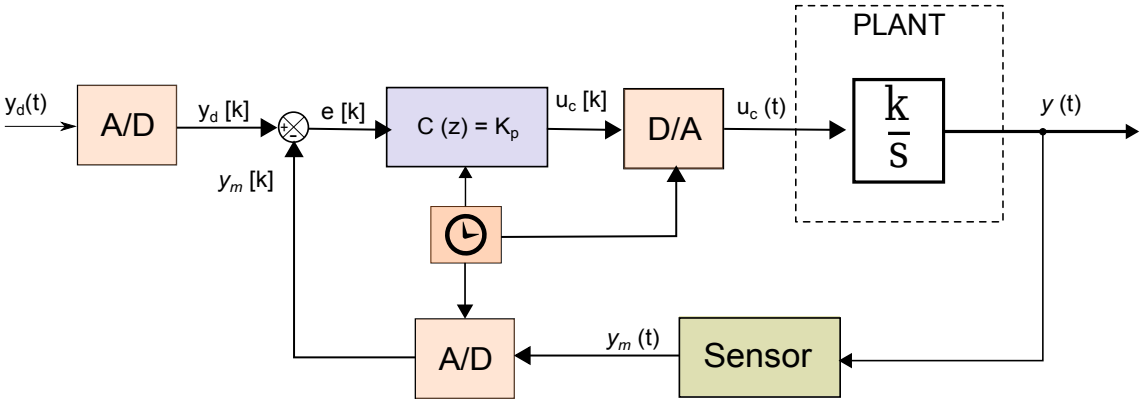

Figure 4.4: Position control scheme with $k = -0.07$ and $K_p = 100$.

By applying proportional control for position tracking, it is evident that the plant is a simple integrator. The results are illustrated in Figure 4.5. It is apparent that a proportional controller can provide satisfactory closed-loop performance. However, it worth to mention that a feed-forward control action being a function of time derivative of the reference signal could improve tracking performance. The results depicted in Figure 4.5b corroborate the relationship

$$\frac{Y(s)}{U(s)} \approx \frac{-0.07}{\mathrm{s}}\,.$$

On the other hand, for the force control case, a fixed gain proportional controller may not be able to keep force tracking in the desired levels required by the fatigue test norm. Indeed, from Figure 4.6 and Figure 4.7, one can verify that the fatigue test norm is violated when the K_{sp} changes by jumps.

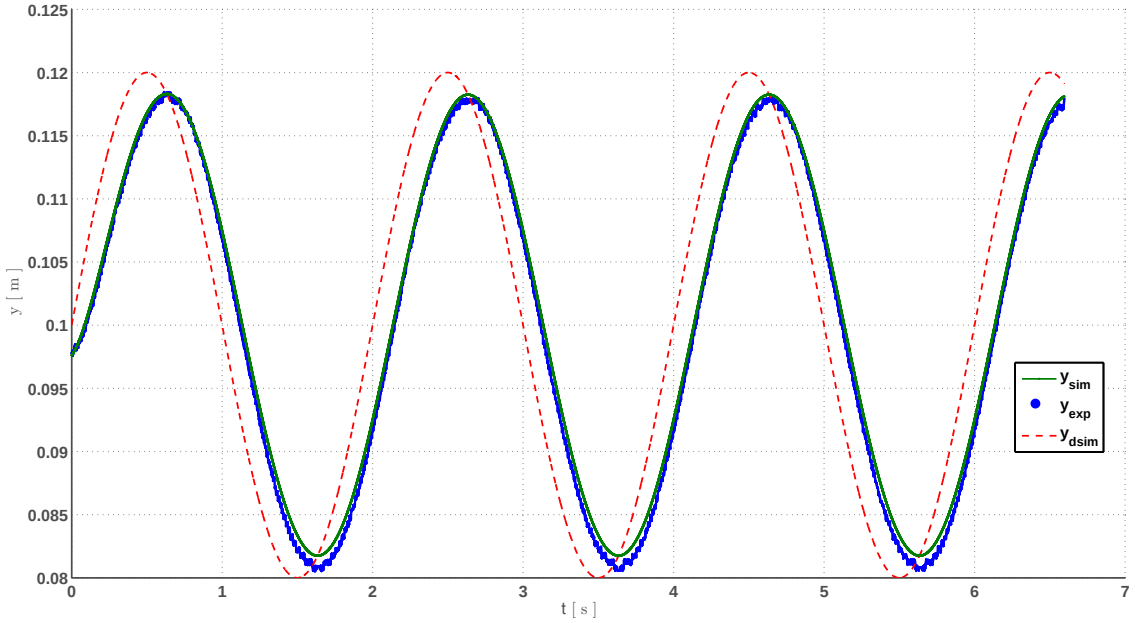

(a)

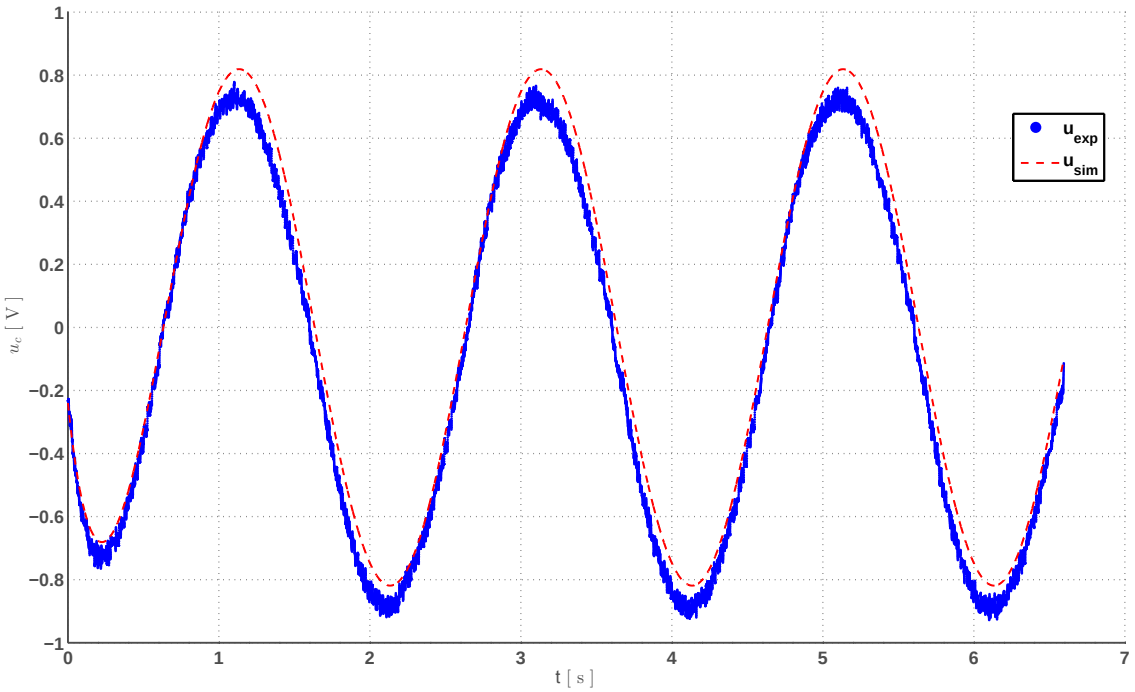

(b)

Figure 4.5: Experimental and simulation results for piston position tracking using a simple proportional controller: (a) piston position and (b) control signal.

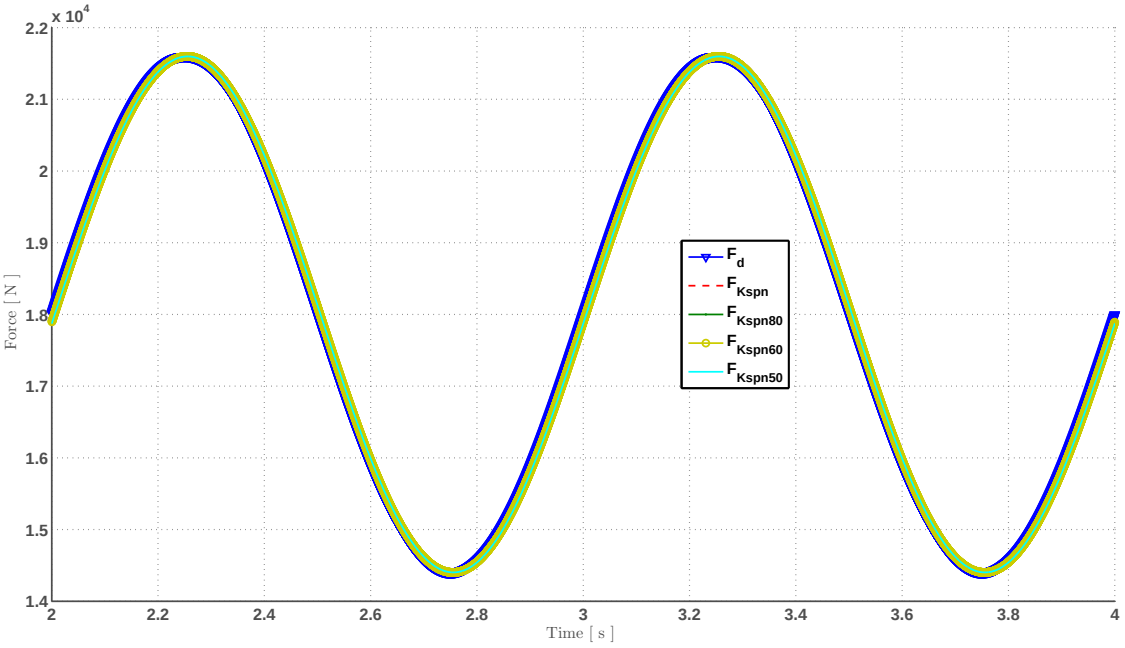

(a)

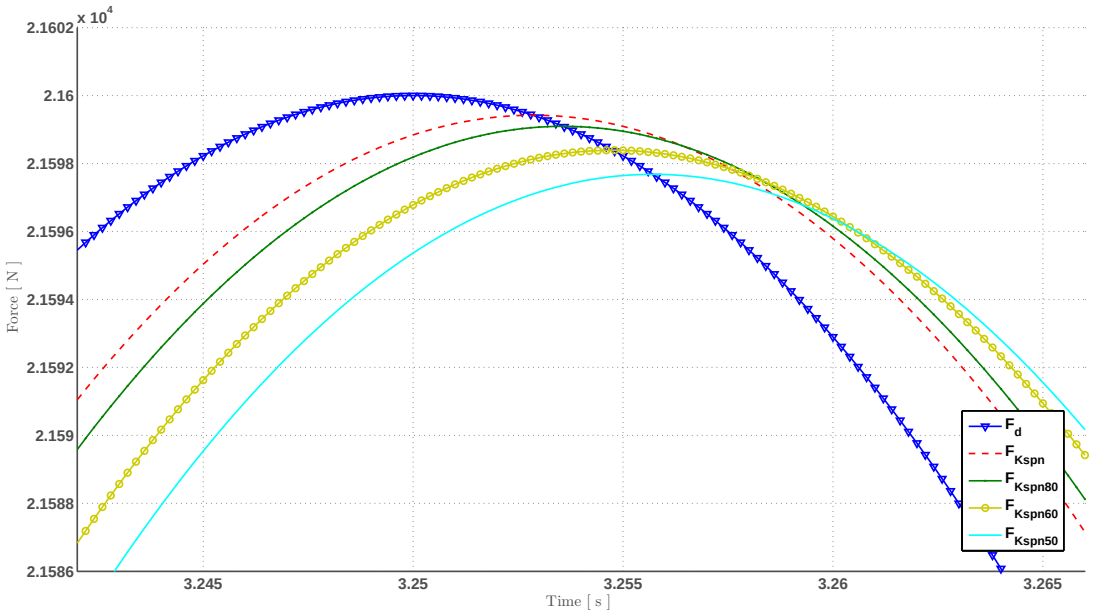

(b)

Figure 4.6: Simulation results for force tracking with a simple fixed gain proportional controller: (a) force time behavior and (b) zoom in the force time behavior. F_d is the desired force, F_{spn} is the force considering the nominal value of the specimen stiffness constant when $a = a_1$, F_{spn80} is the force considering 80% of its nominal value, F_{spn60} is the force considering 60% of its nominal value and F_{spn50} is the force considering 50% of its nominal value.

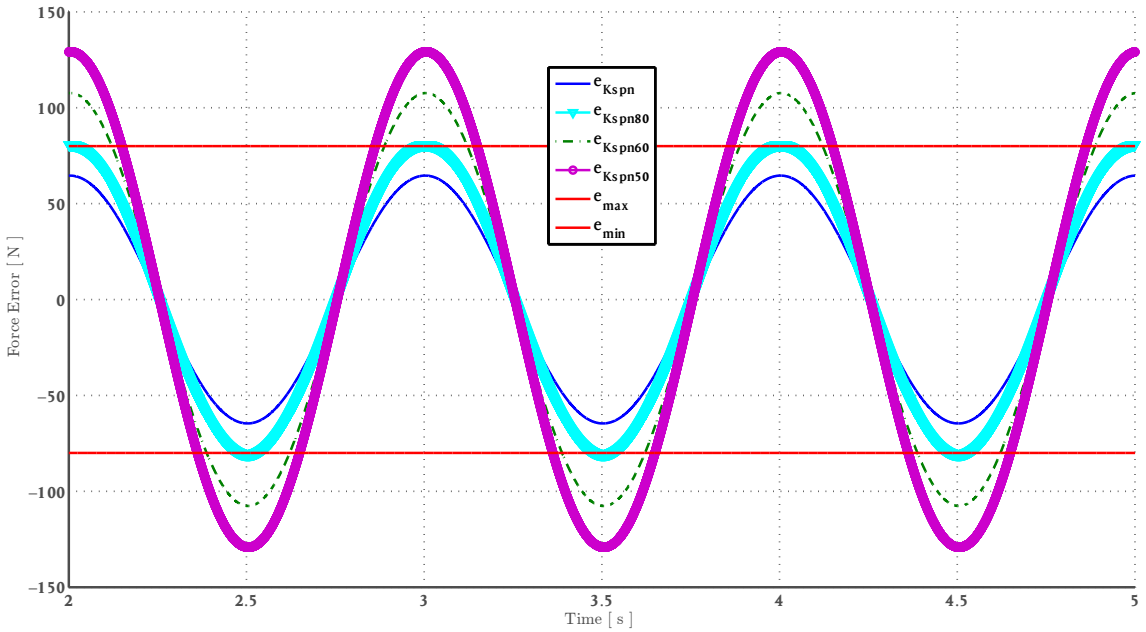

(a)

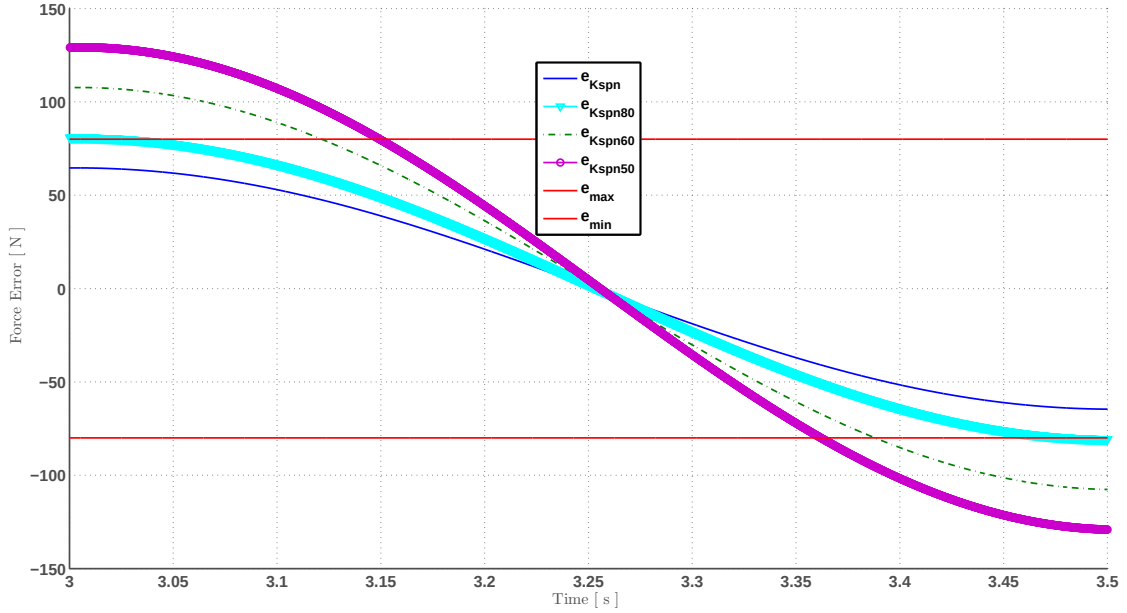

(b)

Figure 4.7: Simulation results for force tracking with a simple fixed gain proportional controller: (a) force error time behavior and (b) zoom in the force error time behavior.. The red solid line are the maximum deviations excepted by (ASTM E647, 2008). The blue solid line represents the error e_{Kspn} considering the nominal value of the specimen stiffness constant when $a = a_1$, e_{Kspn80} is the error considering 80% of its nominal value, e_{Kspn60} is the error considering 60% of its nominal value and e_{Kspn50} is the error considering 50% of its nominal value.

The closed-loop system with a proportional control (fixed gain) was simulated considering that K_{sp} varies as shown in Figure 4.3. The results are shown in Figure 4.8. Note that the fatigue test norm is violated after 2500 cycles.

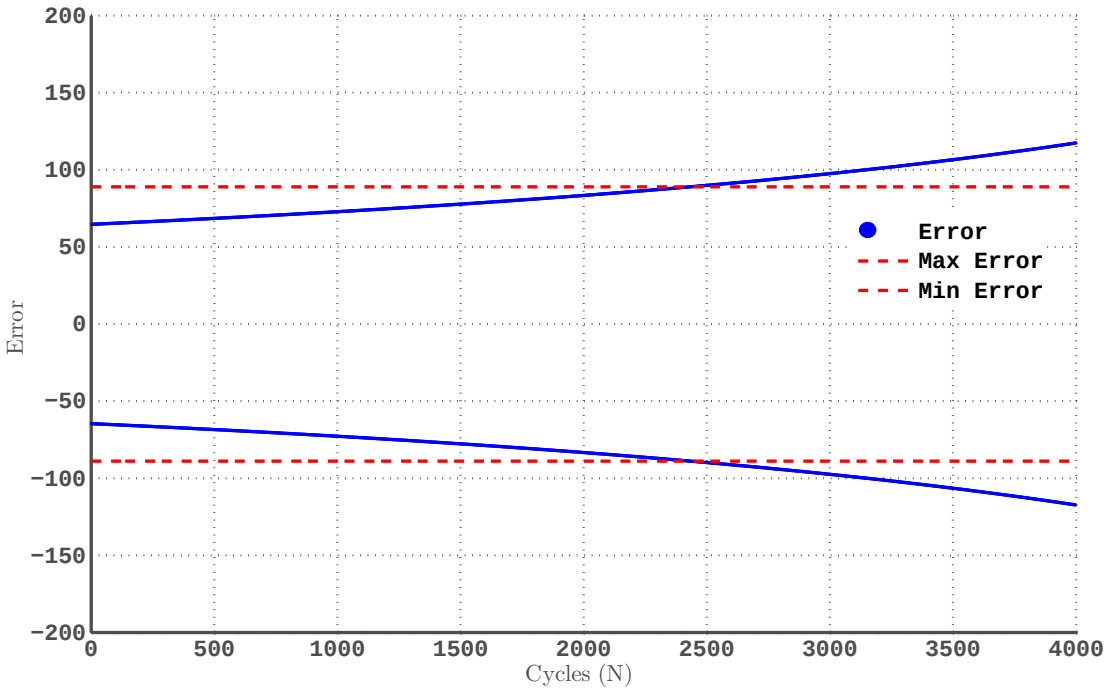

Figure 4.8: Simulation results: force time behavior. The blue line corresponds to the force oscillations envelop. The red line corresponds to the maximum force error allowed by the fatigue test norm.

4.2 Proposed force control

In order to simplify the notation, here onwards, the force applied at the specimen is considered as the plant output y. Moreover, the plant is represented by a integrator (with time varying gain) with input u being the valve input command.

The plant can be described by

$$\dot{y} = -0.07 K_{sp}\, u\,,$$

where K_{sp} varies slowly with time, that is, $\dot{K}_{sp} \approx 0$.

If the HTM force control reaches its steady state, it is desired that the associated force output signal can be approximated by the *desired trajectory* $y_d(t)$ which is

assumed to be in the form

$$y_d(t) = \theta_1^d \sin(\omega t) + \theta_2^d, \tag{4.7}$$

where ω is the (known) fatigue testing frequency, θ_1^d is the desired amplitude for the force oscillations while θ_2^d is the corresponding mean value.

Thus, by restricting the class of admissible control signals to be of the form $u(t) = u_1(t)\cos(\omega t) + u_2(t)$, during the transient process of the HTM force control, the output signal can be characterized as $y(t) = \theta_1(t)\sin(\omega t) + \theta_2(t)$ for appropriate control signals $u_1(t)$ and $u_2(t)$ and output signals $\theta_1(t)$ and $\theta_2(t)$. In other words, the plant output presents a sinusoidal wave of time-varying amplitude.

The force applied to the specimen during a fatigue test must be precisely controlled. The desired peak force during the test is required to be maintained within $\pm 2\%$ of the desired range.

The aim of the control law u is to drive the *output tracking error*

$$e(t) = y(t) - y_d(t) \tag{4.8}$$

to zero or to some small neighborhood of zero (practical tracking). However, since in the fatigue test context the phase shift between y and y_d is irrelevant, the tracking problem is reformulated as two regulation problems as follows.

Reducing tracking to regulation

In fact, the tracking problem can be formulated as a regulation problem which consists in finding an output-feedback control law $u(t) = u_1(t)\cos(\omega t) + u_2(t)$ such that both output errors $e_1 = \theta_1 - \theta_1^d$ and $e_2 = \theta_2 - \theta_2^d$ tend to a neighborhood of zero as $t \to \infty$.

The main idea is to reduce the tracking problem into two regulation problems: force oscillation amplitude regulation and force DC-component regulation, see Figure 4.9.

Amplitude and DC component estimator

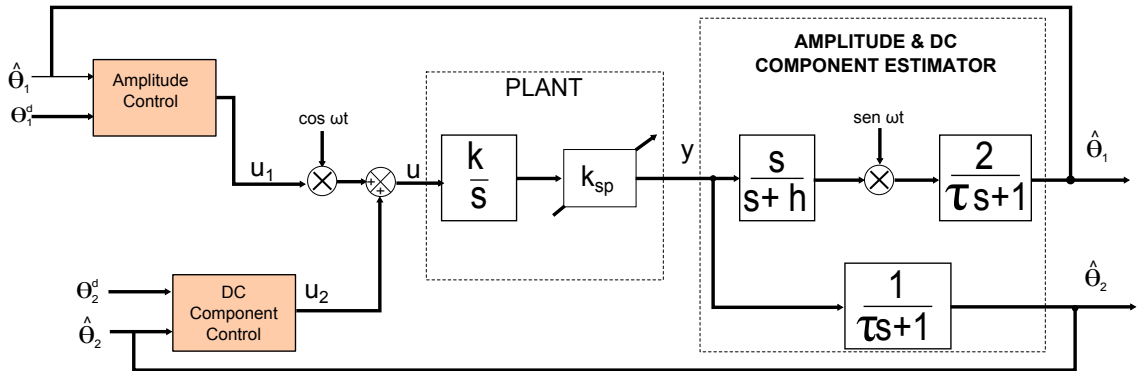

Figure 4.9: The proposed force control. The main idea consists in two separated control strategies: one for the force oscillation amplitude and other one for the force DC-component.

Since the output y is assumed to be of the form $y(t) = \theta_1(t)\sin(\omega t) + \theta_2(t)$ one can obtain estimatives for the amplitude θ_1 and the DC-component θ_2 as follows.

The amplitude θ_1 can be estimate by[‖]

$$\hat{\theta}_1 = \frac{2}{\tau s + 1}\left[\sin(\omega t) z(t)\right] ,$$

where τ is a positive design constant and z is the output of the high pass filter

$$z = \frac{s}{s+h} y = y - \frac{h}{s+h} y ,$$

The high pass filter $\dfrac{s}{s+h}$, applied to the output in the form $y = \theta_1(t)\sin(\omega t) + \theta_2(t)$, serves to remove $\theta_2(t)$, i.e.,

$$\frac{s}{s+h} y \approx \theta_1(t)\sin(\omega t) .$$

This signal is then "demodulated" by multiplication with $\sin(\omega t)$ giving

$$\theta_1(t)\sin^2(\omega t) .$$

Now, since $2\sin^2(\omega t) = 1 - \cos(2\omega t)$ only the DC component pass through the law

[‖]The symbol "s" represents either the Laplace variable or the differential operator "d/dt", according to the context. The output y of a linear time invariant (LTI) system with transfer function $H(s)$ and input u is denoted by $y = H(s)u$.

pass filter $\frac{2}{\tau s+1}$. Hence, $\hat{\theta}_1 \approx \theta_1$.

The mean value can be directly estimated via first order linear filtering. The following estimate is considered

$$\hat{\theta}_2 = \frac{1}{\tau s+1} y \,.$$

The proposed control law

An integral controller $u_1(t)$ is proposed to drive the error signal $e_1(t) = \hat{\theta}_1 - \theta_1^d$ to zero, i.e.,

$$u_1 = \frac{k_1}{s} e_1 \,,$$

and a proportional control law is employed to reduce the error signal $e_2(t) = \hat{\theta}_2 - \theta_2^d$, i.e.,

$$u_2 = k_2 e_2 \,.$$

The proposed control law is then given by

$$u(t) = u_1(t)\sin(\omega t) + u_2(t) \,.$$

Stability analysis

The complete stability analysis is omitted, only a sketch of the proof is provided. The closed loop control scheme is illustrated in Figures 4.10a and 4.10b. First, by using the Averaging Analysis (KHALIL, 2001), one can disregard the high frequency terms (terms depending on the frequency ω) in both closed loops schemes illustrated in Figures 4.10a and 4.10b.

Therefore, for a fixed value of the spring constant K_{sp} it is evident from Figure 4.10b that $u_2(t)$ tends to zero as $t \to \infty$ for any positive value for k_2, due to the presence of the plant integrator in the closed loop. Moreover, the error signal $\tilde{\theta}_2$ also converges to zero as $t \to \infty$. Consequently, in the closed loop control system shown in Figure 4.10a, the control signal $u_2(t)$ can be regarded as a vanishing and uniformly norm bounded input disturbance. Thus, from a simple root locus analysis it is clear

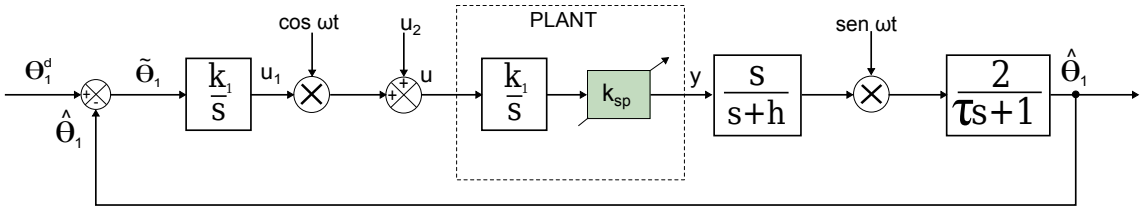

(a)

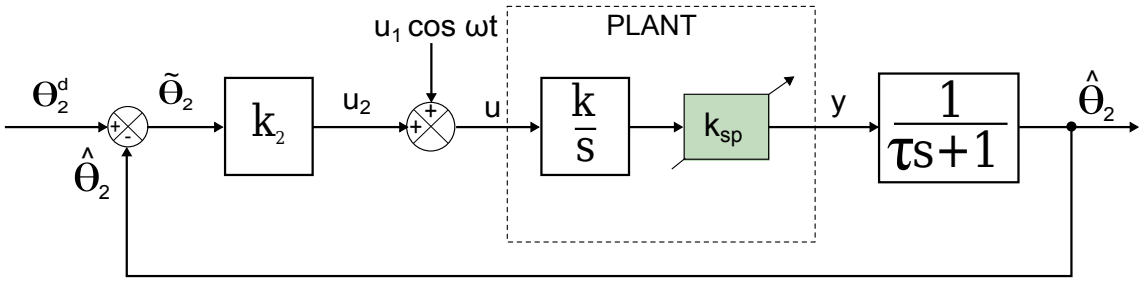

(b)

Figure 4.10: (a) force oscillations amplitude regulation and (b) force DC-component regulation.

that the closed loop system given in Figure 4.10a is stable for sufficient small gain $k_1 > 0$, leading to the conclusion that the error signal $\tilde{\theta}_1$ converges to zero as $t \to \infty$.

4.2.1 Simulation results

The aim of the following simulation is to evaluate the control performance with slow variations in K_{sp}, similar to what happens during real fatigue tests.

The plant model is $\dfrac{-0.07}{s}$ and the low and high pass filters are implemented with $\tau = 40$ and $h = 1/\tau$. The control gains k_1 and k_2 are: $k_1 = -4.5 \times 10^{-5}$ and $k_2 = -1 \times 10^{-4}$. The reference signal is a sinusoid such that y_d has amplitude $\theta_1^d = 2 \times 10^3$, DC-component $\theta_2^d = \ 20 \times 10^3$ and frequency equals to $1\,[\,\mathrm{Hz}\,]$. The plant initial condition is $y(0) = \theta_2^d / K_{sp}(0)$, this condition can be achieved with some pre-loading procedure. The equivalent specimen spring constant is initialized with the value $K_{sp}^{nom} = K_{sp}(0) = 1.04 \times 10^5$.

The data used in this simulation is based in real experimental procedure. The time varying behavior of K_{sp} is illustrated in Figure 4.11b in accordance with Figure 4.3

and the corresponding crack propagation is depicted in Figure 4.11a. The results are given in Figures 4.13a, 4.13b and 4.14. One can observe the closed loop control action by noting that the amplitude of the oscillations in the control signal increases with time as K_{sp} decreases, see Figure 4.12.

The corresponding force behavior and control effort are given in Figures 4.13 and 4.12, respectively. The increase in the amplitude of the control effort u_1 is a consequence of the specimen equivalent stiffness reduction depicted in Figure 4.12a. The corresponding piston position can be noted in Figure 4.14. It is important to observe that the fatigue testing requirements are not violated (ASTM E647, 2008), (ISO-12108, 2002) which are represented by the horizontal limits shown in Figures 4.13a and 4.13b.

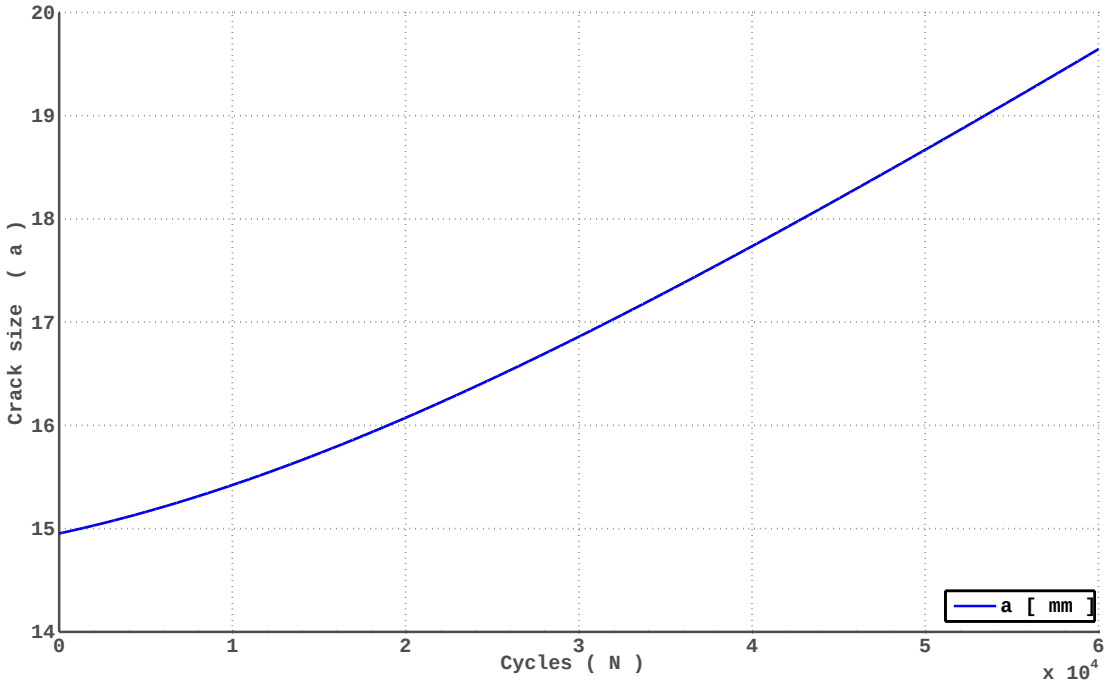

(a)

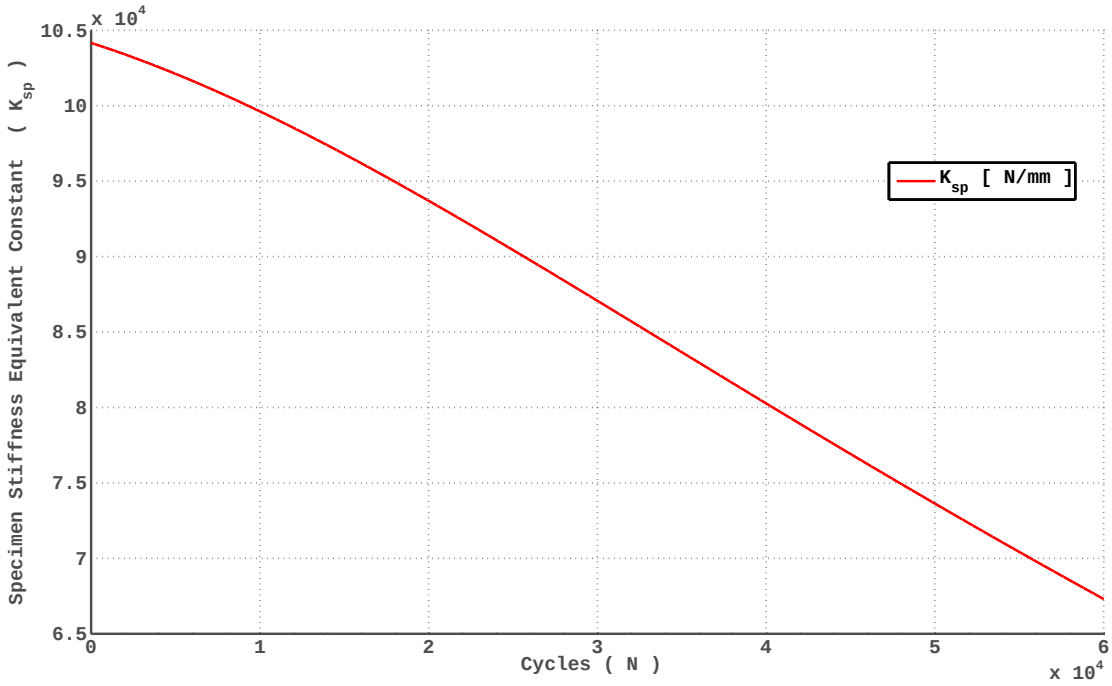

(b)

Figure 4.11: Simulation results: (a) crack propagation and (b) K_{sp} time varying behavior.

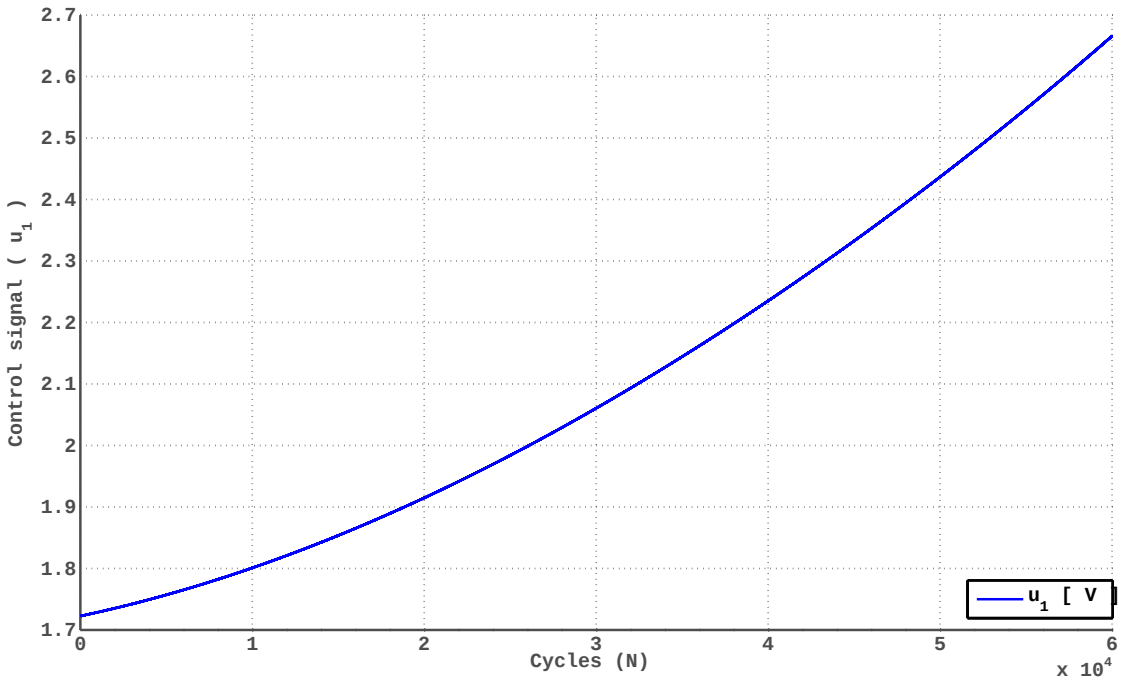

(a)

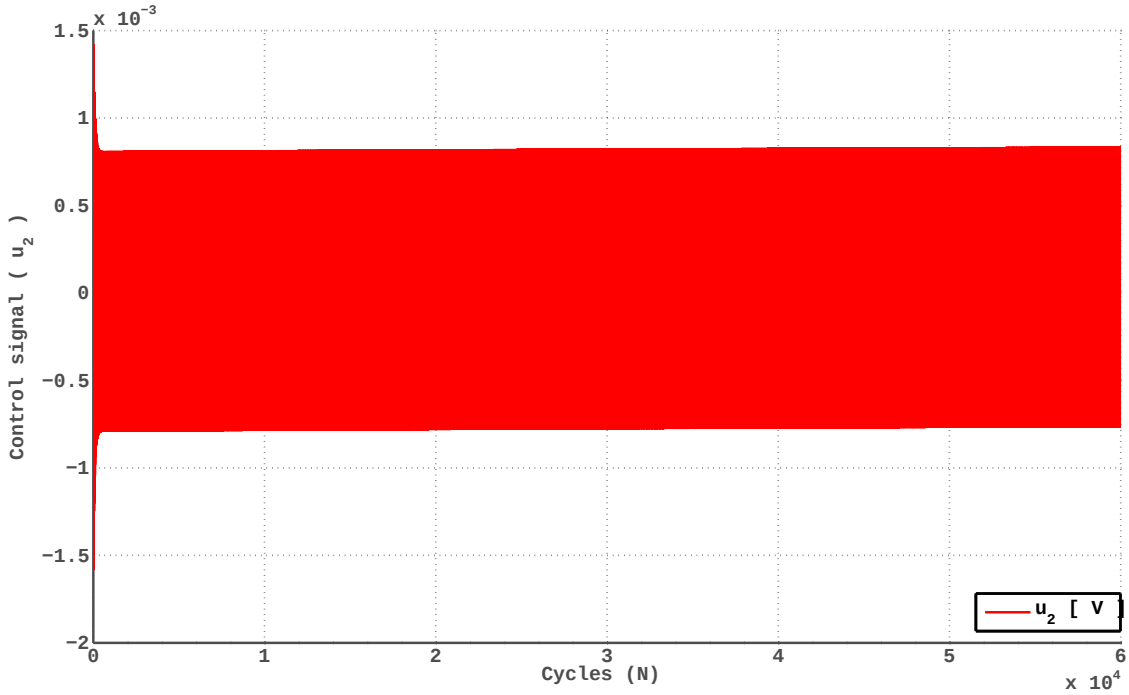

(b)

Figure 4.12: Simulation results: control signal (a) u_1 and (b) u_2.

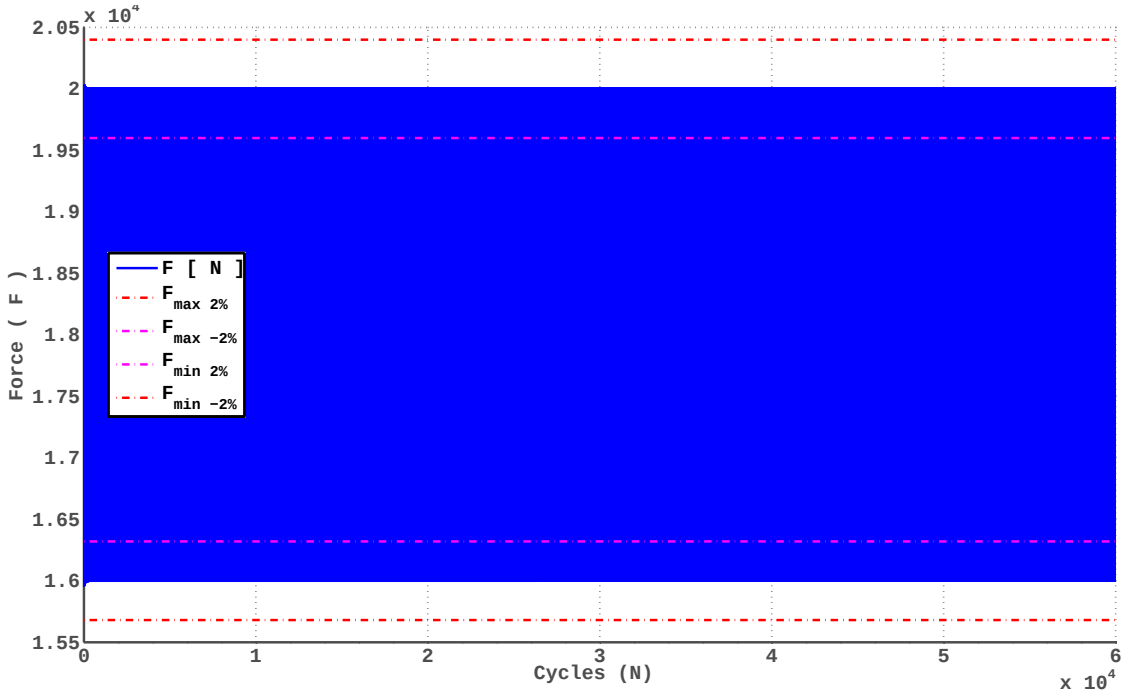

(a)

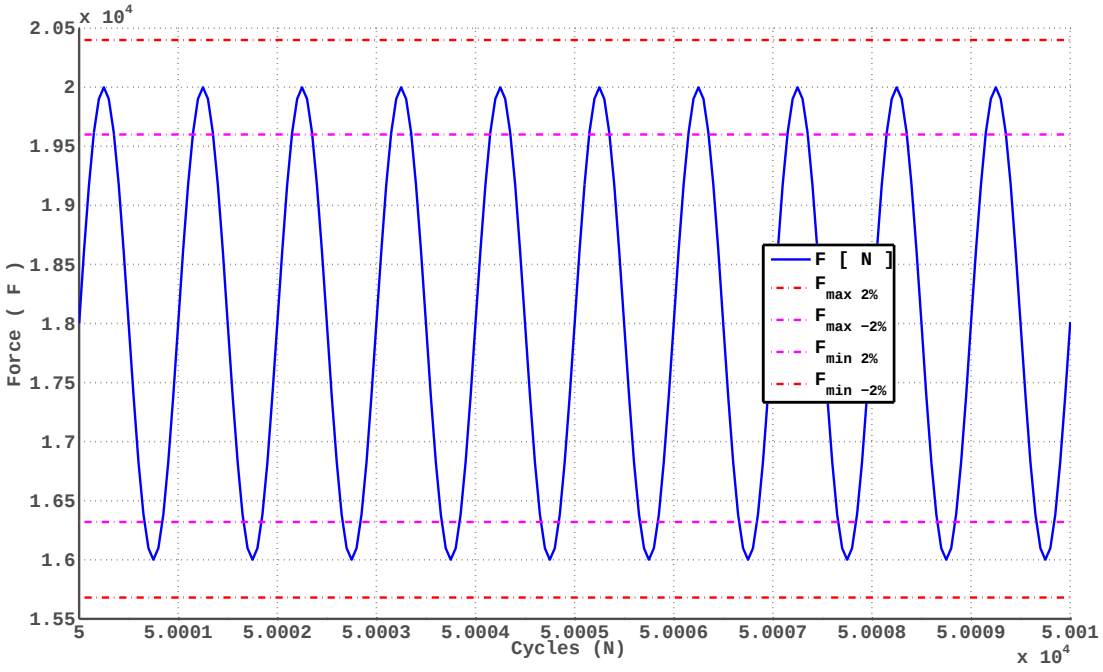

(b)

Figure 4.13: Simulation results: force applied at the specimen: (a) the entire fatigue test simulation (N =6 $\times$ 10^4) and (b) zoom around (N =5 $\times$ 10^4).

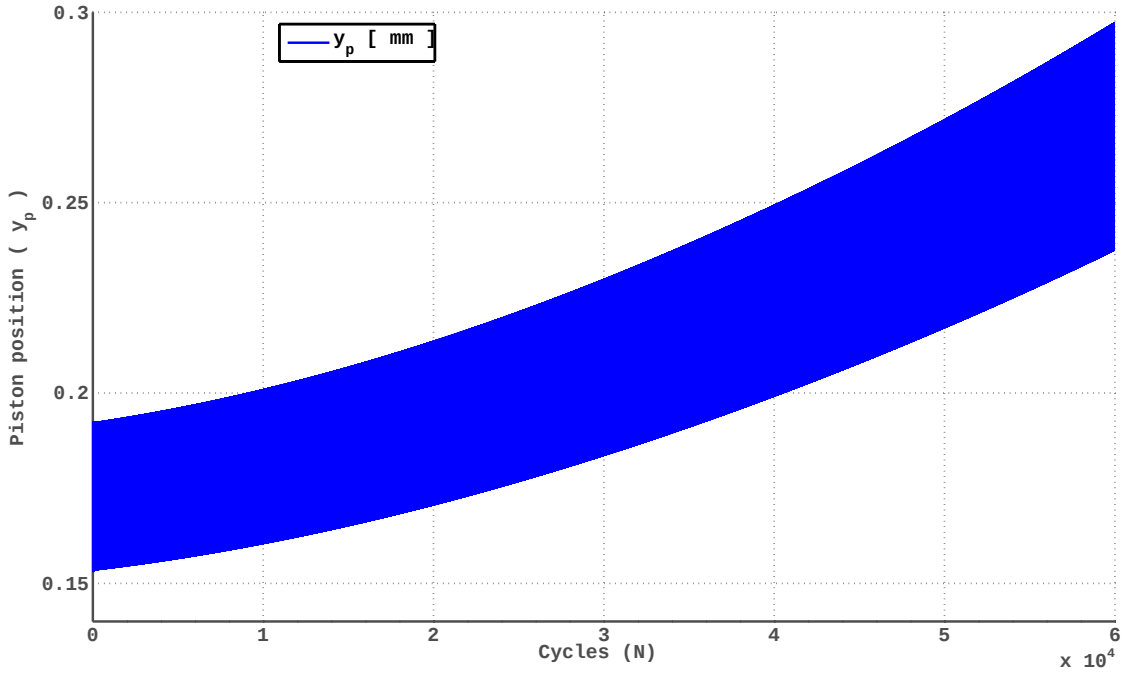

Figure 4.14: Simulation results: piston position.

Chapter 5

Conclusion and future work

The motivation for this work is a real engineering problem faced by the LNDC: to develop a fatigue testing machine for materials that are subjected simultaneously to mechanical stress, high pressure, and corrosive environment. Although there are many testing machines available on the market, soon it was realized that the literature is not specially rich in this context.

The testing machines focused in this dissertation are those hydraulically actuated. Thus, a detailed survey on this class of machines is provided. In particular, the review focuses on the modeling and control aspects of hydraulic systems. The main issues are identified and detailed explained. Theory and standards for the fatigue testing are also presented including a discussion of the most relevant variables and parameters for a test.

For operations at low frequencies, a simple model for control design is obtained. It is shown that the hydraulic actuated testing machine can be modeled by a simple integrator from the servo-valve input to the piston position. The integrator gain is identified and validated. As a result, its control is quite simple. Indeed, a proportional control can solve satisfactorily the position tracking problem. However, a more elaborate control scheme is needed to solve the force tracking problem.

It is well known that the fatigue testing evolves, the specimen crack increases while its equivalent stiffness constant reduces with time. Although, the specimen and force feedback are not available in the test bench, it is verified via numerical

simulation that the specimen equivalent stiffness variation can be compensated by an appropriate force feedback. Indeed, by applying a sinusoidal modulated control signal, it is possible to regulate the force amplitude and mean value within the fatigue testing standards. The feasibility of this control strategy is evaluated via numerical simulations even when the equivalent stiffness constant is subjected to jumps.

On the other hand, for operations at high frequencies, it is verified that a more elaborated model for the actuation system is required to assure a high-performance of the closed-loop position/force control. In this sense, friction force and servo-valve dynamics identification are required.

It is verified that Coulomb and Stribeck friction forces are needed for an accurate friction modeling at low velocities.

Some topics for future work are:

- Investigate the effect of the valve dynamics and nonlinearities when taken into account.
- Investigate the behavior of the closed-loop system including the specimen and force feedback information.
- Investigate other force control strategies. Adaptive control schemes should be considered for analysis and experiments.

References

AGUIRRE, L. A. **Introdução À Identificação de Sistemas**: técnicas lineares e não-lineares aplicadas a sistemas reais. 3.ed. Belo Horizonte, MG, Brasil: Editora UFMG, 2007.

AHN, K. K.; DINH, Q. T. Self-tuning of quantitative feedback theory for force control of an electro-hydraulic test machine. **Control Engineering Practice**, [S.l.], v.17, n.11, p.1291–1306, Nov 2009. .

AKERS, A. *et al.* **Hydraulic Power System Analysis (Fluid Power and Control)**. Boca Raton, FL, USA: CRC Press, 2006.

ALLEYNE, A.; HEDRICK, J. Nonlinear adaptive control of active suspensions. **IEEE Trans. Contr. Syst. Technol.**, [S.l.], v.3, n.1, p.94–101, Mar 1995. .

ALLEYNE, A.; LIU, R. A simplified approach to force control for electro-hydraulic systems. **Control Engineering Practice**, [S.l.], v.8, n.12, p.1347–1356, May 2000. .

ALVA, J. G. C. *Controle por Aprendizado de Sistemas Servo-Hidráulicos de Alta Frequência*. 2008. Dissertação de Mestrado — Pontifícia Universidade Católica do Rio de Janeiro, PUC-RIO, Rio de Janeiro, RJ, Brasil. .

ANDERSON, T. L. **Fracture Mechanics**: fundamentals and applications. 3.ed. Boca Raton, FL, USA: CRC Press: Taylor & Francis, 2005.

ANDERSON, W. **Controlling Electrohydraulic Systems**. 1.ed. New York: Marcel Dekker, Inc., 1989. .

ARMSTRONG-HÉLOUVRY, B. *et al.* A survey of models, analysis tools and compensation methods for the control of machines with friction. **Automatica**, Tarrytown, NY, USA, v.30, n.7, p.1083–1138, July 1994. .

ASTM E1820. **ASTM E1820-08 – Standard Test Method for Measurement of Fracture Toughness**. West Conshohocken, PA, USA: American So-

ciety for Testing and Materials (ASTM International), 2008. Standard Practice, .

ASTM E647-08e1. **ASTM E647-08e1 – Standard Practice for Verification of Constant Amplitude Dynamic Forces in an Axial Fatigue Testing Systems**. West Conshohocken, PA, USA: American Society for Testing and Materials (ASTM International), 2011. Standard Practice, .

ASTM E647. **ASTM E647-08 – Standard Test Method for Measurement of Fatigue Crack Growth Rates**. West Conshohocken, PA, USA: American Society for Testing and Materials (ASTM International), 2008. Standard Practice, .

ASTM E648-11. **ASTM E648-11 – Standard Practice for Presentation of Constant Amplitude Fatigue Test Results for Metallic Materials**. West Conshohocken, PA, USA: American Society for Testing and Materials (ASTM International), 2011. Standard Practice, .

BAUER, G. **Ölhydraulik**: grundlagen, bauelemente, anwendungen (german edition). Wiesbaden, Deutschland: Vieweg+Teubner Verlag, 2011. .

BESSA, W. M. *et al.* Sliding Mode Control with Adaptive Fuzzy Dead-Zone Compensation of an Electro-Hydraulic Servo System. **Journal of Intelligent and Robotic Systems**, Hingham, MA, USA, v.58, n.1, p.3–16, Apr. 2010. .

BESSA, W. M. *et al.* An Adaptive Fuzzy Dead-Zone Compensation Scheme and its Application to Electro-Hydraulic Systems. **Jornal of Brazilian Society of Mechanical Science and Engineering**, [S.l.], v.XXXII, n.1, p.1–7, January-March 2010. .

BOSCH REXROTH. **Proportional pressure reducing valve, pilot operated – Type DRE(M) and DRE(M)E**. [S.l.]: Rexroth Bosch Group, 2003. Manual, .

BOSCH REXROTH. **Direction servo valve in 4 ways – Type 4WS.2E**. [S.l.]: Rexroth Bosch Group, 2005. Manual, .

BOSCH REXROTH. **Hydraulic cylinder mill type – Series CDH2 / CGH2 / CSH2**. [S.l.]: Rexroth Bosch Group, 2007. Manual, .

BOSCH REXROTH. **Analogue amplifier – Type VT-SR2**. [S.l.]: Rexroth Bosch Group, 2009. Manual, .

CALLISTER, W. **Fundamentals of materials science and engineering** : an interactive etext. New York: Wiley, 2001.

CANUDAS-DE-WIT, C.; GE, S. S. Adaptive friction compensation for systems with generalized velocity/position friction dependency. In: DECISION AND CONTROL, 1997., PROCEEDINGS OF THE 36TH IEEE CONFERENCE ON. **Anais...** [S.l.: s.n.], 1997. v.3, p.2465 –2470. .

CANUDAS-DE-WIT, C. *et al.* A new model for control of systems with friction. **IEEE Transactions on Automatic Control**, [S.l.], v.40, n.3, p.419–425, Mar. 1995. .

CLARKE, D. Adaptive control of a materials-testing machine. In: ADAPTIVE CONTROL (DIGEST NO: 1996/139), IEE COLLOQUIUM ON. **Anais...** IEE, 1997. .

COELHO, L. d. S.; CUNHA, M. A. B. Adaptive cascade control of a hydraulic actuator with an adaptive dead-zone compensation and optimization based on evolutionary algorithms. **Expert Systems with Applications**, [S.l.], v.38, n.10, p.12262–12269, Sep 2011. .

CULLEN, W. H. *et al.* **Automated Test Methods for Fracture and Fatigue Crack Growth (ASTM Special Technical Publication)**. West Conshohocken, PA, USA: ASTM, 1985. .

CUNDIFF, J. S. **Fluid Power Circuits and Controls**: fundamentals and applications (mechanical and aerospace engineering series). Boca Raton, Florida, USA: CRC Press, 2001. .

CUNHA, M. A. B. *Controle em Cascata de um Atuador Hidráulico*: contribuições teóricas e experimentais. 2001. Doutorado — Programa de Pós-Graduação em Engenharia Elétrica da Universidade Federal de Santa Catarina, Florianópolis, SC, Brasil.

CUNHA, M. A. B.; GUENTHER, R. Adaptive Cascade Control of a Hydraulic Actuator with an Adaptive Dead-Zone Compensation. **ABCM Symposium Series in Mechatronics**, [S.l.], v.2, p.385–392, 2006. .

CUNHA, M. Adaptive Cascade Controller Applied to a Hydraulic Actuator. **2005 International Conference on Control and Automation**, [S.l.], v.1, p.622 – 627, 2005. .

CUNHA, T. B. *Hydraulic Compliance Control of the Quadruped Robot HyQ*. 2013. Phd — University of Genoa. Istituto Italiano di Tecnologia (IIT), Genova, Italy. .

FILHO, J. R. B. R. *Análise Teórico-Experimental de Falhas em Válvulas Direcionais Servoproporcionais*. 2009. Dissertação de Mestrado — Programa de Pós-Graduação em Engenharia Mecância, Universidade Federal de Santa Catarina, Florianópolis, SC, Brasil. .

FLOHIL, J. J. *Active friction compensation in the hydraulic actuators of the Ampelmann system*. 2012. Master of Science — Delft University of Technology, Delft, The Netherlands. .

GUAN, C.; PAN, S. Adaptive sliding mode control of electro-hydraulic system with nonlinear unknown parameters. **Control Engineering Practice**, [S.l.], v.16, n.11, p.1275–1284, Nov 2008. , .

HOSFORD, W. **Mechanical behavior of materials**. Cambridge New York: Cambridge University Press, 2010.

BRAUN, A. A. *et al.* (Ed.). **Applications of Automation Technology in Fatigue and Fracture Testing and Analysis**: fourth volume (astm special technical publication// stp) (vol 4). West Conshohocken, PA, USA: ASTM International, 2002. .

ISO-12108. **ISO12108 — Metallic materials – Fatigue Testing – Fatigue Crack Growth Method**. [S.l.]: International Organization of Standardization (ISO), 2002. Standard Practice, .

ISO-1291-1. **ISO1291-1 — Fluid Power Systems And Components – Graphic Symbols And Circuit Diagrams – Part 1**: graphic symbols. [S.l.]: International Organization of Standardization (ISO), 2012. Standard Practice.

JELALI, M.; KROLL, A. **Hydraulic Servo-systems**: modelling, identification, and control. London New York: Springer, 2003. , .

KASPRZYCZAK, L.; MACHA, E. Selection of settings of the PID controller by automatic tuning at the control system of the hydraulic fatigue stand. **Mechanical Systems and Signal Processing**, [S.l.], v.22, p.1274–1288, Sept. 2008. .

KHALIL, H. K. **Nonlinear Systems**. 3rd edition.ed. [S.l.]: Prentice Hall, 2001.

KIM, M. Y.; LEE, C.-O. An experimental study on the optimization of controller gains for an electro-hydraulic servo system using evolution strategies. **Control Engineering Practice**, [S.l.], v.14, n.2, p.137 – 147, 2006. .

LEDEZMA-PÉREZ, J. A. *Controle Robusto de Força em Atuadores Hidráulicos Aplicando a Teoria de Realimentação Quantitativa*. 2012. Dissertação de Mestrado — Programa de Pós-Graduação em Engenharia Mecância, Universidade Federal de Santa Catarina, Florianópolis, SC, Brasil. .

LEE, S. R.; SRINIVASAN, K. Self-Tuning Control Application to Closed-Loop Servohydraulic Material Testing. **Journal of Dynamic Systems, Measurement, and Control**, [S.l.], v.112, n.4, p.680, 1990. .

LINSINGEN, I. v. **Fundamentos de Sistemas Hidráulicos**. Florianópolis, SC, Brasil.: Editora da UFSC, 2001. 399 p.p.

LNDC/COPPE/UFRJ. *Laboratório de Ensaios Não Destrutivos, Corrosão e Soldagem*. Disponível em: <http://www.metalmat.ufrj.br/lndc/english/about.htm>. Acesso em: 20 set. 2012.

MAKKAR, C. *et al.* A new continuously differentiable friction model for control systems design. In: ADVANCED INTELLIGENT MECHATRONICS. PROCEEDINGS, 2005 IEEE/ASME INTERNATIONAL CONFERENCE ON. **Anais...** [S.l.: s.n.], 2005. p.600–605. .

MERRITT, H. E. **Hydraulic Control Systems**. New York, USA: John Wiley & Sons, Inc., 1967. .

MORGAN, J. M.; MILLIGAN, W. W. A 1kHz Servohydraulic Fatigue Testing System. In: HIGH CYCLE FATIGUE OF STRUCTURAL MATERIALS, Warrendale, PA, USA. **Anais...** [S.l.: s.n.], 1997. p.pp. 305–312. .

NIKSEFAT, N.; SEPEHRI, N. Robust force controller design for a hydraulic actuator based on experimental input-output data. In: AMERICAN CONTROL CONFERENCE, 1999. PROCEEDINGS OF THE 1999. **Anais...** [S.l.: s.n.], 1999. v.5, p.3718 –3722 vol.5. .

OLSSON, H. *et al.* Friction Models and Friction Compensation. **European Journal of Control**, [S.l.], v.4, n.3, p.176 – 195, 1998. .

PELLOUX, R. M. N.; BROOKS, S. D. Hydraulic Tension-Compression Fatigue Machine. **Review of Scientific Instruments**, [S.l.], v.35, n.11, p.1564–1567, July 1964. .

PEREIRA-DIAS, D. *et al.* Control of Hydraulic Actuated Fatigue Testing Machines – A review. In: INTERNATION CONGRESS OF MECHANICAL ENGINEERING (COBEM2013), 22., Ribeirão Preto, SP. **Anais...** ABCM, 2013. p.9370–9381. .

PEREIRA-DIAS, D. *et al. Modelagem e identificação do Sistema de posicionamento de uma máquina hidráulica.* Submitted to 20th Brazilian Conference on Automation – 20 to 24 of September, 2014. Belo Horizonte, Brazil.

PEREIRA, P. I. I. *Análise Teórico-Experimental de Controlador Para Sistemas Hidráulicos.* 2006. Dissertação de Mestrado — Programa de Pós-Graduação em Engenharia Mecânica, UFSC, Florianópolis, SC, Brasil. .

PLUMMER, A. R. Robust electrohydraulic force control. **Proceedings of the Institution of Mechanical Engineers, Part I: Journal of Systems and Control Engineering**, [S.l.], v.221, n.4, p.717–731, Jan 2007. .

RABIE, M. G. **Fluid Power Engineering**. New York, NY, USA: The McGraw-Hill Companies, Inc., 2009. .

RODERMOND, S. *Modelling, identification and control of a multivariable hydraulic servo system.* 2006. Master Thesis — Technische Universiteit Eindhoven, Eindhoven, Nederlands. .

ROMANO, R. A.; GARCIA, C. Karnopp Friction Model Identification for a Real Control Valve. In: WORLD CONGRESS THE INTERNATIONAL FEDERATION OF AUTOMATIC CONTROL, 17., Seoul, Korea. **Proceedings...** [S.l.: s.n.], 2008. .

SÁNCHEZ, E. C. M. *et al.* Learning Control and Neuro-Fuzzy Learning Control to Increase the Frequency of Fatigue Tests. In: ABCM SYMPOSIUM SERIES IN MECHATRONICS, Rio de Janeiro, RJ, Brasil. **Anais...** [S.l.: s.n.], 2012. v.5, p.pp. 231–244. .

SARZOSA, D. F. *et al.* Fatigue crack growth assessments in welded components including crack closure effects: experiments and 3-D numerical modeling. **International Journal of Fatigue**, [S.l.], v.47, p.279–291, Feb 2013.

SCHWARTZ, C. *Modelagem e Análise de um dispositivo de amortecimento de fim de curso auto-ajustável para cilindros hidráulicos.* 2004. Dissertação de Mestrado — Programa de Pós-Graduação em Engenharia Mecânica, Universidade Federal de Santa Catarina, Florianópolis, SC, Brasil. .

SERRANO, M. I. *Controle de Força de um Servoatuador Hidráulico atráves da Técnica de Linearização por Realimentação*. 2007. Dissertação de Mestrado — Programa de Pós-Graduação Em Engenharia Elétrica – UFRGS, Porto Alegre, RS, Brasil. .

SHIH, T. T.; WEI, R. P. **A Study of Crack Closure in Fatigue**. Bethlehem, PA, USA: Lehigh University, 1973. Report.

SIROUSPOUR, M. R.; SALCUDEAN, S. On the Nonlinear Control of Hydraulic Servo-System. In: IEEE INTERNATIONAL CONFERENCE ON ROBOTICS & AUTOMATION, 2000., San Francisco, CA, USA. **Proceedings...** [S.l.: s.n.], 2000. , .

SIX, K. *et al.* A time-delayed dynamic inversion scheme for mechatronic control of hydraulic systems. In: ADVANCED INTELLIGENT MECHATRONICS, 2001. PROCEEDINGS. 2001 IEEE/ASME INTERNATIONAL CONFERENCE ON. **Anais...** [S.l.: s.n.], 2001. v.2, p.1232 –1238. .

SOHL, G. A.; BOBROW, J. E. Experiments and simulations on the nonlinear control of a hydraulic servosystem. **IEEE Transactions on Control Systems Technology**, Notre Dame, IN ,USA, v.7, n.2, p.238–247, Mar. 1999. .

STOTEN, D. P.; BENCHOUBANE, H. Robustness of a minimal controller synthesis algorithm. **International Journal of Control**, [S.l.], v.51, n.4, p.851–861, Jan 1990. , .

SZPAK, R. *Análise Teórico-Experimental do Comportamento das Pressões em Posicionadores Hidráulicos*. 2008. Dissertação de Mestrado — Programa de Pós-Graduação em Engenharia Mecância, Universidade Federal de Santa Catarina, Florianópolis, SC, Brasil. .

TANAKA, M. C. *et al.* Feedback Linearization with Fuzzy Compensation for Electro-Hydraulic Actuated Systems. In: *ABCM Symposium Series in Mechatronics - Vol. 5*. Rio de Janeiro, RJ, Brasil: ABCM, 2012. p.438–446. , .

TRAN, X. B. *et al.* Modeling of dynamic friction behaviors of hydraulic cylinders. **Mechatronics**, [S.l.], v.22, n.1, p.65–75, Feb 2012. , .

VALDIERO, A. C. *Controle de Robôs Hidráulicos com Compensação de Atrito*. 2004. Tese de Doutorado (D.Sc.) — Programa de Pós-Graduação em Engenharia Mecância, Universidade Federal de Santa Catarina, Florianópolis, SC, Brasil. .

VALDIERO, A. C. **Modelagem Matemática de Robôs Hidráulicos**. Ijuí, RS, Brasil: Editora Unijuí, 2012.

VOSSOUGHI, G.; DONATH, M. Dynamic Feedback Linearization for Electrohydraulically Actuated Control Systems. **Journal of Dynamic Systems, Measurement, and Control**, [S.l.], v.117, n.4, p.468, 1995. ,.

WANG, X. *An Active Disturbance Rejection Control Solution For Electro-Hydraulic Servo Systems*. 2012. Master Thesis — Cleveland State University, Clevand, USA. .

WEIBULL, W. **Fatigue Testing and Analysis of Results**. London, UK: Pergamon Press, 1961.

YAO, J. *et al.* Friction compensation for low velocity control of hydraulic flight motion simulator: a simple adaptive robust approach. **Chinese Journal of Aeronautics**, [S.l.], v.26, n.3, p.814 – 822, 2013.

Appendix A

Parameter set for simulation and experimental setup

The experimental implementation was conducted at LNDC of the Graduate Program in Metallurgical and Materials Engineering (PEMM) of the Federal University of Rio de Janeiro. This implementation is part of an initiative to development national technology for fracture mechanics and fatigue testing.

The test bench is shown in Figure A.1 and it is composed of: a load cell, a double-rod cylinder, a SV, an accumulator, a relief valve, filtering system, cooling system and a fixed displacement pump (BOSCH REXROTH, 2007), (BOSCH REXROTH, 2005), (BOSCH REXROTH, 2009), (BOSCH REXROTH, 2003). Tables A.1, A.2, A.3 and A.4 describe each individual component.

Table A.1: Technical Details of servo valve (SV)

	DESCRIPTION	UNIT
Manufacture	Bosch Rexroth	
Model	4W2S2M10-51/75B11ET315K31EV	
MRN	RP900909219	
Product	Servo valve for external electronics, two stage, with mechanical feedback	
Electrical operator	Torque-motor	
Filtering	necessary (high level of contamination)	
Hysteresis	~ 0.1 to 0.5 %	
Maximum Freq.	100.0 to 200.0 [Hz]	
Nominal flow rate at ΔP =70 [bar]	75	[$\mathrm{L\,min^{-1}}$]
Control signal	± 60	[mA]
External control electronics	VT-SR2-12/1-60	
MRN	RP	
Input signal	± 10	[V]

Table A.2: Technical Details of double-rod cylinder

	DESCRIPTION	UNIT
Manufacture	Bosch Rexroth	
Model	CGH2MF3/80/56/200	
MRN		
Piston area	$Ap = 5.0265 \times 10^{-4}$	[$\mathrm{m^2}$]
Rod area	$Ar = 2.5635 \times 10^{-4}$	[$\mathrm{m^2}$]
Stroke length	$L = 200 \times 10^{-3}$	[m]
Maximum displacement velocity	$\dot{y} \mid_{\max} = 5 \times 10^{-1}$	[$\mathrm{m\,s^{-1}}$]
Maximum operating pressure	$P_s \mid_{\max} = 25$	[MPa]

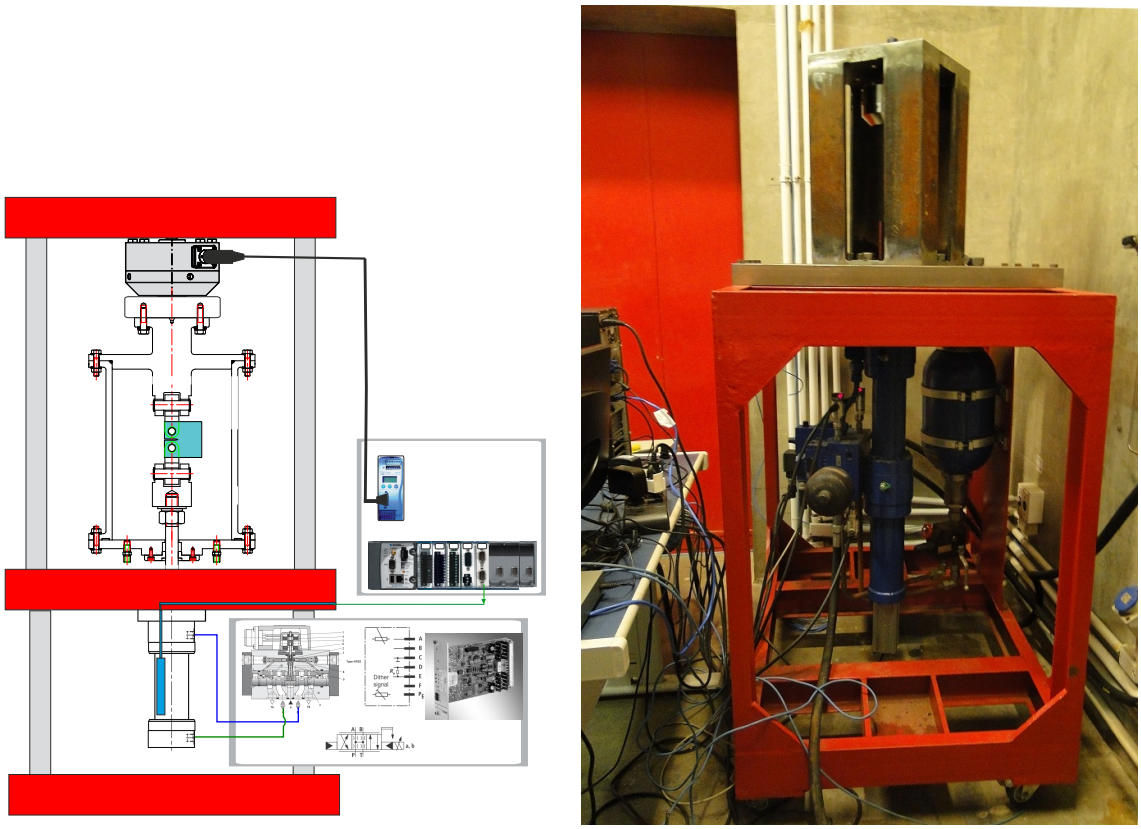

(a) (b)

Figure A.1: Schematic and Test bench of HTM: (a) Hydraulic circuit of HTM at LNDC and (b) Test bench of the hydraulic actuated fatigue testing machine (HTM) for the preliminary testing at LNDC

Table A.3: Main characteristics of hydraulic power unit (HPU)

Hydraulic Fluid	Mineral Oil	
Manufacture	LUBRAX	
Bulk modulus	$\beta_{\text{estimated}} = 10$	[GPa]
Density	ρ= 874	[kg m^{-3}]
Supply Pressure	$P_s = 19$	[MPa]
Temperature	37	[°C]

Table A.4: Details of Pressure Electronic Transducers

Manufacture	BOSCH-REXROTH	
Model	HEDE 10A1-2x/400K41G24/1/V	
MRN	R901022978	
Operation range	$P = 0$ to 400	[bar]
Output signal	$P = 0$ to 10	[V]
Supply Voltage	24	[V]

Table A.5: Details of Position Transducers

Manufacture	BALLUFF MICROPULSE	
Model	BTL5-H110-M0200-B-S94	
Operation range	0 to 200	[mm]
Output signal	Position CAN DATA Frame	4 bytes
	Velocity CAN DATA Frame	2 bytes
Position resolution	5	[µm]
Velocity resolution	0.1	$[\,\mathrm{mm\,s^{-1}}\,]$
Supply Voltage	24	[V]

Appendix B

Example output data of a fatigue test

Table B.1: Example Output Data of a Fatigue Test

Specimen Type: CT					
Dimensions:	B: 6.35 mm R: 0.8 n: 3	W: 50.8 mm	a_0: 12.7 mm		
#	Cycles [ ]	a_i [mm]	$\hat{a}_i$ [mm]	ΔK [MPa $\sqrt{m}$]	ΔP [N]
1.00e+00	0.00e+00	1.52e+01	0.00e+00	0.00e+00	4.45e+03
2.00e+00	1.55e+04	1.60e+01	0.00e+00	0.00e+00	4.45e+03
3.00e+00	2.21e+04	1.67e+01	0.00e+00	0.00e+00	4.45e+03
4.00e+00	3.02e+04	1.71e+01	8.21e-05	1.93e+01	4.45e+03
5.00e+00	3.61e+04	1.77e+01	8.56e-05	1.98e+01	4.45e+03
6.00e+00	4.14e+04	1.82e+01	8.10e-05	2.03e+01	4.45e+03
7.00e+00	4.69e+04	1.87e+01	8.55e-05	2.08e+01	4.45e+03
8.00e+00	5.01e+04	1.89e+01	8.65e-05	2.10e+01	4.45e+03
9.00e+00	5.44e+04	1.91e+01	8.82e-05	2.14e+01	4.45e+03
1.00e+01	6.03e+04	1.98e+01	9.83e-05	2.20e+01	4.45e+03
1.10e+01	6.52e+04	2.03e+01	1.05e-04	2.26e+01	4.45e+03
1.20e+01	7.02e+04	2.09e+01	1.13e-04	2.33e+01	4.45e+03
1.30e+01	7.47e+04	2.14e+01	1.15e-04	2.39e+01	4.45e+03
1.40e+01	8.01e+04	2.20e+01	1.22e-04	2.47e+01	4.45e+03
1.50e+01	8.39e+04	2.25e+01	1.25e-04	2.54e+01	4.45e+03
1.60e+01	8.81e+04	2.30e+01	1.31e-04	2.61e+01	4.45e+03
1.70e+01	9.15e+04	2.35e+01	1.38e-04	2.68e+01	4.45e+03
1.80e+01	9.56e+04	2.40e+01	1.48e-04	2.77e+01	4.45e+03
1.90e+01	9.90e+04	2.46e+01	1.55e-04	2.86e+01	4.45e+03
2.00e+01	1.02e+05	2.51e+01	1.58e-04	2.95e+01	4.45e+03
2.10e+01	1.05e+05	2.56e+01	1.70e-04	3.03e+01	4.45e+03
2.20e+01	1.08e+05	2.61e+01	1.76e-04	3.14e+01	4.45e+03
2.30e+01	1.12e+05	2.66e+01	1.88e-04	3.25e+01	4.45e+03
2.40e+01	1.13e+05	2.71e+01	1.93e-04	3.32e+01	4.45e+03
2.50e+01	1.17e+05	2.77e+01	2.14e-04	3.48e+01	4.45e+03
2.60e+01	1.19e+05	2.81e+01	2.28e-04	3.58e+01	4.45e+03
2.70e+01	1.21e+05	2.87e+01	2.66e-04	3.73e+01	4.45e+03
2.80e+01	1.22e+05	2.89e+01	2.82e-04	3.77e+01	4.45e+03
2.90e+01	1.23e+05	2.92e+01	2.89e-04	3.85e+01	4.45e+03
3.00e+01	1.24e+05	2.96e+01	3.22e-04	3.98e+01	4.45e+03
3.10e+01	1.26e+05	3.01e+01	3.41e-04	4.09e+01	4.45e+03
3.20e+01	1.27e+05	3.07e+01	4.19e-04	4.31e+01	4.45e+03
3.30e+01	1.29e+05	3.11e+01	5.12e-04	4.48e+01	4.45e+03
3.40e+01	1.30e+05	3.16e+01	0.00e+00	4.69e+01	4.45e+03
3.50e+01	1.31e+05	3.24e+01	0.00e+00	0.00e+00	4.45e+03
3.60e+01	1.31e+05	3.30e+01	0.00e+00	0.00e+00	4.45e+03
3.70e+01	1.32e+05	3.36e+01	0.00e+00	0.00e+00	4.45e+03

Source: extracted and adapted from (ASTM E647, 2008, Table X1.2)

Glossary

bulk modulus

of a substance measures the substance's resistance to uniform compression. It relates the change in pressure divided by the fractional change in volume at a constant temperature. Its unit is $[\,\mathrm{N\,m^{-2}}\,]$, the same as that of pressure.

CANOpen

is a communication protocol and dive profile specification for embedded systems based on CAN (Controller Area Network).

Index